FOSSIL ENERGY

15
9-22-95

DOE/BC/14652-15

(DE95000141)

DISPERSION MEASUREMENT AS A METHOD OF QUANTIFYING GEOLOGIC CHARACTERIZATION AND DEFINING RESERVOIR HETEROGENEITY

FINAL REPORT

By
D.E. Menzie

May 1995

Performed Under Contract No. DE-AC22-90BC14652

The University of Oklahoma
Norman, Oklahoma

Bartlesville Project Office
U. S. DEPARTMENT OF ENERGY
Bartlesville, Oklahoma

DISCLAIMER

DISCLAIMER

Portions of this document may be illegible in electronic image products. Images are produced from the best available original document.

DOE/BC/14652-15

Distribution Category UC-122

Dispersion Measurement as a Method of Quantifying Geologic Characterization and Defining Reservoir Heterogeneity

Final Report

By
D.E. Menzie

May 1995

Work Performed Under Contract No. DE-AC22-90BC14652

Prepared for
U.S. Department of Energy
Assistant Secretary for Fossil Energy

Gene Pauling, Project Manager
Metairie Site Office
900 Commerce Road, East
New Orleans, LA 70123

Prepared by
The University of Oklahoma
Norman, Oklahoma

Acknowledgements

The support of this research project by the U.S. Department of Energy has been essential in developing experimental techniques for the determination of dispersion measurements as a method of quantifying reservoir characterization and defining reservoir heterogeneity. The cooperation and encouragement of our research effort by colleagues in the School of Petroleum and Geological Engineering, the administrators of the Energy Center and the University of Oklahoma are gratefully appreciated.

I would like to acknowledge the invaluable contributions of:

S. R. Shadizadeh
Nadeem A. Malik
Sylvanus N. Nwosu
Yan Li
Shixin Chen
Saba Tahmassebi
Wei Wang
Dianli Han

Contents

List of Tables

List of Figures

Abstract

The main objective of this research project is to investigate dispersion as a method of quantifying geological characterization and defining reservoir heterogeneity in order to enhance crude oil recovery. The dispersion of flow of a reservoir rock (dispersion coefficient and dispersivity) was identified as one of the physical properties of a reservoir rock by measuring the mixing of two miscible fluids, one displacing the other in a porous medium.

A rock was 100% saturated with a resident fluid and displaced by a miscible fluid of equal viscosity and equal density. Some specific experiments were performed with unequal densities. Produced fluid was analyzed by refractometer, nuclear reaction, electrical conductivity and X-ray scan.

Several physical and flow characteristics were measured on the sand rock sample in order to establish correlations with the measured dispersion property. Absolute permeability, effective porosity, relative permeability, capillary pressure, the heterogeneity factor and electrical conductivity were used to better understand the flow system.

Linear, transverse, 2-D and 3-D dispersions were measured and used to characterize the rock heterogeneity of the flow system. A new system of measuring dispersion was developed using a gas displacing gas system in a porous medium. An attempt was also made to determine the dispersion property of an actual reservoir from present day well log data on a producing well.

Executive Summary

A significant part of the remaining hydrocarbon reserves of the United States remains in developed oil fields where the oil cannot be produced economically by primary production . Oil production from these pressure depleted reservoirs is increasing due to recently accelerated developments such as water flooding and other enhanced oil recovery methods. Non-uniform permeability of a oil reservoir (flow heterogeneity) is a major factor in the recovery of oil.

This study investigated the use of dispersion measurement as a method of defining reservoir heterogeneity and its effect on oil recovery. An important objective was to develop innovative methods to measure this property of the reservoir rock. The research was performed as eight tasks over a four year period.

Task 1 To investigate various methods of measuring dispersion, dispersion coefficient, and dispersivity of a reservoir rock;

Task 2 To develop a new method of evaluating dispersion in a miscible system using Oxygen-18 water and nuclear reaction analysis;

Task 3 To relate the dispersion flow property to other properties of a rock such as relative permeability and capillary pressure;

Task 4 To attempt to obtain the dispersion flow property of a reservoir rock by using well log data;

Task 5 To study the interconnection of linear, transverse, 2D and 3D dispersion;

Task 6 To study the differential equations describing dispersion flow;

Task 7 To develop a new method of using X-ray scan to determine dispersion along the length of a rock;

Task 8 To use a gas of one composition to displace a second gas of a different composition in order to measure a flow property of a porous medium.

The various tasks were investigated over the four year period of the research project. The report presents a summary of the entire study including tasks 1 to 8 and contains a record of all work and findings of this contract.

CHAPTER 1

Introduction

Recovery of oil and gas from complex reservoirs is inefficient because our understanding of the pore structure of reservoir rocks is inadequate to explain and predict internal variability and the paths of fluid flow in reservoirs. Improved recovery of hydrocarbons will require significant advances in our ability to characterize the reservoir rocks. Many parameters have been defined for this purpose such as porosity, permeability, specific surface area, formation resistivity factor, tortuosity, capillarity, pore size distribution and so on. All of these rock properties are used in the oil industry to describe a reservoir rock.

However, none of the above parameters can uniquely characterize the mixing ability of miscible fluids within a reservoir rock. The mixing process is relevant to many problems involving underground flow such as the migration of fertilizers towards aquifers, leaks of chemical or nuclear wastes stored in low-permeability rocks, the spreading of chemicals, and miscible flooding for enhanced oil recovery. This latter process is usually termed the dispersion phenomenon. A knowledge of the mixing ability of the miscible fluids in a porous rock will add a new dimension to reservoir characterization. This is critical to improve the efficiency of enhanced oil recovery.

The unsteady state mixing of two miscible fluids displacing one another in a porous rock is governed by a dispersion phenomena. In a heterogeneous porous medium, two basic mechanisms drive the dispersion process. This is a result of the chaotic nature of the pore level velocity field force on the flowing fluids. In a heterogeneous porous medium, flowing streamtubes are dissipated, continually break-up and rejoin together at the junction of flow channels. This leads to a variation in length of streamlines across the porous system. This accounts for the kinematic mechanism of dispersion in rock. Changing pore geometry, pore orientation and local permeabilities across the rock cause a change in flow velocity. These mechanisms cause a concentration front of fluid particles to spread as flow takes place. The extent of the spread of the concentration front of the fluid mixing is a measure of dispersion. This experimental investigation was designed to develop, measure and study dispersion, the dispersion coefficient, and dispersivity to determine their correlation with other rock properties in order to be able to predict oil recovery.

CHAPTER 2

Determination of Dispersivity and Correlations with Rock Properties

2.1 Introduction

Dispersion is a common problem in ground water hydrology, chemical engineering processes, and enhanced oil recovery techniques where an injected fluid displaces the reservoir oil. There are two types of dispersion in relation to the direction of gross fluid flow: i.e., longitudinal and transverse. Research on dispersion began in the early 1950's and a great deal of literature is available on this topic. The reference list at the end of this report includes available dispersion reports.

There are two possible extremes for the form of the dispersion coefficient D: (1) directly proportional to velocity, and (2) proportional to velocity squared. Put mathematically, respectively:

$$D = \alpha_d U \qquad (2.1.1)$$

and,

$$D = \alpha_d U^2 \qquad (2.1.2)$$

Experiments seem to indicate that the first of these forms corresponds to physical reality. This implies that there is no mixing of material on adjacent streamlines. The constant α_d, with the dimension of length, has been termed as dispersivity. The dispersivity is expressed as the quotient of the dispersion coefficient and interstitial fluid velocity. Local dispersivities are of the order of 10^{-2} to 1 cm for laboratory experiments and range from 10^{-1} to 10^{2} m for tracer tests in porous media as calculated in the field[133]. Some typical values for local longitudinal dispersivity are also shown in the order of 10^{-2} to 1 m[91]. Values in the range of 3 to 200 m have also been reported[36], but these values may not be physically meaningful. In order to obtain meaningful predictions of contaminant movement at existing sites and to apply advection-dispersion models to new or proposed sites, an accurate way of quantifying dispersivity has to be developed. The values calculated in the field tracer tests are biased by the scaling effect. It appears that dispersivity increases with distance from the injection point.

The purpose of the present study was to obtain data from laboratory core displacement tests and to calculate the dispersion coefficient and dispersivity in order to characterize the reservoir rock. Using both cores and plugs taken from Berea sandstone, such rock properties as porosity, absolute permeability and the heterogeneity factor were measured. Using Brigham's[36] method, the dispersivity values for each core and plug were determined. In a manner similar to the correlation of reservoir fluid property , which is well developed in the literature, an attempt was made to

correlate dispersivity with the rock properties listed above. Using a non-linear multiple regression technique, dispersivity values were calculated and their scattering pattern on a cross-plot was simulated by the Monte Carlo method. A statistical analysis is presented to determine the validity of the regression models developed in this study.

2.2 Experiment

This section contains the method and equipment used in performing the miscible displacement experiments for calculation and testing of dispersivity for Berea sandstone cores.

2.2.1 Experimental Method

The experimental setup and apparatus is shown in Figure 2.2.1. The plug and cores used were 1 and 2 inches in diameter with lengths ranging from 2 to 6 inches. A block of Berea sandstone was obtained from Cleveland Quarry (Amherst, Ohio) and the 6 inch long cores were cut from that block. The 1 inch diameter plugs with a length of 2.5 inches were taken from a 224 feet thick Red Fork sand reservoir.

Air permeability was measured with a dry air source. The liquid permeability was measured to establish the final value of permeability since it is purely a rock property and does not depend upon the type of fluid used (air or liquid).

In the displacement run, naphtha, crude oil, iso-octane, and a combination of all these fluids were used as the displaced and displacing fluids. Thus the displacement process was miscible. The combination of the fluids was chosen so that the fluids had equal densities and viscosities.

During the displacement run, the effluent concentrations of the displacing fluid were determined by measuring the refractive index of the effluent fluid. The displacing fluid was injected until its concentration in the effluent reached 100%.

2.2.2 Calculation of Dispersivity

The calculation of dispersivity and the interpretation of the data were performed by plotting the concentration values against the volumes injected and also by plotting the parameter λ versus the displacing fluid concentration on probability paper. The parameter λ is defined as:

$$\lambda = \frac{\frac{V}{V_p} - 1}{\sqrt{\frac{V}{V_p}}} \qquad (2.2.1)$$

where, V_p = pore volume, cm^3,
V = volume injected, cm^3.

In the plot of λ versus effluent concentration, a straight line was drawn and from this straight line the values of λ_{90} and λ_{10} corresponding to 90% and 10% displacing liquids concentration, respectively, were read. The dispersion coefficient, D, was then calculated by the following equation:

$$D = \frac{UL(\lambda_{90}-\lambda_{10})^2}{3.635^2} \qquad (2.2.2)$$

where, U = average interstitial velocity, cm/sec,
L = length of plug or core, cm.

The dispersivity α_d was then calculated as follows:

$$\alpha_d = \frac{D}{U} \qquad (2.2.3)$$

The heterogeneous system is defined as one in which the recovery at one pore volume solvent injected in a matched viscosity flood is less than 99%. The degree of heterogeneity of a system is given by the factor H. Koval defined H as follows:

$$H = \frac{K}{E} \qquad (2.2.4)$$

where, K = parameter characterizing the viscosity effects,
E = effective viscosity ratio,
V_{pi} = pore volume injected for complete or 100% displacement,

$$K = V_{pi}=H*E \qquad (2.2.5)$$

$$E = (0.79 + 0.22\, V_r^{1/4})^{1/4} \qquad (2.2.6)$$

$$V_r = \mu_{resident}/\mu_{displacing} \qquad (2.2.7)$$

Table 2.2.1 is the database for plugs and Table 2.2.2 is the database for cores. Note that one data point consists of an individual value for dispersivity, porosity, absolute permeability and the heterogeneity factor. There are 37 data points including both core and plug databases.

The databases are obtained exclusively from calculations based on laboratory displacement data. Unlike fluid property correlation[3] (e.g. bubble point pressure for crude oil), there is no known method to smooth the measured data before using them for establishing correlations. Nonetheless, an attempt was made in this study to see if the permeability data could be adjusted by means of a single variable correlation with the porosity. If such a correlation exists, the correlated permeability values may be considered in place of the experimentally determined permeability values, and the former may then be used to fit in the proposed regression model for dispersivity.

Table 2.2.1 Plug Data

Serial Number	Fluid Property	Run #	Plug #	ϕ (%)	k (md)	H	α_d (cm)
1	IDN	35	1	14.70	18.00	3.03	0.157
2	IDN	36	2	13.40	13.00	2.81	0.2105
3	IDN	37	3	17.90	26.00	2.04	0.1357
4	IDN	38	4	14.82	14.00	2.15	0.1858
5	IDN	39	5	15.54	8.80	3.38	0.0526
6	IDN	40	6	17.09	29.00	2.36	0.3249
7	IDN	41	7	9.85	26.00	2.39	0.3574
8	NDI	45	7	9.85	26.00	4.26	0.2865
9	IDN	42	8	15.63	58.00	2.00	0.2010
10	NDI	46	8	15.63	58.00	2.30	0.2791
11	IDN	43	9	16.06	33.17	2.14	0.1208
12	IDN	47	11	18.12	35.00	1.833	0.2234
13	IDN	48	12	11.90	72.00	2.658	0.2042
14	IDN	49	13	13.15	119.0	2.476	0.0626
15	IDN	52	19	13.15	6.45	3.5313	0.8042
16	IDN	53	20	15.20	225.0	2.182	0.0852
17	IDN	54	21	16.90	125.0	2.383	0.2505
18	IDN	55	22	16.50	200.0	2.156	0.1160
19	IDN	57	24	16.07	170.0	2.427	0.1979

IDN = Iso-Octane 89% diesel oil 11% displacing naphtha,
NDI = Naphtha displacing Iso-Octane 89% diesel oil 11%,
ϕ = Porosity, %,
k = Permeability, md,
H = Heterogeneity Factor,
α_d = Dispersivity, cm.

Table 2.2.2 Core Data

Serial No.	Fluid Property	Run #	Core #	ϕ (%)	k (md)	H	α_d (cm)
1	NDC	4	1B	22.6	225.0	2.0	6.17
2	NDC	5	2B	22.6	15.0	2.37	1.45
3	NDC	7	3B	18.1	90.0	2.20	3.30
4	NDC	10	4B	19.6	98.0	1.72	3.39
5	NDC	12	5B	19.8	143.0	2.26	3.93
6	NDC	14	6B	22.8	680.0	2.00	6.30
7	CDN	8	3B	18.1	90.0	3.30	0.07
8	CDN	9	4B	19.6	98.0	3.40	0.08
9	CDN	11	5B	19.8	143.0	5.57	0.12
10	CDN	13	6B	22.8	680.0	3.30	0.13
11	NCDIS	6	3B	18.1	90.0	1.93	0.37
12	NCDIS	19	7B	17.1	8.40	1.80	0.11
13	ISDN	31	10B	21.5	300.0	1.75	0.142
14	NDIS	32	1B2B	18.9	163.0	1.72	0.477
15	DODN	34	11B	20.2	68.0	2.00	0.0784
16	NODIS	28	8B	21.7	250.0	1.57	0.09
17	NODIS	3	9B	20.3	215.0	1.7767	0.1893
18	NODIS	3	11B	17.2	93.0	1.2510	0.0989

NDC = Naphtha displacing crude oil,
CDN = Crude oil displacing naphtha,
NCDIS = Naphtha 90% diesel 10% displacing iso-octane,
NODIS = Naphtha 80% diesel 20% displacing Iso-Octane 89% diesel oil,
ISDN = Iso-Octane 89% diesel oil 11% displacing naphtha,
NDIS = Naphtha displacing Iso-Octane 89% diesel oil 11%,
DODN = Diesel oil displacing naphtha,
ϕ = Porosity, %,
k = Permeability, md,
H = Heterogeneity Factor,
α_d = Dispersivity, cm.

2.3 Regression of Experimental Results

2.3.1 Fitting of the Non-Linear Regression Models

The goal of the present study was to correlate dispersivity, α_d, with porosity, ϕ, permeability, k, and the heterogeneity factor, H. In order to accomplish this, the following types of non-linear regression models were envisaged:

(a) Direct non-linear multiple regression:

$$\alpha_d = a\phi^b k^c H^d \qquad (2.3.1)$$

(b) Iterative non-linear multiple regression:

$$\alpha_d = a\phi^b k^c \pm H^d \qquad (2.3.2)$$

Equation 2.3.1 is direct because the non-linear can be removed by logarithmic transformation resulting in Equation 2.3.3. The least square method has to be applied only once to determine the regression parameters a, b, c and d.

$$Log(\alpha_d) = Loga + bLog\phi + cLogk + dLogH \qquad (2.3.3)$$

In contrast, a logarithmic transformation of Equation 2.3.2 did not readily linearize the equation. In fact, there is no known transformation method to linearize Equation 2.3.2 in terms of the unknown parameters a,b,c and d. To fit the regression model represented by Equation 2.3.2, the following iterative procedure was used. Equation 2.3.2 can be written as:

$$Log(\alpha_d \pm H^d) = Loga + bLog\phi + cLogk \qquad (2.3.4)$$

Assuming arbitrarily a value of the parameter d, Equation 2.3.4 becomes linear in terms of the remaining regression parameters. Therefore, the method of least square now can be applied to determine parameters a, b and c. Another value of d was assumed and the process was repeated for a few hundred times automatically using a FORTRAN code developed to perform the calculation. The purpose of this iteration was to find the optimum value of d for which the coefficient of determination, R^2, is maximum. Thus the iterative non-linear regression involved multiple use of the least square method for the determination of regression parameters.

It was felt that smoothing of the permeability data by establishing a permeability-porosity correlation, if feasible, could result in a better correlation for dispersivity. For the k-ϕ databases used in this study, correlation of the type:

$$k = a_1 \Phi^{b_1} \qquad (2.3.5)$$

was observed. In the regression models represented by Equation 2.3.1 and 2.3.2, both experimental and smoothed ϕ data were used separately.

2.3.2 Solution Method and Results

The regression model represented by Equation 2.3.1 or 2.3.3 can be readily solved by using the SAS package or LOTUS spreadsheet. To solve the iterative model represented by Equation 2.3.2 or 2.3.4, however, there is no procedure in the SAS package. The use of the LOTUS spreadsheet is also not possible. Therefore a FORTRAN program was developed to implement the iterative algorithm as outlined in section 2.3.1. The program is general and strong in the sense that it incorporates an automatic switching algorithm to select the variable that appears in Equation 2.3.2. Later an analysis of the fitted model suggested that the use of a random number and the Monte Carlo simulation might result in an improvement of the model. Exploring this idea, another FORTRAN program was developed.

The results of the regression models are presented in Figure 2.3.1 through 2.3.6. These are the various cross-plots of the experimental α_d plotted against the calculated α_d. The chaotic scatter of data in Figure 2.3.1 resulted from the use of unsmoothed porosity (or permeability) data in the regression model. When the porosity (or permeability) data was smoothed using Equation 2.3.5, the dispersivity cross plot showed a marked improvement, as shown in Figure 2.3.7. Later in section 2.3.3, it will be shown that the regression model using smoothed porosity (or permeability) data can be further improved by the application of the Monte Carlo technique. Using the parameters a,b,c and d, the two types of correlation for dispersivity finally take form, as represented by Equation 2.3.1 and 2.3.2, respectively:

$$\alpha_d = 1.4217 \phi^{-0.9918} k^{-0.2113} H^{-0.5429} \qquad (2.3.6)$$

and,

$$\alpha_d = 1.91192 \phi^{-0.130611} k^{-0.004} - H^{-0.006} \qquad (2.3.7)$$

Equations 2.3.6 and 2.3.7 are based on the data obtained from the plugs. The parameters are different for data obtained from the cores. These Equations are shown below:

$$\alpha_d = 1.21 * 10^{-8} \phi^{6.15} k^{-0.05} H^{-1.07} \qquad (2.3.8)$$

and,

$$\alpha_d = 4.2743*10^{-3}\phi^{2.12181}k^{0.00251}-H^{0.72} \qquad (2.3.9)$$

If the cores and plugs are used together, the regression equations become:

$$\alpha_d = 0.0025\phi^{1.8404}k^{-0.0153}H^{-0.6007} \qquad (2.3.10)$$

and,

$$\alpha_d = 0.3568\phi^{0.5523}k^{0.0346}-H^{0.425} \qquad (2.3.11)$$

A modified version of Equation 2.3.1 was also studied. The parameter c associated with permeability k was fixed as 0.5 in order to maintain dimensional homogeneity of the equation:

$$\alpha_d = 0.0558\phi^{-0.8213}k^{0.5}H^{1.7073} \qquad (2.3.12)$$

The results are shown in Figure 2.3.8. As the results show, there is no obvious gain in the value of R^2, but the cross plot in Figure 2.3.8 has shown some improvement over the model represented by Equation 2.3.1.

2.3.3 Discussion of the Regression Models

To find a measure of a linear model which fits a set of data, the multiple regression equivalent of R^2, the coefficient of determination was used. It is defined as:

$$R^2 = 1-\frac{\sum(y_i-y_i)^2}{\sum(y_i-y_i)} = 1-\frac{SSE}{SS_{yy}} \qquad (2.3.13)$$

where, y_i is the predicted value of y_i for the model.

The value $R^2 = 0$ implies a complete lack of fit of the model to the data, and $R^2 = 1$ implies a perfect fit, with the model passing through every data point.

For Equation 2.3.6, $R^2 = 0.1541$ and for Equation 2.3.7, $R^2 = 0.14$. Although these values are very small, it is too early to say that dispersivity cannot be correlated at all with such reservoir properties as were used in the present study. This speculation stems from the fact that although permeability k usually is correlated with porosity, there are many cases where these properties cannot be correlated at all. Using the core data used in this study, a k-ϕ correlation of the type of Equation 2.3.5 was investigated, where a_1 and b_1 were determined to be $2.366*10^{-6}$ and 5.929, respectively. The corresponding R^2 value was equal to 0.27 which was low as in the case of Equation 2.3.1 and 2.3.2. Thus for the cores studied, k cannot be correlated with ϕ. Further study could be conducted to determine what happens to the dispersivity correlation when a good k-ϕ correlation exists for a given type of rock.

The test statistic used to test the overall model was the F-test. This test statistic is defined as:

F = Mean sum of square of deviations from mean/ Mean sum of square of errors (2.3.14)

The upper tail values of the F distribution are given in the standard table. This test statistic is defined as:

$$F = \frac{\frac{R^2}{\delta}}{\frac{(1-R^2)}{[n-(\delta+1)]}} \qquad (2.3.15)$$

where, n = number of data points,
δ = number of parameters in the model - 1.

The F test statistics become large as the coefficient of determination R^2 becomes large. To determine how large F must be at a given value of α_d at which the model is useful for predicting y, the rejection level set is given by:

$$F_{calc.} > F_{\alpha} \qquad (2.3.16)$$

Like the R^2 analysis, the F-test was calculated for both the k-ϕ model and the α_d model. The values of the one-tailed test statistic-F were calculated using Equation 2.3.15 for 10% probability of Type 1 error. For the k-ϕ model:

$$R^2 = 0.27 \qquad \delta = 1 \qquad n = 15$$

Therefore,

$$F_{calc} = \frac{\frac{R^2}{\delta}}{\frac{(1-R^2)}{[n-(\delta+1)]}} = 4.82 \qquad (2.3.17)$$

where as, $F_{0.10} = 3.14$ **(from F-table)**

Thus $F_{calc} > F_{0.10}$, which means that the k-ϕ model has an overall utility.

For the α_d model represented by Equation 2.3.12, $R^2 = 0.35$, $\delta = 2$, n = 13, $F_{calc} = 2.72$, $F_{0.10}=2.92$, and $F_{calc} < F_{0.10}$ which indicates that the model does not have an overall utility for prediction purposes. It may be noted that $F_{0.10} = 2.67$ for n = 19, i.e., if the number of data points is increased from n = 13 to n = 19, the model is most likely to be valid. Since an increase in n is also attended by an increase[3] in R^2, a glance at Equation 2.3.15 shows that for n = 19, the F_{calc}

will also be greater than 2.72. The F-test thus suggests that in order to use the model represented by Equation 2.3.1, more than 13 data points are necessary. The results of the F-test for the other α_d models are shown in Table 2.3.1.

Table 2.3.1 Testing of Overall Utility of Dispersivity Models

Data Type	Model	R^2	n	δ	F_{calc}	$F_{0.10}$	Remarks
Plugs	1	0.1541	17	3	0.7892	2.56	Needs more data points
Cores	1	0.1380	18	3	0.7476	2.52	
Combine	1	0.0960	35	3	1.0977	2.27	
Plugs	2	0.2351	19	3	1.5377	2.49	
Cores	2	0.1328	19	3	0.7131	2.52	
Combine	2	0.1072	37	3	1.3208	2.26	
Plugs	Modified	0.3519	13	2	2.7147	2.92	

From Table 2.3.1, it can be seen that the F-test does not imply overall validity of the models. For all the data types and/or models, probably more data points are needed in order to determine the model parameters.

The dispersivity cross-plot (Figure 2.3.7) shows an interesting feature. It may be observed that as dispersivity increases, the relative scattering of the calculated dispersivity also increases. This indicates that the regression model may be more accurate at lower dispersivity values than at higher ones. Although there is no distinct mathematical trend in the scattering, it can be seen that almost all the points are contained within a conical section generated by a line measuring θ_1 degree above the perfect fit 45° line and another at $-\theta^o_2$ below. Obviously, if $\theta_{1,2}=0^o$, then it indicates a 100% correlation, which is, of course, not attainable in a realistic sense. On the other hand, if $\theta_1=45^o$ and/or $-\theta_2=45^o$, then there is no correlation at all. Therefore, the ratio $\upsilon^2=\theta/45$ provides a measure of goodness of the correlation developed. Therefore $\upsilon^2 \rightarrow 0$ implies a good correlation, $\upsilon^2 \rightarrow 1$ shows no correlation. In our case, $\upsilon_1^2=0.19$ and $\upsilon_2^2=0.11$, which are closer to 0 than 1. Although these numbers seem to be good, a concrete assessment of this measure of goodness of correlation will necessitate the application of the calculated dispersivity values in a reservoir simulator to study the sensitivity on history matching.

By measuring the angle θ_1 and θ_2 and assuming that the data scattering is somewhat random within these two limits of θ, a random correction factor, ω, given by:

$$\omega = \frac{1}{\tan(45^0 \pm \theta)} \qquad (2.3.18)$$

may be applied. Then the modified regression model may be written as:

$$\alpha_d = (a \phi^b k^c H^d) * \omega \qquad (2.3.19)$$

The correction factor, ω, is generated by the Monte Carlo simulation which is facilitated by the assumption that θ may be chosen at random[130]. Using Equation 2.3.19, a set of α_d values were calculated and the cross plot was superimposed (Figure 2.3.9) onto the crossplot obtained without applying the correlation factor. It is observed in Figure 2.3.9 that the data scattering has reduced to some extent, indicating an improvement in the correlation.

Instead of calculating a single value of α_d from Equation 2.3.19 for a set of ϕ, k and H values, a large number of α_d values can be calculated using the Monte Carlo program. These α_d values should display a mound shaped distribution with a mean located somewhere near the middle of the vertical line segment CD. To obtain this point, about 225 dispersivity points were calculated using Equation 2.3.19 and the arithmetic mean was taken. The procedure was repeated for each of the observed dispersivity values. Using these calculated statistical average values of dispersivity, a crossplot was made (Figure 2.3.10). Obviously Figure 2.3.10 has better reproducibility than Figure 2.3.9.

2.4 Conclusions and Recommendations

Based on the review of literature and work carried out in this study, the following conclusions and recommendations are made.

2.4.1 Conclusions

(1) Comparison of results from the regression models showed that the use of smoothed porosity or permeability data resulted in a considerable improvement of the correlation.

(2) Exploiting the trend of the data scattering in the dispersivity cross-plot, a method for applying a correlation factor to the correlations was derived. In this, the Monte Carlo technique was also utilized.

(3) The statistical analysis of the fitted regression models indicated that probably more experimental data points are needed to determine the regression parameters in order to facilitate prediction of dispersivity in terms of rock properties used in this study.

(4) The value of dispersivity can not exclusively be calculated by using reservoir rock properties used in this study.

2.4.2 Recommendations

(1) Laboratory experiments as outlined in this study should be redesigned for better reproduction of experimental data. This will help in reproducibility and sensitivity of data.

(2) Besides rock properties, some fluid properties may also be included in the regression models.

(3) The study may be carried out for various types of sandstones. The phenomenon of dispersivity may also be studied for limestone.

(4) More than non-linear additive terms may be included in the iterative type regression models. This will necessitate the development of a new mathematical approach to determine the regression parameters.

2.5 Nomenclature

D	dispersion coefficient, cm^2/sec
E	effective viscosity ratio
F	value of F-test statistics from tables
F_{calc}	value of F-test statistics calculated
H	heterogeneity factor
K	parameter characterizing viscosity effects
k	permeability, md
L	length, cm
n	number of data points
R^2	coefficient of determination
SSE	sum of squares for error
SS_{yy}	sum of squares of deviations
U	average flow velocity, cm/sec
V	volume injected, cm^3
V_p	pore volume, cm^3
V_{pi}	pore volume injected, cm^3
V_r	viscosity ratio of resident fluid to displacing fluid
y	dependent variable
y	estimator of the mean value of y

Greek Letters

α_d	dispersivity, cm
δ	number of data parameters in model 1
ϕ	porosity, percent
λ_{10}	value at 10% of displacing liquid concentration
λ_{90}	value at 90% of displacing liquid concentration
μ	viscosity, cp
ω	correction factor

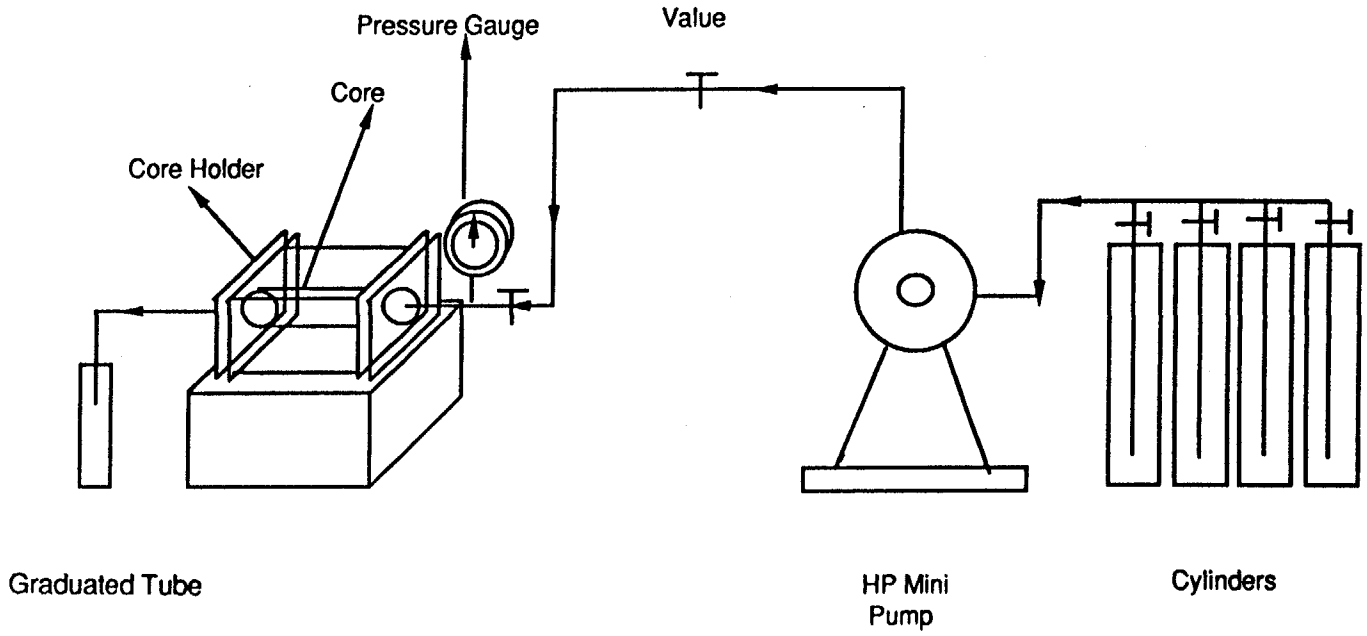

Figure 2.2.1 Experimental Setup for Miscible Displacement Runs

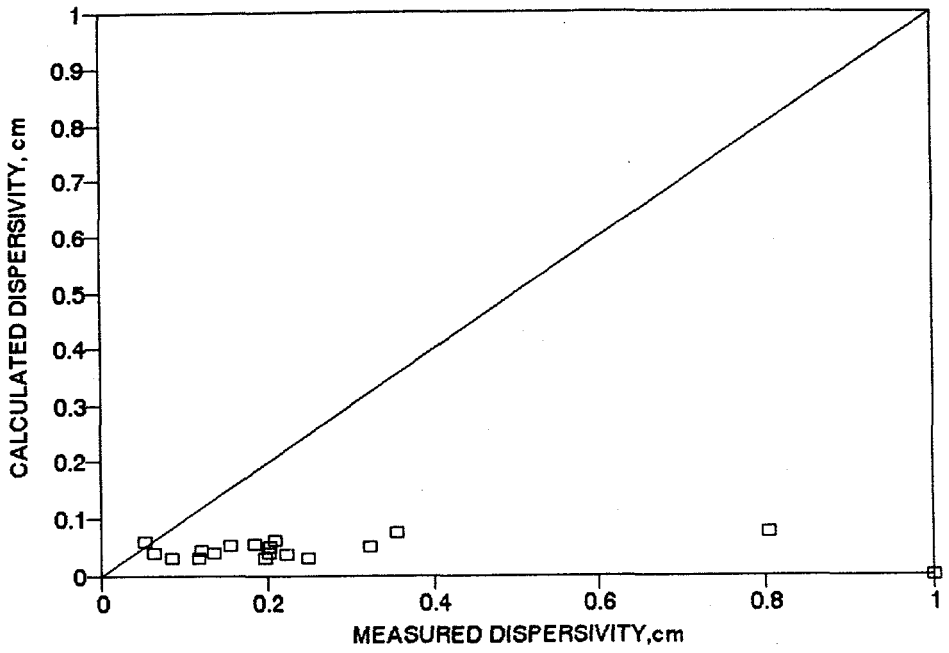

Figure 2.3.1 Cross Plot (Model 1: Berea Sandstone Plugs)

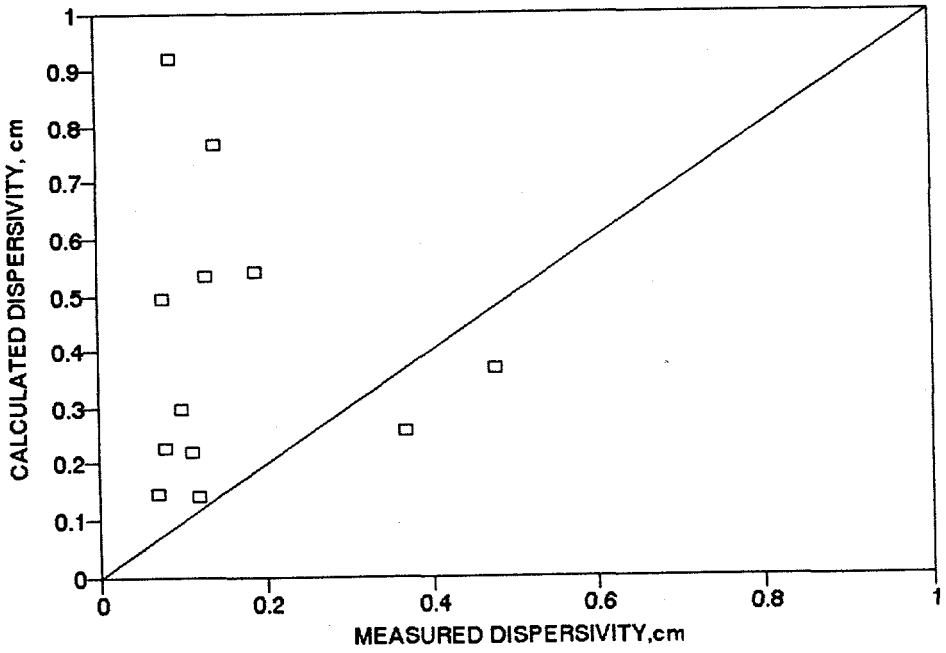

Figure 2.3.2 Cross Plot (Model 1: Berea Sandstone Cores)

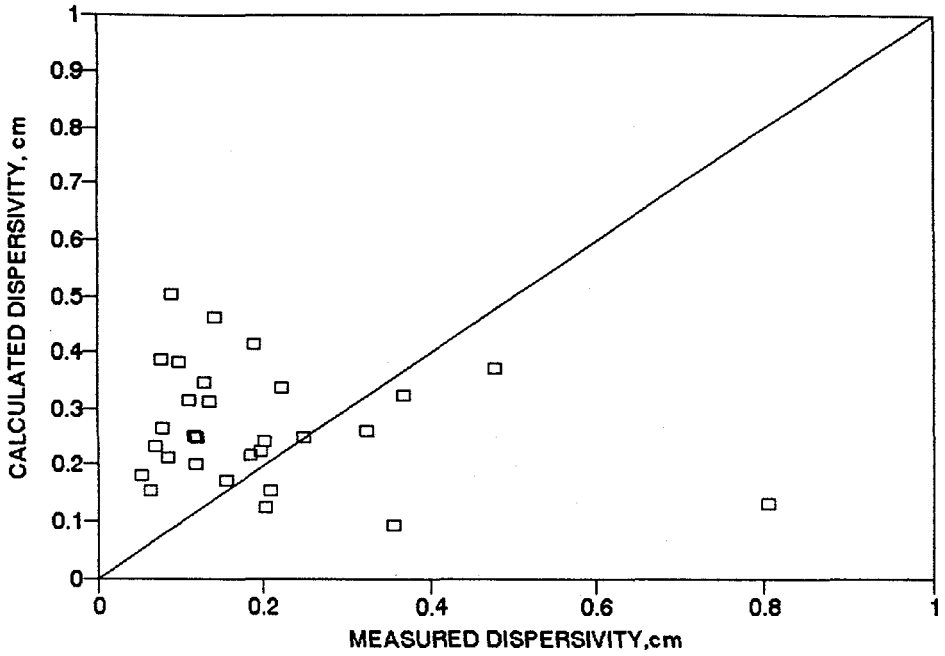

Figure 2.3.3 Cross Plot (Model 1: Berea Sandstone Plugs and Cores)

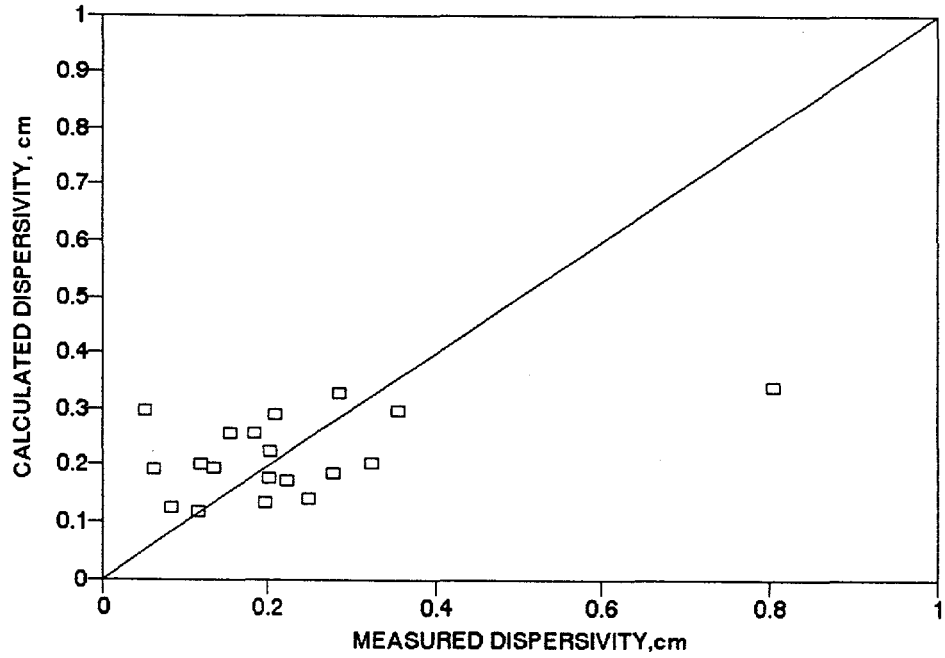

Figure 2.3.4 Crossplot of Dispersivity (Model 2: Berea Sandstone Plugs)

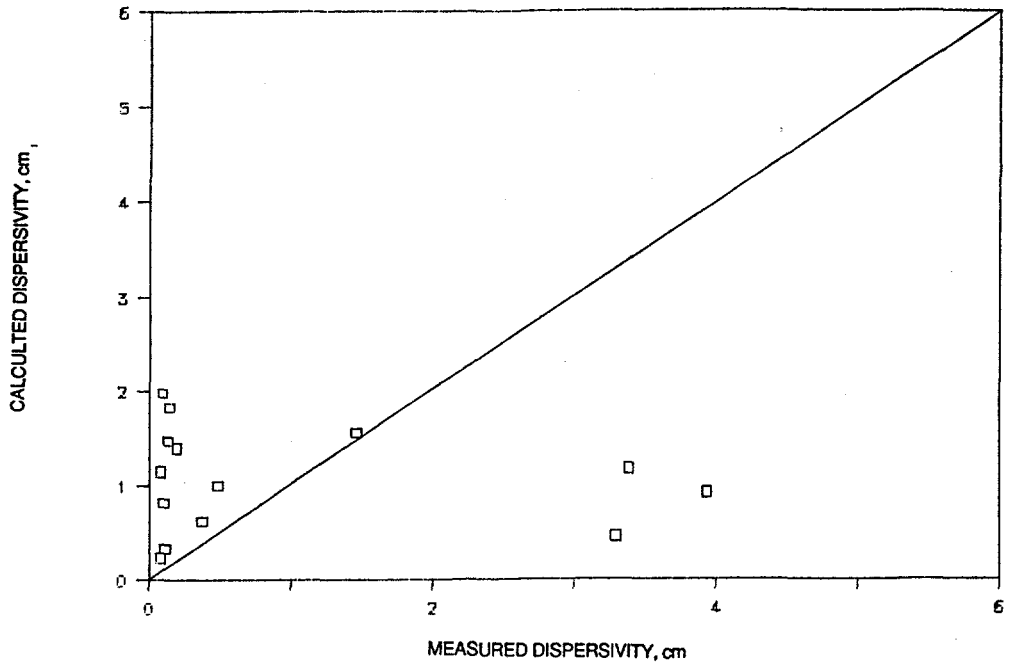

Figure 2.3.5 Crossplot of Dispersivity (Model 2: Berea Sandstone Cores)

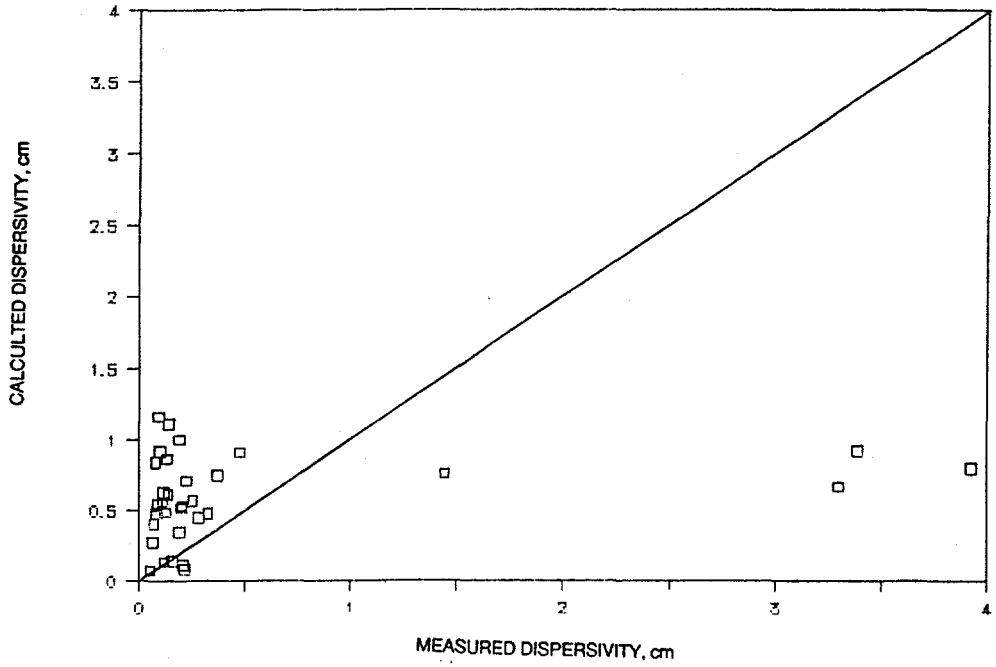

Figure 2.3.6 Crossplot of Dispersivity (Model 2: Berea Sandstone Plugs and Cores)

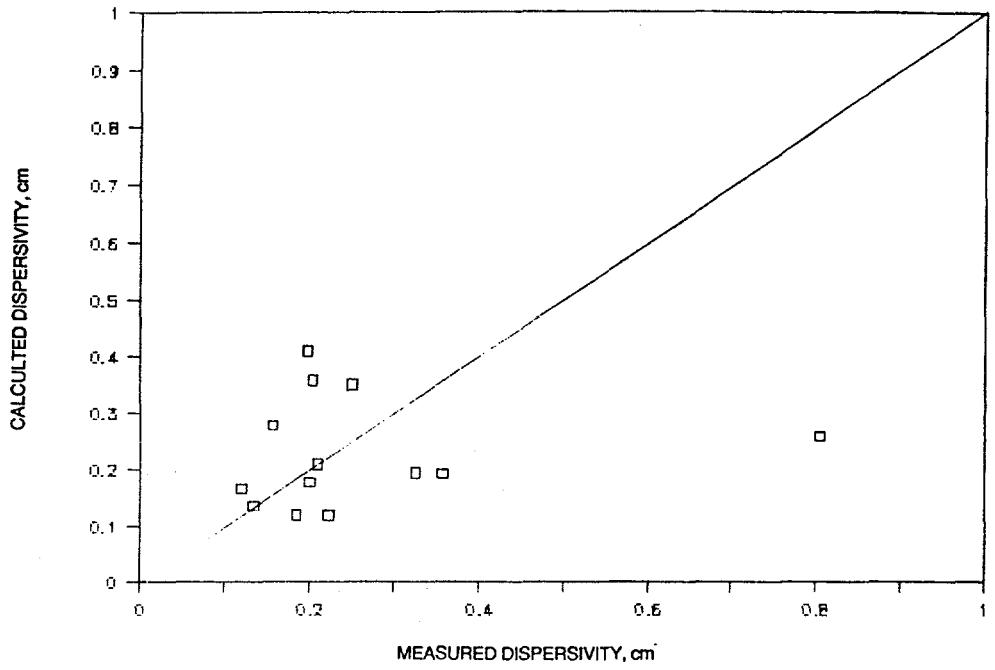

Figure 2.3.7 Crossplot of Dispersivity (With Smooth Porosity for Berea Sandstone Cores Using Model 1)

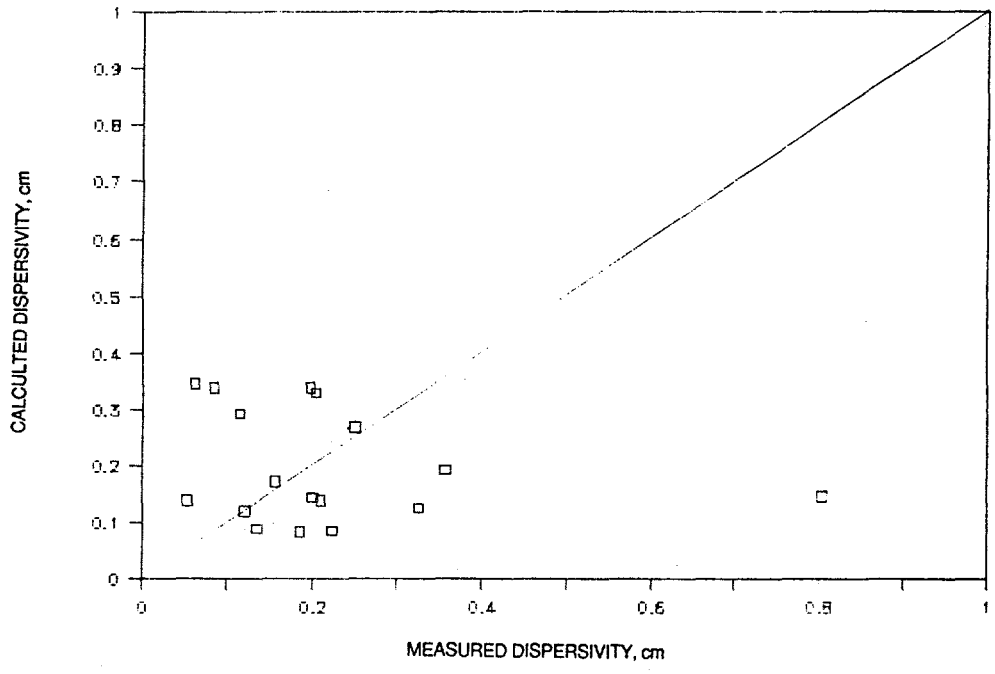

Figure 2.3.8 Crossplot of Dispersivity (Dimensionally Homogeneous Model for Berea Sandstone Plugs)

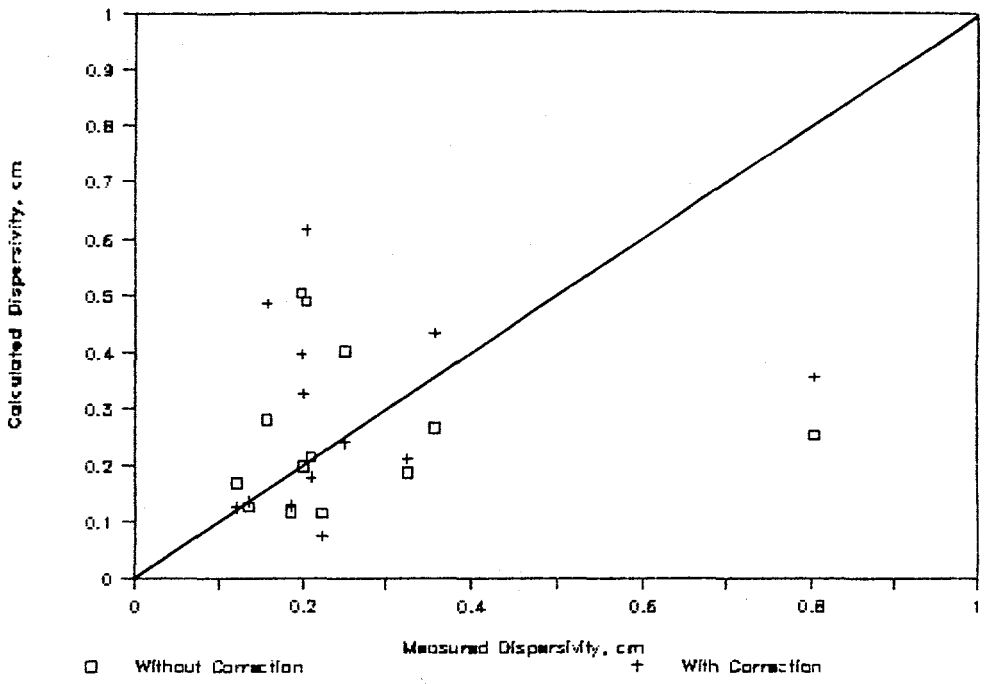

Figure 2.3.9 Crossplot of Dispersivity (With Correction Factor)

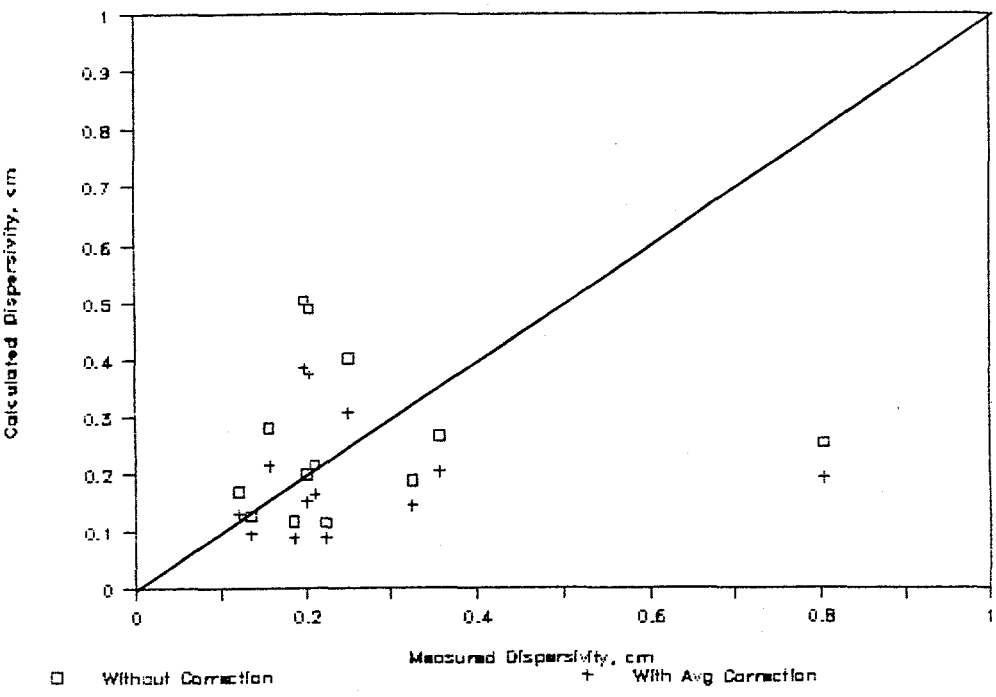

Figure 2.3.10 Crossplot of Dispersivity (With Average Correction Factor)

CHAPTER 3

Measurement of Dispersivity by Nuclear Reaction Analysis

The dispersion of water in a consolidated porous medium was measured using the $^{18}O(p,\alpha)^{15}N$ nuclear reaction. A reservoir rock core was saturated with water enriched to 0.56 atom % of ^{18}O. During a miscible displacement of the resident ^{18}O enriched water by a brine solution with natural ^{18}O abundance, effluent mixtures of the fluids were collected as a function of time and pore volume injected. The targets used for the nuclear reaction analysis were prepared by anodic oxidation of tantalum at constant voltage. The Ta_2O_5 film was bombarded with 0.73 MeV protons and the resulting reaction alpha particles were recorded. The number of the reaction alpha particles proportional to the ^{18}O concentration in the effluent mixture was used as the concentration index for the determination of the water dispersion profile and rock dispersivity.

3.1 Introduction

Radioactive and non-radioactive tracers have been applied in the study of dispersion of water in porous geological material[190,76]. Tritiated and deuteriated water, soluble ions, or a combination of these, have been identified as satisfactory water soluble tracers[85]. ^{18}O enriched water and the $^{18}O(p,\alpha)^{15}N$ nuclear reaction were used to measure the dispersion profile in an oil reservoir core and the dispersivity of the core. The resident fluid (^{18}O enriched water) was displaced by a diluted brine solution in a miscible flooding process. When miscible fluids move through porous material, mixing of the two fluids takes place both as a result of molecular diffusion due to spontaneous mixing, and convection due to the dynamic motion of the fluids and the existing concentration gradient[36,108]. This type of mixing is defined as dispersion and may be influenced by differences in the viscosity and density of the miscible fluids, fluid velocity, and the pore-size distribution.

The detailed derivation of the basic equations for isotope tracer analysis by nuclear reaction and the mathematical formulation of the dilution process based on two compartment kinetics is presented in ref.[177] Here only the result is given by expressing the ^{18}O concentration of the effluent fluid as:

$$C_E(^{18}O) = \frac{R_\alpha(ES) - C(BS)}{1 - C(BS)} \qquad (3.1.1)$$

The quantity $R_\alpha(ES) = N_\alpha(E)/N_\alpha(S)$ is the ratio of the alpha particle count rate $N_\alpha(E)$ obtained from the Ta_2O_5 targets prepared from the effluent fluid and $N_\alpha(S)$ the alpha particle count rate from targets prepared from the ^{18}O enriched water used to initially saturate the core. The quantity $C(BS)$ is the ratio of the ^{18}O concentration of the displacing fluid, C_B, (brine in this case) and the ^{18}O concentration of the enriched water, C_S, initially used to saturate the core. The concentration C_S and

C_B are proportional to the alpha count rate $N_\alpha(S)$ and $N_\alpha(B)$ respectively. The concentration ratio $C(BS) = C_B/C_S = N_\alpha(B)/N_\alpha(S)$ can be determined by measuring the alpha particle rate $N_\alpha(B)$, from targets made from the displacing fluid before it is injected, and $N_\alpha(S)$.

Expressing the ^{18}O concentration of the effluent fluid as given in Equation 3.1.1 has the advantage that only count rate ratios appear so that no absolute calibration is needed. In order to readily compare the results of the nuclear reaction analysis (NRA) with the results of the conventional method of oil reservoir dispersivity measurements, where the index of the refraction of the displacing fluid is the indicator, it is convenient to introduce the "brine" concentration of the effluent fluid defined as:

$$C_E(B) = 1 - C_E(^{18}O) \qquad (3.1.2)$$

This definition assumes that the ^{18}O concentration of the displacing fluid (brine) before being introduced into the core is C_B and the ^{18}O concentration of the resident water in the core is C_S.

The expressions for the dispersion coefficient and the reservoir dispersivity as given in refs. [36] and [165] are respectively:

$$K_D = \frac{UL(\lambda_{90} - \lambda_{10})^2}{(3.625)^2}, \qquad \alpha_D = \frac{K_D}{U} \qquad (3.1.3)$$

The average interstitial velocity $U = q/A\phi$, q is the average injection flow rate, A the cross sectional area of the reservoir core, L the length of the core, and ϕ the porosity of the core as a fraction of the pore volume. The quantities, λ_{90} and λ_{10} ($\lambda=(R_V-1)/\text{sqrt } R_V$) represent 90% and 10% concentration of the displacing fluid, respectively. $R_V = V/V_P$ is the ratio of the effluent volume injected at any time during the displacement and the pore volume of the core.

3.2 Experiment

The core sample was saturated with ^{18}O enriched water (C_S = 0.56%), after the porosity, permeability and pore volume had been determined[165,164]. The resident ^{18}O enriched water was displaced using 8% brine solution which had an index of refraction equal to 1.3358. Fluid samples (about 5 cc) of the effluent mixture were collected as a function of time and pore volume injected. The index of refraction of the effluent fluid samples was measured with a refractometer. The displacement of the ^{18}O enriched resident water continued until the cumulative displaced fluid reached more than 1.5 times the pore volume and the refractive index matched that of the brine solution.

The nuclear reaction analysis was done using a proton beam with an energy of 0.73 MeV from the University of Oklahoma Van de Graaff accelerator. A beam current between 200 to 400 nA and an average dose of about 100 μC on target was used. The targets were prepared by anodizing pure tantalum metal foil at a constant applied voltage of 100 V and an initial current density of 10 mA/cm^2 in 2 cc of the effluent fluid mixture for 10 minutes of oxidation time. A complete description of the technique is given in ref. [177].

3.3 Results and Discussion

The data and results of the miscible displacement measurement are summarized in Table 3.3.1. Column (3), labeled $R_\alpha(ES)$, gives the ratio of the alpha particle counts from the Ta_2O_5 targets prepared from aliquots of the effluent fluid and the ^{18}O enriched water initially used to saturate the core sample. It is expected that $R_\alpha(ES)=1$ at the beginning of the miscible displacement. This is observed to be the case within the 1% experimental uncertainty.

Table 3.3.1 Data for the Miscible Displacement of 0.56 Atom % ^{18}O Enriched Water by An 8% Brine Solution at a Pressure of 42 psig Through A Berea Sandstone Core Sample

(1)	(2)	(3)	(4)	(5)	(6)	(7)
Injection Time (10^{-3}sec)	Pore Volume Injected	$R_\alpha(ES)$	Index of Refraction	$C_E(B)$ (%)		λ
				NRA	Ind. of Ref.	
0.868	0.06	0.996	1.3340	0	0	-3.837
1.447	0.13	0.996	1.3340			-2.413
2.183	0.23	0.995	1.3340			-1.606
2.883	0.33	0.995	1.3340			-1.166
3.583	0.43	1.004	1.3340			-0.869
4.233	0.52	0.969	1.3340	4.9		-0.666
5.023	0.64	0.989	1.3340	1.7		-0.450
5.648	0.73	0.987	1.3340	2.1		-0.316
6.234	0.83	0.962	1.3340	6.0		-0.187
6.853	0.90	0.911	1.3340	14.0		-0.105
7.515	1.00	0.766	1.3348	36.8	44.4	0
8.077	1.08	0.608	1.3350	61.7	55.6	0.077
8.631	1.17	0.522	1.3355	75.2	83.3	0.157
9.410	1.26	0.479	1.3355	82.0	83.3	0.232
10.213	1.39	0.439	1.3356	88.2	88.9	0.331
11.213	1.50	0.432	1.3358	89.3	100	0.408
11.633	1.59	0.404	1.3358	93.8	100	0.468

Berea Sandstone Core:

Pore Volume=54.7 cm^3 Bulk Volume=308.9 cm^3
Porosity=17.71% Permeability=3.1 md
Fluid Velocity=0.0021 cm/s Core Length=15.24 cm
Core Area=20.27 cm^2

After the volume of the injected brine solution is 1.5 times the core volume, the index of refraction of the effluent fluid is equal to the index of refraction of the injected brine. If this indicates complete replacement of the resident water by brine, then, assuming a natural concentration $C_B = 0.204$ atom% ^{18}O for the brine, one would expect that $R_\alpha(ES) = C(BS) = 0.364$. A measurement of this ratio from brine and resident water before the beginning of the miscible displacement gave $N_\alpha(B)/N_\alpha(S) = 0.36$ in good agreement with the expected value. However, the observed ratio $R_\alpha(ES) = 0.40$ after the fraction of the core volume injected had reached 1.59 indicates a small amount of resident fluid still present in the fluid mixture collected during the late part of the injection period which can not be observed by the refraction index method. The concentration obtained via the index of refraction method is based on a calibration curve which assumes that the observed index of refraction at the end of the displacement (after 1.5 pore volumes have been injected) indicates the effluent fluid to be 100% brine.

Figure 3.3.1 shows the dispersion profile for the Berea sandstone core sample. The concentration $C_E(B)$ is plotted against the pore volume injected. The solid circles represent the concentration values based on the index of refraction measurement using the method described by Menzie *et al* in ref. [164]. The open circles are the concentration obtained from NRA. It is evident that the two methods predict breakthrough at the same pore volume injected. The shape of the curves is typical for a zone in which mixing of two miscible fluids is taking place. However, the points based on NRA show a "tailing", beginning at 0.5 pore volumes injected.

The observed flow pattern may be expected in certain porous systems during the displacement of two miscible fluids. It has been argued[76], however, based on data obtained for Berea cores, that tailing may not be a characteristic of all porous systems. If that is true for the Berea core used in this study, then the fact that the tailing is absent in the index of refraction method seems to point out that observation of tailing may depend on the sensitivity of the method used in determining the dispersion curve. The NRA method is based on the isotopic dilution of the resident ^{18}O enriched fluid by the displacing brine solution, and is very sensitive to small concentration changes during the mixing of the two fluids.

The λ-values given in Table 3.3.1 can be used to determine λ_{10} and λ_{90} by plotting them against the effluent brine concentration on a probability coordinate paper[36]. The extent of the mixing during the displacement may be determined from the straight line region of such a plot. The values of λ determined from the intercept with the 90% and 10% effluent "brine" concentration were found to be 0.20 and -0.10, respectively. With the λ values so determined the dispersion coefficient and the dispersivity are determined as 0.00022 cm^2/sec and -0.104 cm, from Equation 3.1.3 for both methods.

The measurement we have described shows that water labeled with ^{18}O can be used as a resident fluid in the experimental determination of oil reservoir rock dispersivity. The high sensitivity of the method allows the observation of small concentration changes. The necessity of an accelerator for the analysis may not be a serious detriment to the method since the oxide targets are easy to prepare and very stable and can be transferred to an accelerator laboratory for analysis.

3.4 Nomenclature

A	cross section area of reservoir core, cm^2
C_B	^{18}O concentration of displacing fluid
C_S	^{18}O concentration of enriched water
C_E	concentration of effluent fluid
C(BS)	the ratio of the ^{18}O concentration of the displacing fluid to the ^{18}O concentration of the enriched water
K_D	dispersion coefficient, cm^2/sec
L	length of the core, cm
$N_\alpha(E)$	alpha particle count rate obtained from the Ta_2O_5 targets prepared from the effluent fluid
$N_\alpha(S)$	alpha particle count rate from targets prepared from the ^{18}O enriched water
q	average injection flow rate, cm^3/sec
R_v	the ratio of injection pore volume to pore volume, V/V_p
$R_\alpha(ES)$	the ratio of the alpha particle count rate obtained from the Ta_2O_5 targets prepared from the effluent fluid to the alpha particle count rate from targets prepared from the ^{18}O enriched water
U	average interstitial velocity, cm/sec
V	injection pore volume, cm^3
V_p	pore volume of the core, cm^3

Greek letters

α_D	dispersivity, cm
ϕ	porosity of the core, %
λ_{10}	λ value at 10% concentration of the displacing fluid ($\lambda=(R_v-1)/\text{sqrt } R_v$)
λ_{90}	λ value at 90% concentration of the displacing fluid ($\lambda=(R_v-1)/\text{sqrt } R_v$)

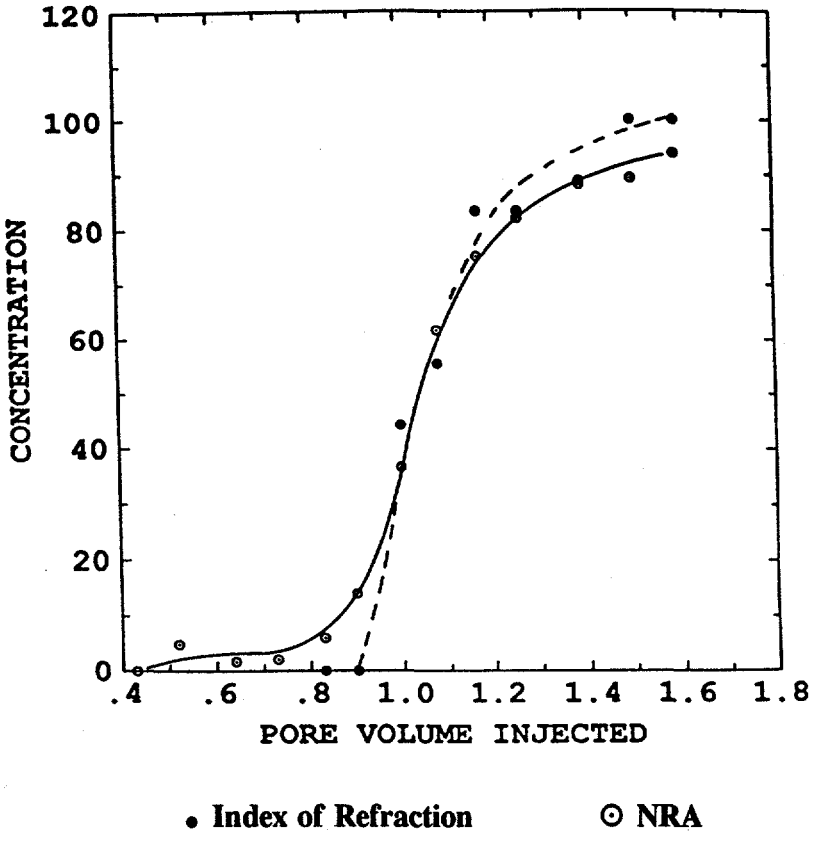

Figure 3.3.1 Effluent Concentration $C_E(B)$ as a Function of Pore Volume Injected During Miscible Displacement of ^{18}O Enriched Water in a Sandstone with a Brine Solution

CHAPTER 4

Dispersion Characteristics and Determination of Flow Characterization

One of the most challenging aspects of reservoir engineering in the petroleum industry is to evaluate the flow system in a heterogenous reservoir. The purpose of this study was to develop new knowledge whereby the flow characterization in a porous medium or reservoir can be determined using dispersion measurements.

A series of miscible displacement tests were conducted on Berea and Brown sandstones with different permeabilities, system lengths and heterogeneities. The analytical methodologies were utilized for dispersion measurements: (1) X-ray computed tomograph (CT) method, (2) X-ray linear core scanning method, and (3) refractive index method. This research provides new knowledge and background that can be used to assist reservoir engineers to define the flow system in a heterogeneous reservoir.

4.1 Introduction

Dispersion is an important phenomenon known to depend fundamentally on the properties of porous media and flow conditions. When a solute is injected into a saturated porous medium, the solute will move along the flowing channels of the media at different velocities depending on the size and shape of the pore channels. Menzie and Dutta (1989) have shown that the dispersion coefficients can be correlated with the rock properties of the media. This discovery has brought attention to dispersion research using laboratory and field dispersion measurements in the area of determination of the flow characterization of a porous medium or a reservoir. In order to develop a method to determine the flow characterization from dispersion measurements, a fundamental understanding of the dispersion phenomena in a small-scale heterogeneous rock is needed.

The specific objectives of the study are as follows:

(1) To develop different laboratory methods which can be utilized to study the dispersion characteristics in porous media. These methods should be able to measure (a) the local heterogeneity or variation of porosity and permeability of a porous medium, and (b) the in-situ and effluent concentration profiles of the displacing fluid flowing through porous media during miscible displacement.

(2) To develop a fundamental understanding of the features of dispersivity in a porous medium from laboratory experimental results.

(3) To determine the relationships between dispersion, permeability, system length, and heterogeneity using small-scale heterogeneous porous media.

(4) To develop a method to determine the flow characterization in a reservoir using the dispersion measurement.

4.2 Experimental Methods and Apparatus

Three laboratory experimental methods were used to study dispersion and the characteristics of rocks in this study. They are (1) X-ray Computed Tomograph (CT) method, (2) X-ray linear core scanning method, and (3) Refractive index method.

4.2.1 X-Ray Computed Tomography

X-ray Computed Tomography (CT) scanning is a powerful tool for studying small-scale rock heterogeneities of core samples and visualizing fluid displacement inside of cores. The CT scanning method gives computer enhanced X-ray photographs of cross-sectional slices of an object.

A miscible displacement system was set up on the CT scanning table as shown in Figure 4.2.1. The two miscible fluids used in this study were MN919 and ID1090. MN919 was a mixture containing 91% naphtha and 9% mineral oil. ID1090 was a mixture containing 10% iododecane and 90% naphtha. The two liquids had equal viscosity but unequal density. The properties of both fluids are provided in Table 4.2.1.

Table 4.2.1 The Properties of Fluids Used in CT Scanning

Material	Density (at 74 °F)	Viscosity (cp at 74 °F)
Naphtha (N)	0.75	0.57
Mineral Oil (M.O)	0.86	27.9
Iododecane (I.D)	1.257	3.6
MN919 (9% (M.O)+91% (N))	0.76	0.69
ID 1090 (10% (ID)+90% (N))	0.80	0.69

4.2.2 X-Ray Linear Core Scanning Method

The X-ray linear core scanning system uses the basic principle of the X-ray absorption method. This method was developed to measure the oil saturation in a core (Boyer, Morgan, and Muskat, 1947). This technique is currently being used by several major oil companies and service companies to measure saturation during the measurement of relative permeability.

A miscible displacement system was set up on the X-ray table as in Figure 4.2.2 to measure the concentration profile during a miscible displacement. In addition to the concentration measurement, the X-ray linear core scanning system was also used to determine the X-ray intensity curves and porosity profile of the cores. These were used to characterize the different core samples. Two miscible fluids, MN919 and ID1090, were used for the dispersion test using the X-ray linear core scanning method.

4.2.3 Refractive Index Method

The refractive index method has become a standard method used to measure the dispersion coefficient in the petroleum industry (Menzie and Dutta, 1989). This method provides an accurate, highly qualified, and economical measurement of an effluent concentration profile.

The experimental effluent analysis apparatus was set up as in Figure 4.2.3. Effluent fluid samples were collected using a "CYGNET" fraction collector. The refractive index of the sample was measured using an Abbe-type refractometer which is a device that uses the optical properties of a given fluid to distinguish the relative percentages in a fluid mixture. Isoxy and naphtha were selected as the two miscible fluids. Isoxy was a mixture of 53% isooctane and 47% orthoxylene. Isoxy and naphtha had approximately equal densities and viscosity, while their refractive index values were different. The properties of these liquids are listed in Table 4.2.2.

Table 4.2.2 Physical Properties of the Liquids Used in the Refractive Index Measurement

Material	Density (at 74°F)	Viscosity (cp at 74°F)	Refractive Index (at 74°F)
Isooctane (I.S)	0.64	0.50	1.3907
Orthoxylene (O.L)	0.87	0.82	1.5050
Naphtha (N)	0.74	0.63	1.4192
Isoxy (47% (O.L) + 53% (I.S))	0.78	0.63	1.4450

4.3 Experimental Results

Eighty-three experimental runs were carried out on eight types of cores in this investigation. Of the eighty-three runs, three were measured using the CT scanner, twenty-five were measured using the linear X-ray core scanning system, and fifty-five were measured using the refractometer.

Five Berea sandstone cores (YA, YB, YC, YD, and YH) and one brown sandstone core (YE) were used to study dispersion characteristics. Berea cores were labeled YA, YB, YC, YD, and YH to distinguish the different permeabilities. Cores labeled YF and YG were man-made heterogeneous cores which were combined from a series of Berea core segments with different permeabilities. Cores labeled YE consisted of Brown sandstone. All cores used in this study had a 3.8 cm diameter except core YH1 which had a 5.1 cm diameter. The lengths of the cores ranged from 7.6 to 76.2 cm.

4.3.1 Experimental Results Measured by a CT Scanner

Three experimental runs using the CT scanning method were conducted on Berea core YB8 in order to study the dispersion characteristics of the Berea sandstone.

The first CT scanning run was used to scan the dry, clean core at each half-inch increment over the length of the Berea core which was a combination of four core segments (YB1, YB2, YB3 and YB4) with a total length of 76.2 cm. Four cross-section images were taken in the middle of each segment at 4.8, 28.7, 40.6, and 73.7 cm of the core as shown in Figure 4.3.1 to 4.3.4. Each image represents a 3 mm thick segment of the sample. In a CT image, the darker region represents the lower density of the material (air), and the lighter region represents the higher density of the material (rock matrix). The images taken at the segments of YB1, YB2 and YB3 show that the structure of these cross-sections is relatively homogeneous, but the image taken at the segment YB4 shows that the pore spatial distribution is not homogenous at that cross-section. Comparing these four images, the YB3 sample is less dense, and the YB4 sample is more dense. In other words, the porosity of YB3 is the highest, and the porosity of YB4 is the lowest. Since the average porosities of the cores YB1, YB2, YB3, and YB4 are 19.9%, 20.1%, 20.5%, and 18.8%, respectively, the CT images represent an accurate porosity level. These CT images indicate that the Berea sandstone is a small-scale heterogeneous sandstone.

The second CT scanning run was used to scan the core saturated with MN919. A series of cross-sectional images recorded at every half-inch increment was obtained. Since the rock matrix of the dry core and the saturated core were the same, the difference between the two scans was determined to be the pore space which was filled with air in the dry core and with liquid in the saturated core. Therefore, the X-ray attenuation coefficients which were obtained on the dry core and on the saturated core were different. Figure 4.3.6 is a CT image of a saturated core at the 57.7 cm location. This is the same location used for the dry core image shown in Figure 4.3.5. It can be seen that the color of the image in Figure 4.3.6 is slightly lighter than that in Figure 4.3.5 because air was substituted for liquid. The two X-ray attenuation coefficients from the dry core and the saturated core were used to calculate the porosity at that location.

The third CT scanning run was used to measure the concentration inside of the core during miscible flooding. ID1090 was used to displace MN919 in this run. A comparison of the cross-section images at the same location was made among the dry core, the core saturated with 100% MN919, and the core saturated with 100% ID1090. The dark color in Figure 4.3.7 and the light color in Figure 4.3.8 show the different X-ray attenuation levels between the two liquids in the core. The ID1090 is a strong X-ray attenuation liquid, resulting in a white color image. The CT numbers measured on the core saturated with 100% MN919 and 100% ID1090 were used to calibrate the concentration curve. The images of the MN919 and ID1090 mixture exhibited colors between the dark color of 100% MN919 and the white color of 100% ID1090.

The porosity profile over the length of core YB8 can be determined from the CT numbers. Figure 4.3.10 shows the porosity profile measured by the CT scanner.

The concentration profiles at different locations of core YB8 were measured while ID1090 displaced MN919. The displacement was at a constant flow rate of 0.015 cc/sec and a stable injection pressure of 1.9 psi. Figure 4.3.11 shows the cross-sectional images of the mixing zone corresponding to 0%, 5.4%, 22%, 52%, 73%, 89%, 96%, and 100% ID1090 concentration measured on core YB8 at 7.2 cm location. The dark region represents the MN919 which is a low X-ray attenuation material, while the light region represents ID1090 which is a high X-ray attenuation material. As the concentration of the ID1090 increased, the light region became larger

and larger from the bottom of the core to the top of the core. Although the density difference between ID1090 and MN919 was only 0.04, the gravity segregation could still be observed in these images.

Figure 4.3.12 shows the concentration profiles measured on YB8 Berea cores using the CT scanner. The concentration curves show that the longer the lengths of the cores, the steeper the S-shaped curve. Figure 4.3.13 shows the derivative curves of these runs. It was observed that the peaks of the derivative curves increased as the system lengths increased and then stabilized at a constant value.

4.3.2 Experimental Results Measured by X-Ray Linear Core Scanning

Twenty five experimental runs were carried out on eight Berea cores and one Brown core using the X-ray core scanning system. Five types of cores (YA, YB, YC, YD, and YE) were scanned using the X-ray core scanning system in order to obtain the X-ray absorption character of the rock.

The X-ray intensity curves were based on the measurements taken on dry, clean core samples before they were coated with JB-Weld and epoxy. An intensity curve for the dry core represents the X-ray attenuation of the rock matrix and the pore space of the core. Figure 4.3.14 shows the six X-ray intensity curves which were measured on the three YA, YB, and YC Berea core samples. The six curves indicate that type YA, YB, and YC Berea cores absorbs X-rays uniformly, so they are uniform rocks.

Figures 4.3.15 and 4.3.16 show the X-ray intensity curves measured on YD and YE Berea cores. They indicate that type YD and YE Berea cores absorb the X-ray non-uniformly. The non-uniform X-ray absorption may be caused by either rock material or pore structure.

Three porosity profiles of Berea cores (YA1, YB5, and YH1) were obtained using the X-ray linear core scanning system. Figures 4.3.17 to 4.3.19 show the porosity profiles of Berea cores YA1, YB1 and YH1. It can be observed that cores YA1 and YB1 have relatively uniform porosity distribution, but core YH1 has a non-uniform porosity profile.

Two miscible displacements were conducted on Berea core YH1. Nine concentration profiles of the mixing front were measured in the first run at different times during the displacement of MN919 by ID1090. Six concentration profiles were obtained in the second run at different times during the displacement of ID1090 by MN919. Figures 4.3.20 and 4.3.21 show the concentration profiles obtained from these two measurements.

4.3.3 Experimental Results Measured by Refractometer

Concentration profiles were measured on five different cores (YA, YB, YC, YD Berea, and YE Brown cores), which have different permeabilities, to study the effect of permeability on dispersion. Figures 4.3.22 and 4.3.23 show the concentration curves measured on different cores. It was observed that the shape of the concentration changed as the permeabilities of rock changed.

Concentration profiles were measured on core samples with different lengths using two processes to investigate the effect of length on dispersion. Figure 4.3.24 shows the concentration profiles measured in the first process, in which the core segments were combined into different lengths of cores. The concentration profiles show that as the length of the core increases, the slope of the curve increases. Figure 4.3.25 shows that the peaks of the derivative curves also increase with increasing system length and then stabilize at a constant value.

Figures 4.3.26 and 4.3.27 show the concentration profiles and derivative curves in the second process, in which the measurement was first conducted on a longer core. Then the longer core was cut into short cores. The same process was also used for other cores. These experiments illustrate that the shape of the concentration curve changes as the system length changes; the peak of the derivative curve increases as the system length increases.

The experimental runs were carried out on two man-made heterogeneous core samples. Core YF was a combination core composed of two 15.2 cm core segments. Core YG was a combination core composed of four 7.6 cm core segments. All of these core segments have different permeabilities.

Two experimental runs were conducted on the YF core based on the direction of the fluid. In the first experiment, the fluid flowed from the low permeability side to the high permeability side. In the second experiment, the fluid flowed from the high permeability side to the lower permeability side YA10. The same experimental procedures were also conducted on the YG core.

From the experiments, it was concluded that the concentration profile is not affected by the order of change of permeability so the dispersivity is not affected by the order of change of permeability. The beginning portion of the concentration curve of the combination core is different from the ones of the original cores. However, the later portion of the concentration curve of the combination core overlaps with those of the original cores.

4.4 Dispersion Characteristics in Coreflooding

4.4.1 Dispersion Factor

A new parameter, dispersion factor DF_{ML}, was defined in this study. This parameter is a single value which can be used to represent the characteristics of the concentration profile and its derivative curve. The dispersion factor is independent of the system length so it can be used in the sensitivity analysis of dispersion.

The dispersion factor is observed as a variation in slope of the lognormal distribution curve. It was defined by the following equation:

$$DF_{ML} = \frac{\left(\frac{V}{V_p}\right)_{84.1\%} - \left(\frac{V}{V_p}\right)_{50\%}}{\left(\frac{V}{V_p}\right)_{50\%}} \qquad (4.4.1)$$

where: DF_{ML} = dispersion factor (dimensionless),
V = volume injected (cm^3),
V_p = one pore volume (cm^3),
$(V/V_p)_{50\%}$ = pore volume injected at 50% concentration (dimensionless), and
$(V/V_p)_{84.1\%}$ = pore volume injected at 84.1% concentration (dimensionless).

The dispersion factor is a non-dimensional value from 0 to 1 which is directly proportional to the degree of dispersion. A value of zero is indicative of piston displacement without dispersion, while a value of one is indicative of large dispersion. The dispersion factor represents the spread of the mixing fluid in terms of variation. It could be used as a characteristic parameter of the concentration and derivative curves.

Figure 4.4.1 shows the concentration profiles measured on different length samples of YA Berea cores. It was observed that the slopes of the curves of the shorter cores are steeper than those of the longer cores. As the system length increases, the slope of the distribution curves stabilizes.

4.4.2 Effect of Rock Properties on Dispersion

The relationship between the dispersion factor and permeability shows that dispersion is very sensitive to rock permeability. However, it is not a linear function of rock permeability. X-ray attenuation analysis shows that Berea sandstone is not homogeneous, which indicates that dispersion may also be dependent upon the rock characterization. For a relatively homogeneous X-ray absorption rock, dispersion decreases as permeability increases, while for a relatively non-homogeneous X-ray absorption rock, dispersion increases as permeability increases.

Dispersivity appears to be a length dependent parameter which increases as the system length increases after the system length is longer than a critical length. But the dispersion factor is not a length dependent variable and can therefore be used to evaluate the characteristics of a reservoir. A critical length can be determined from laboratory experimental data. In a dispersion measurement, different types of reservoir material have different critical lengths. Results indicate that critical lengths are longer in high permeability rock. The critical length is also dependent on the method of measurement. The critical length will be shorter if end-effects can be eliminated.

In order to study the effect of small-scale heterogeneity on dispersion, two man-made heterogeneous cores, YF and YG, were made. Core YF was composed of two core segments and core YG was composed of four core segments. Experiments were conducted on these combined cores. It was observed that the order of the change of the permeability from low to high or from high to low does not affect the dispersion measurement. However, the dispersion factor is dependent upon the heterogeneity of the core. It increases as the heterogeneity of the core increases.

Dispersion behavior was shown to be strongly affected by the density of the displacing fluid. CT images show that dense liquid mixes with lighter liquid from the bottom to the top of a core. When the displacing fluid is more dense, the mixing zone is shorter, breakthrough time occurs later, and the growing rate of the mixing zone length is slower. In contrast, when a less dense displacing fluid is used, the mixing zone is longer, breakthrough time occurs earlier, and the growing rate of the mixing zone is faster.

4.5 Flow Characterization in Miscible Displacement

One of the most significant challenges in reservoir engineering is to determine the heterogeneity of reservoirs and predict the behavior of fluid flowing in the reservoir with respect to space. Reservoir heterogeneity is usually determined by permeability distribution in porous media. Permeability data, which can be obtained from core analysis or pressure tests, is limited by the number and reliability of measurements. Laboratory values must be corrected to account for the overburden effect. In addition, the heterogeneity of a reservoir is not only a function of the permeability, but also a function of the flowing channels of the formation. The existence of fractures and channels in a reservoir cannot be estimated accurately. Therefore, the determination of flow characterization in a heterogeneous reservoir is still a challenging research area which needs to be investigated.

4.5.1 Capillary Tube Model

A capillary tube model was developed to determine the pore flow size distribution from a concentration profile. In the model, the flowing channels are arranged from the largest radius to the smallest radius as shown in Figure 4.5.1. Poiseuille's Equation (Amyx, Bass, and Whiting, 1960) can be applied to each tube as follows:

$$Q_i = \frac{\pi r_i^4 \Delta P}{8 \mu L} \qquad (4.5.1)$$

where: Q_i = the flow rate in a single tube (cc/sec),
ΔP = pressure drop (atm),
μ = viscosity of fluid (cp),
L = length of a tube (cm),
r = radius of a flow channel (cm).

The total flow rate of a bundle of tubes is:

$$Q_t = \sum_{i=1}^{N} \frac{\pi r_i^4 \Delta P}{8 \mu L} \qquad (4.5.2)$$

where: Q_t = total flow rate (cc/sec),
N = total number of the tubes in a medium.

To apply Poiseuille's Equation to miscible displacement, the following assumptions were made:

1. The flow channels are filled with the first fluid, then the second fluid (injection fluid) is injected into the tubes at a constant injection rate.
2. The viscosity and density of these two miscible fluids are the same, therefore no viscous fingering and gravity segregation occur during miscible displacement.
3. The injection fluid will breakthrough first at the flow channel which has the largest equivalent flow radius.
4. After the breakthrough of the injected fluid, the tube will produce only injection fluid.

For a miscible displacement, Poiseuille's Equation was applied to the injection fluid as:

$$Q_t\, C_n = \frac{\pi\, \Delta P}{8\mu L} \sum_{i=1}^{n} r_i^4 \qquad (4.5.3)$$

and to the displaced fluid:

$$Q_t(1 - C_n) = \frac{\pi\, \Delta P}{8\mu L} \sum_{i=n+1}^{N} r_i^4 \qquad (4.5.4)$$

where: C_n = concentration of the displacing fluid measured in the effluent (%),
n = number of tubes which are full of injection fluid,
N = total number of channels.

A cumulative equivalent flow radius $R_{ei,n}$ was defined by the following equation:

$$(R_{ei,n})^4 = \sum_{i=1}^{n} r_{ei}^4 = \frac{8\mu L Q_t C_n}{\pi \Delta P} \qquad (4.5.5)$$

Equation 4.5.5 indicates that the injection fluid flows through each of the "n" channels at each concentration measurement C_n. The cumulative equivalent flow radius $R_{ei,n}$ is directly proportional to the concentration. The cumulative equivalent flow radius $R_{ei,n}$ represents the size of the channels that injection fluid has broken through. When the relative concentration is equal to one, the cumulative equivalent flow radius is at the maximum value because all of the flowing channels produce injection fluid only.

Equivalent flow radius was defined as:

$$r_{ei} = R_{ei,n} - R_{ei,n-1} \qquad (4.5.6)$$

Equivalent pore flow size distribution curves can be obtained by plotting the cumulative equivalent flow radius or the equivalent flow radius versus concentration.

4.5.2 Equivalent Pore Flow Size Distribution of Berea and Brown Sandstones

Seven equivalent pore flow size distribution curves of Berea and Brown cores were developed from concentration profiles. Figure 4.5.2 shows two curves for the YA9 Berea core. The first curve shows the cumulative equivalent pore flow radius which represents the sum of all radii which produced the injecting fluid. The cumulative equivalent pore flow radius increases with the concentration. The second curve shows the equivalent pore flow radius distribution that represents the radius of each channel and which decreases with the increase of concentration. This curve indicates that the earlier portion of the concentration profile represents the characteristics of the mixing fluids which pass through the larger channels, and the later portion of the concentration profiles represents characteristics of the mixing fluids which pass through smaller channels. The equivalent pore flow size distribution curve shows that the pore structure of a YA Berea core is not homogeneous.

The degree of microscopic heterogeneity can be evaluated using the variation of the equivalent pore flow diameter. The variation of pore size distribution can be calculated by the following equation:

$$V_{ps} = \frac{d_{50\%} - d_{84.1\%}}{d_{50\%}} \qquad (4.5.7)$$

where, V_{ps} = pore flow size variation (dimensionless),
$d_{50\%}$ = equivalent pore flow diameter at 50% concentration (cm),
$d_{84.1\%}$ = equivalent pore flow diameter at 84% concentration (cm).

A large variation in pore flow size indicates a large degree of heterogeneity of the rock. Figure 4.5.3 indicates that the dispersion factor increases with pore flow size variation, indicating that the dispersion factor represents the flowing characterization in a small-scale heterogeneity rock. A large dispersion factor is indicative of a large pore flow size variation. Since the dispersion factor is a non-dimensional value, it can be utilized to evaluate the flow characterization in both laboratory and field studies. The dispersion factor calculated from a concentration profile measured in the laboratory represents the flow characterization in a small-scale heterogeneous core, while the dispersion factor calculated from a concentration profile measured in a field test represents the flowing characterization in a large scale reservoir.

4.5.3 Determination of the Flow Characterization Using a Field Dispersion Factor

A concentration profile was measured during a field test conducted in El Dorado, Kansas (Ravnaas, 1981). A fresh water solution was injected in a well (MP-118) to displace salt water in the formation. The concentration was measured in the observation well (MP-131) located at 90 feet from the injection well, shown in Figure 4.5.4. The observation well was positioned directly between the injection and production wells so that sampled flow streamlines were linear throughout the system. The observation well (MP-131) was not perforated through its entire pay zone. It was perforated through a 1-foot interval from 646 to 647 ft. This small interval disrupted the streamline

between the injection and production wells as little as possible. The sampling flow rate from the observation well (MP-131) was 5 barrels per day (bbl/day) and the injection flow rate was 150 bbl/day. The Dykstra-Parson permeability variation showed that the EL Dorado field is a reservoir with a moderate degree of heterogeneity.

The concentration profile and its derivative curve are shown in Figure 4.5.5. The concentration profile measured from the field test was not a typical S-shaped curve and the derivative curve did not show a peak value as the volume injected approached one pore volume. The dispersivity calculated from the concentration profile measured in this field test was 382 cm.

The dispersion factor for the El Dorado field was calculated to be 0.81, which was much higher than most laboratory dispersion factors. This indicates that reservoir heterogeneity is much larger than the microscopic heterogeneity in a reservoir rock.

This study shows that dispersion factors may be used to evaluate the flow characterization in a reservoir. The dispersion factor obtained from a laboratory test may represent the flowing characterization in a small-scale core sample, while the dispersion factor obtained in a field test may represent the flowing characterization in a large-scale formation. Since the dispersion factor is a dimensionless variable, it can be used to evaluate both the laboratory and the field measurements. The results show that the dispersion factor calculated from a field test is much higher than that calculated from a laboratory test. This indicates that the dispersion factor is more representative of a given reservoir than the heterogeneity factor based on the permeability variable.

4.6 Conclusions and Recommendations

4.6.1 Conclusions

The following conclusions can be drawn from this study:

(1) CT scanning and X-ray linear core scanning methods were applied for dispersion measurements in this study. A refractive index method was adopted from a previous study. A comparison of these three methods reveals that both CT scanning and X-ray linear core scanning have the advantage of being able to measure rock and dispersion characteristics inside the core.

(2) The CT images and the porosity profiles measured by the CT scanner and the X-ray linear core scanning system indicate that Berea sandstone is not homogeneous. The results show that Berea sandstone has small-scale heterogeneity. Laboratory results appear to indicate that dispersion is sensitive to rock permeability; however, dispersion is not a linear function of the rock permeability.

(3) The laboratory results show that the dispersion measurement is not stable when the system length is shorter than the critical length. The concentration profile measured on a short core has an early breakthrough and is skewed, which indicates a large dispersion. When the system length is longer than the critical length, the shape of the concentration profile becomes stable and the dispersion factor becomes constant. The critical length of dispersion measured in this research depends on the type of rock and method used for measurement.

(4) Laboratory dispersivity appears to be a length dependent parameter which increases with increasing system length.

(5) The laboratory results indicate that a concentration profile measured on a consolidated core is affected by the flowing channels of porous media. The early portion of a concentration profile may represent the mixing in large flowing channels, and the later portion of a concentration profile may represent the mixing in small flowing channels.

(6) Gravity segregation seems to play an important part in miscible displacement. Dispersion behavior is strongly affected by the density of the displacing fluid. This study shows that for a favorable density displacement, the mixing zone is short, the breakthrough time is late, and the growing rate of the mixing zone length is slow. In contrast, for an unfavorable displacement, the mixing zone is long, the breakthrough time is early, and the growing rate of the mixing zone is fast.

(7) A new parameter, dispersion factor DF_{ML}, has been introduced in this study. The field dispersion factor was found to be much higher than the laboratory dispersion factor, which may indicate that the degree of reservoir heterogeneity is much higher than the degree of microscopic heterogeneity. In addition, the dispersion factor measured in a field test is more representative of a given reservoir than the dispersion factor measured in the laboratory.

4.6.2 Recommendations

Based on this study, the following recommendations are suggested for future study:

(1) A field test is suggested in order to study the features of the dispersion factor. The field test needs to be designed to measure the dispersion factor at different distances between an injection well and a production well. The flow characterization and dispersion can be studied further in the field test.

(2) Further research is suggested that focuses on the substitution of a non-constant dispersion coefficient into the convection-dispersion equation. More theoretical work is required, and analytical and numerical solutions of the modified convection-dispersion equation need to be developed. This can improve the prediction of a miscible displacement.

(3) Gravity segregation appears to play an important part in miscible displacement. Further laboratory and theoretical investigations that focus on the effect of gravity segregation on dispersion are recommended.

(4) Using laboratory results, further research could focus on the correlation between the capillary pressure curve and the concentration profile developed. Because the capillary pressure curve represents the pore size distribution of a rock, the equivalent pore size distribution calculated from the concentration profile could be used to calculate the capillary pressure curve, if the interfacial tension between the two fluids is known.

4.7 Nomenclature

C	concentration, mg/liter
CT	CT number, Hounsfield
$d_{50\%}$	equivalent pore flow diameter at 50% concentration (cm)
$d_{84.1\%}$	equivalent pore flow diameter at 84.1% concentration (cm)
DF_{ML}	dispersion factor
L	length of a core,cm
P	pressure, psi
q	injection rate, cc/sec
Q	flow rate, cc/sec
r	capillary radius, cm
r_{ei}	equivalent pore flow radius, cm
R_{ei}	cumulative equivalent pore flow radius, cm
t	time, sec
V	injection volume, cm^3
V_p	one pore volume of a core, cm^3
V_{ps}	pore flow size variation (dimensionless)
$V_{50\%}$	volume injected at 50% concentration, cm^3
$V_{84.1}$	volume injected at 84.1 concentration, cm^3

Greek Letters

μ	viscosity of the displacing fluid, cp

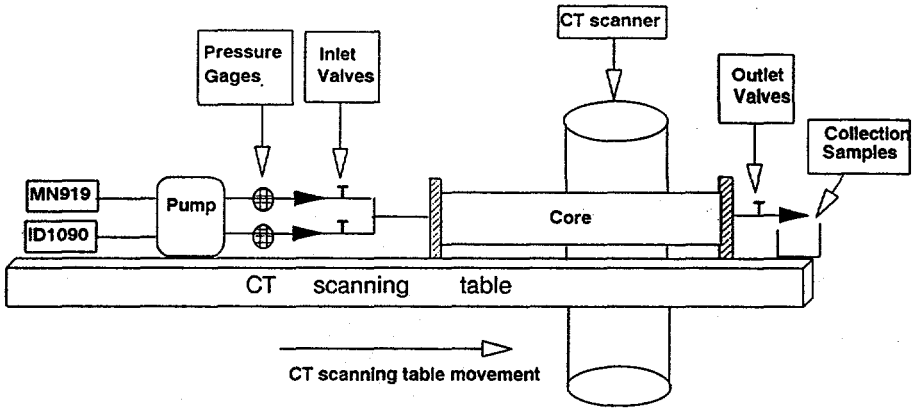

Figure 4.2.1 Schematic Diagram of CT Scanning System

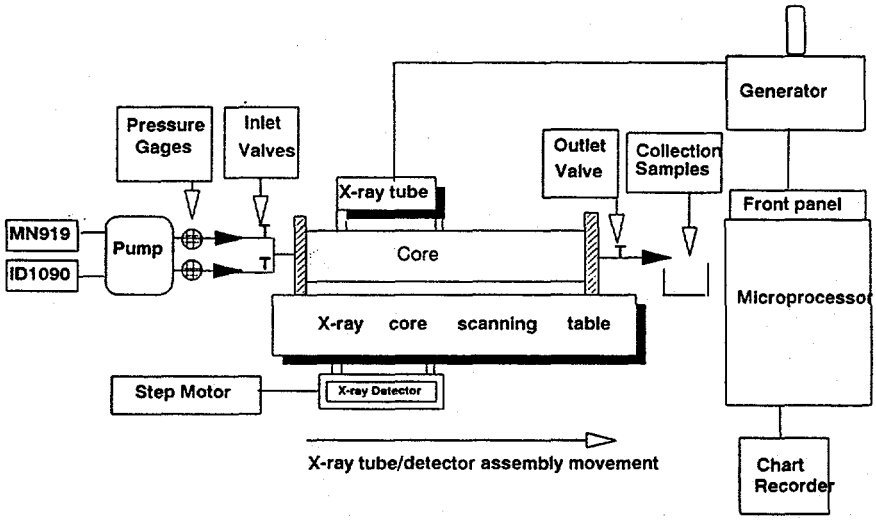

Figure 4.2.2 Schematic Diagram of X-Ray Linear Core Scanning System

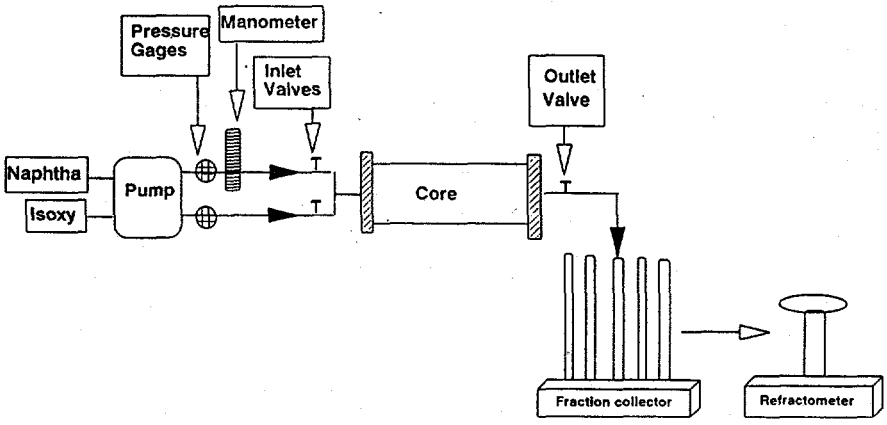

Figure 4.2.3 Schematic Diagram of Effluent Analysis System

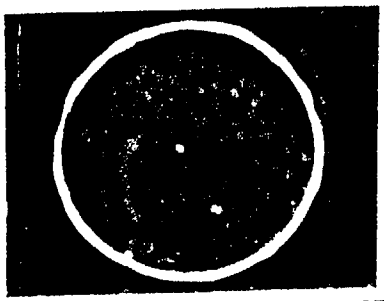

Figure 4.3.1 CT Image at 4.8 cm on YB8 Berea Core (Dry Core)

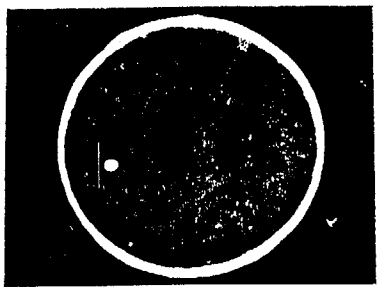

Figure 4.3.2 CT Image at 28.7 cm on YB8 Berea Core (Dry Core)

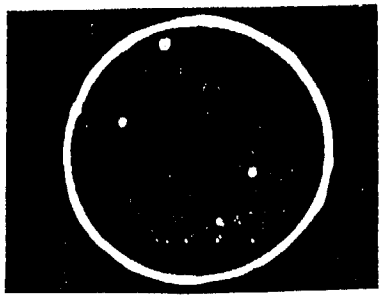

Figure 4.3.3 CT Image at 40.6 cm on YB8 Berea Core (Dry Core)

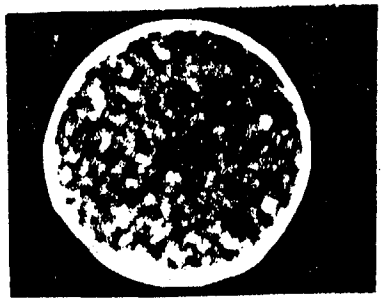

Figure 4.3.4 CT Image at 73.7 cm on YB8 Berea Core (Dry Core)

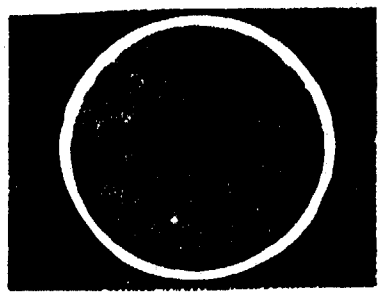

Figure 4.3.5 CT Image at Joint YB3 and YB4 on YB8 Berea Core (Dry Core)

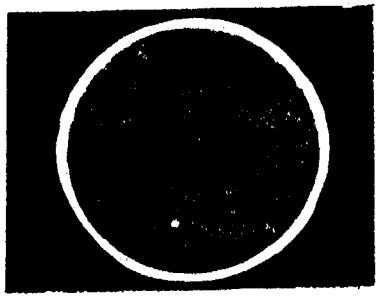

Figure 4.3.6 CT Image at Joint YB3 and YB4 on YB8 Berea Core(Saturated with MN919)

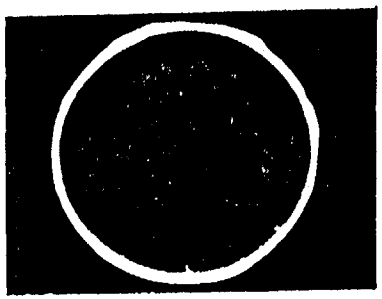

Figure 4.3.7 CT Image at 45.7 cm on YB8 Berea Core (Dry Core)

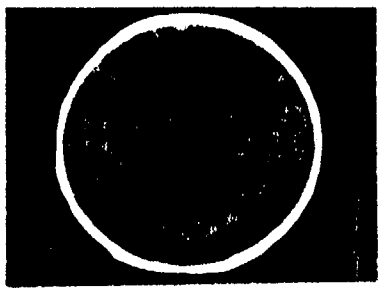

Figure 4.3.8 CT Image at 45.7 cm on YB8 Berea Core(Saturated with MN919)

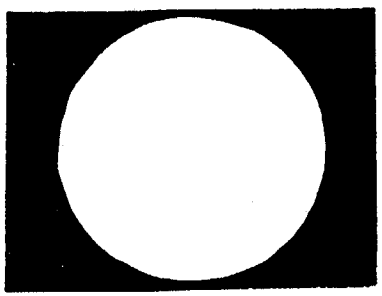

Figure 4.3.9 CT Image at 45.7 cm on YB8 Berea Core (Saturated with ID1090)

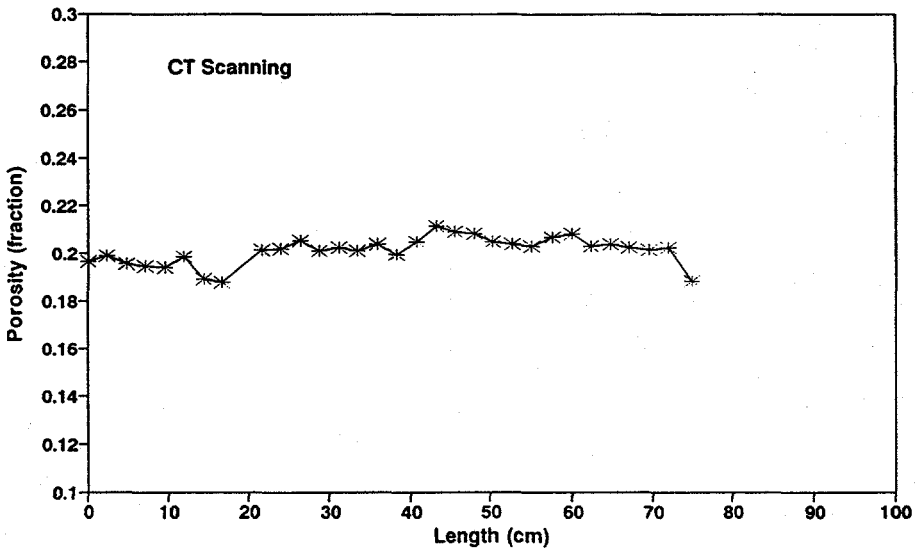

Figure 4.3.10 Porosity Profile of YB8 Berea Core

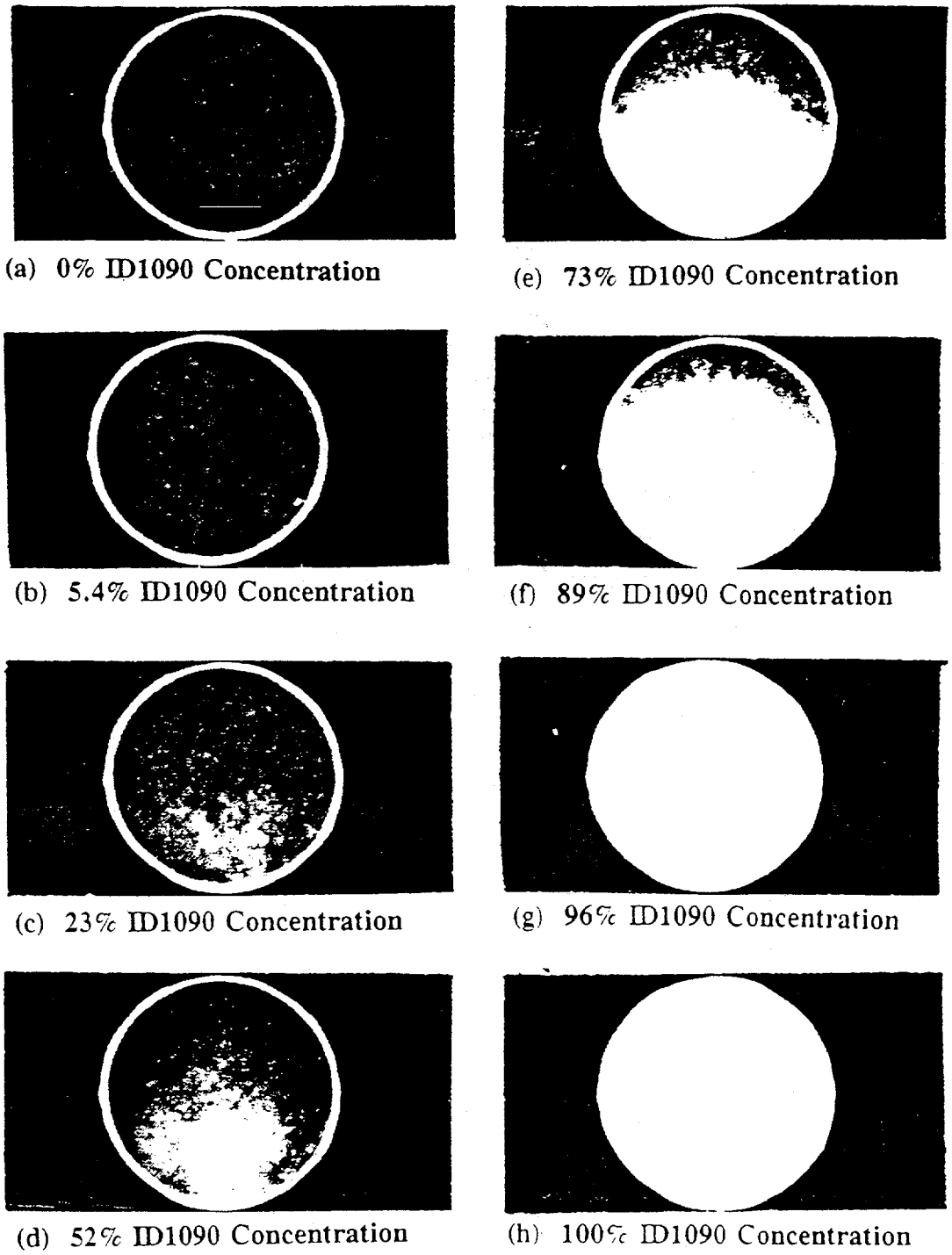

(a) 0% ID1090 Concentration

(e) 73% ID1090 Concentration

(b) 5.4% ID1090 Concentration

(f) 89% ID1090 Concentration

(c) 23% ID1090 Concentration

(g) 96% ID1090 Concentration

(d) 52% ID1090 Concentration

(h) 100% ID1090 Concentration

Figure 4.3.11 CT Images Measured at 7.2 cm Location on Core YB8 Berea Core

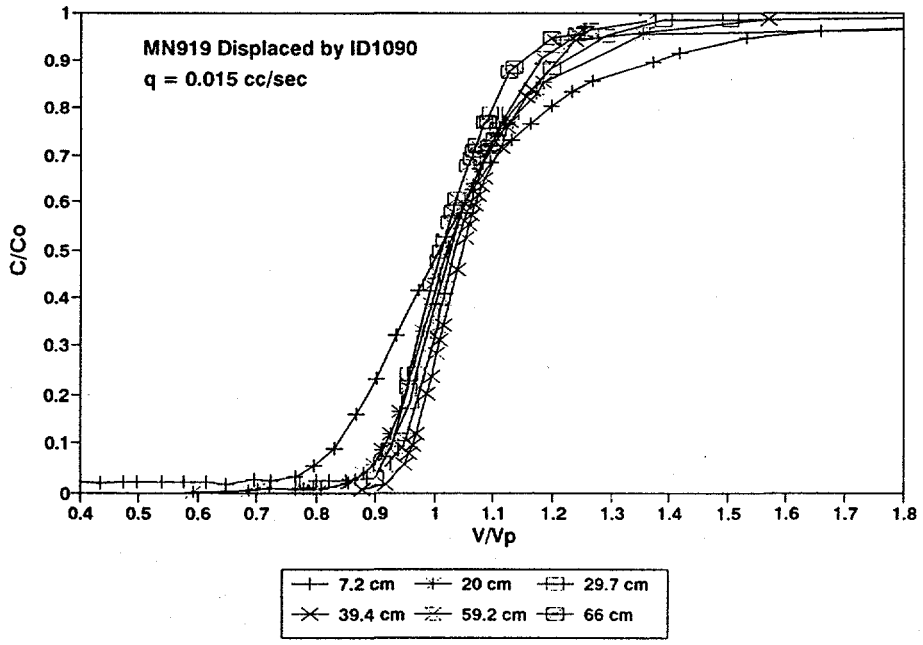

Figure 4.3.12 Concentration Profiles Measured on YB8 Berea Core by CT Scanning Method

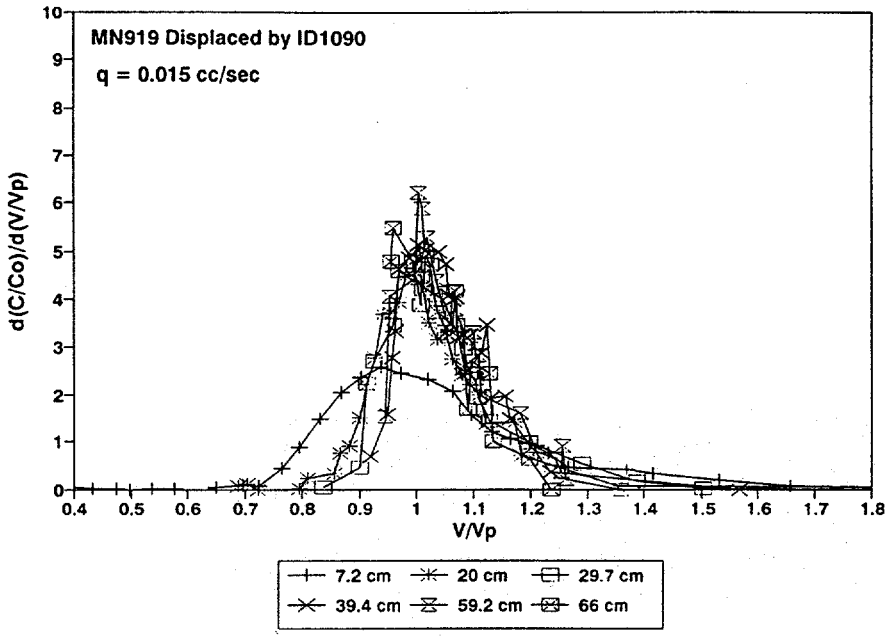

Figure 4.3.13 Derivative Curves Measured on YB Berea Core Using CT Scanning Method

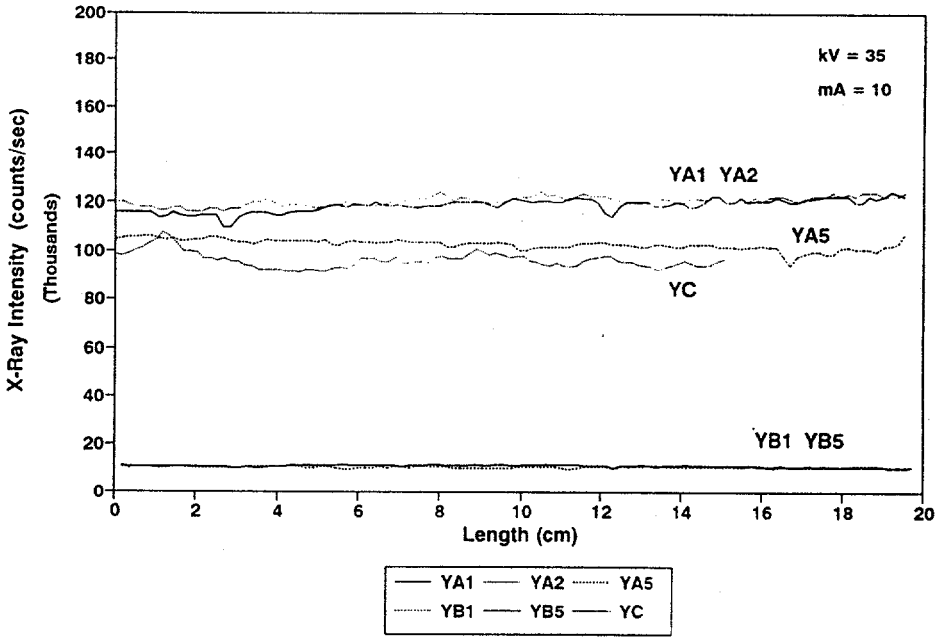

Figure 4.3.14 X-Ray Intensity Curves

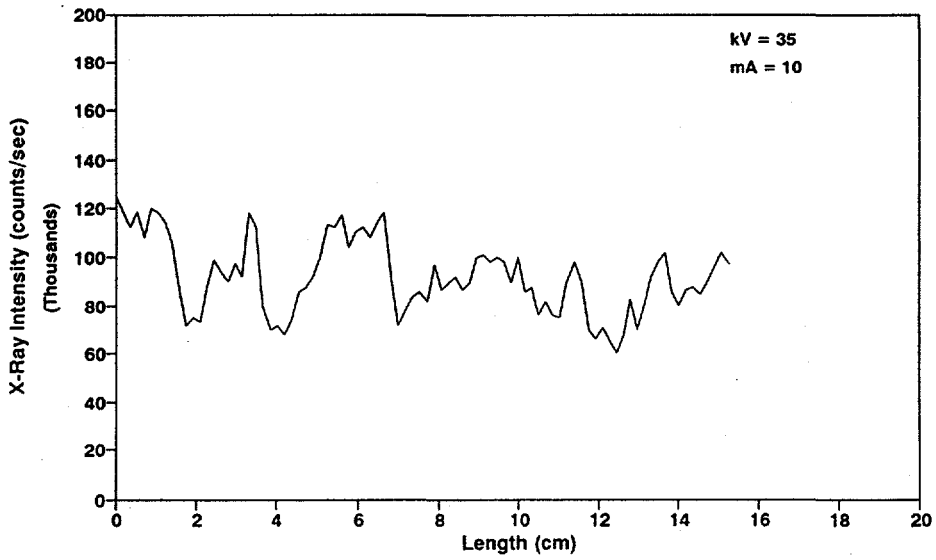

Figure 4.3.15 X-Ray Intensity Curve of YD Berea Core

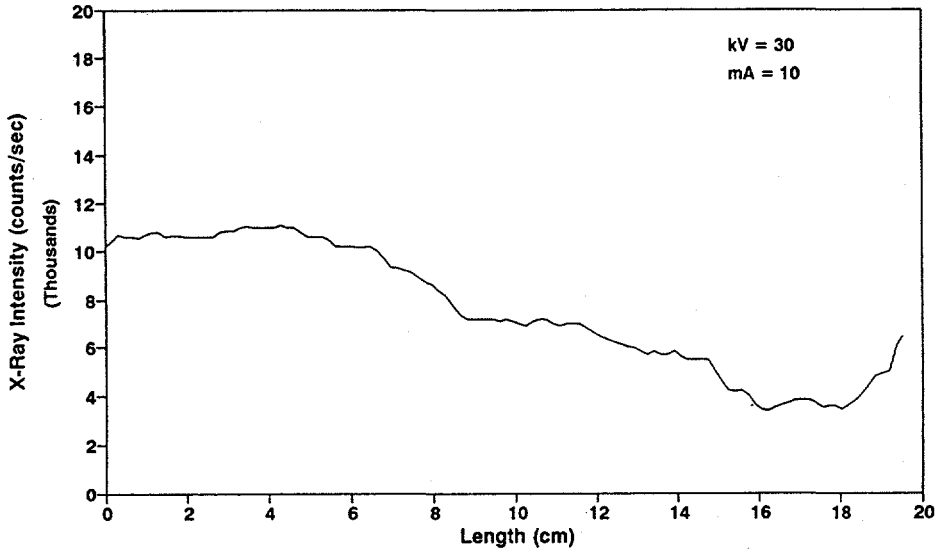

Figure 4.3.16 X-Ray Intensity Curve of YE1 Brown Core

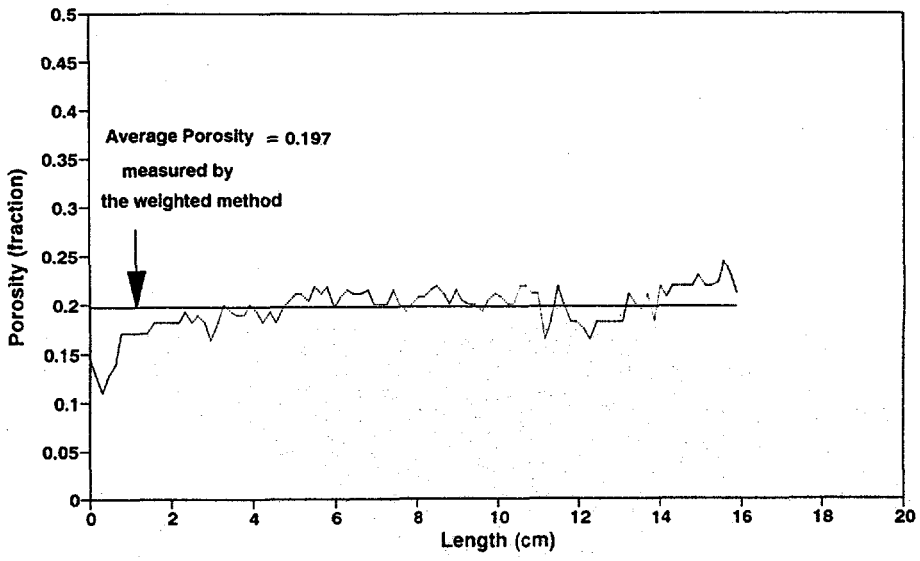

Figure 4.3.17 Porosity Profile Measured on YA1 Berea Core Using X-Ray Linear Core Scanning System

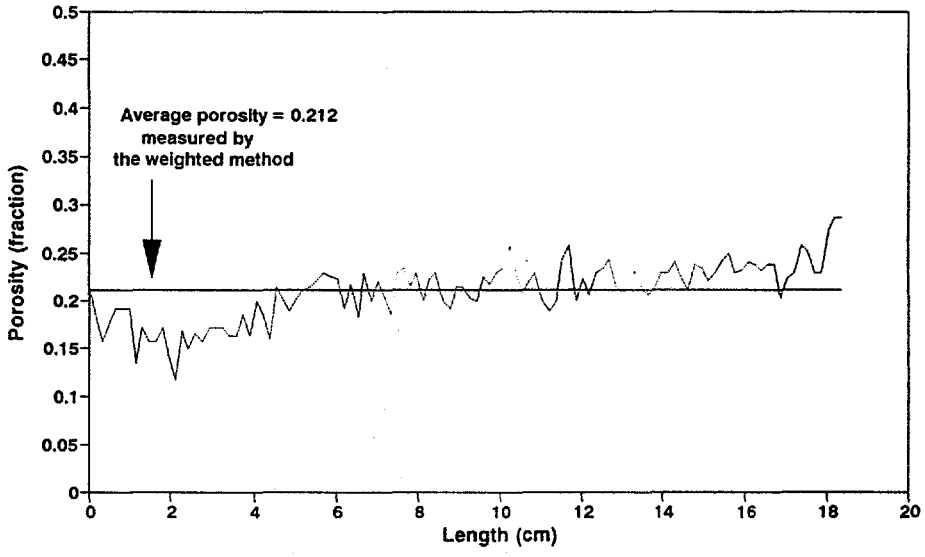

Figure 4.3.18 Porosity Profile Measured on YB5 Berea Core Using X-Ray Linear Core Scanning System

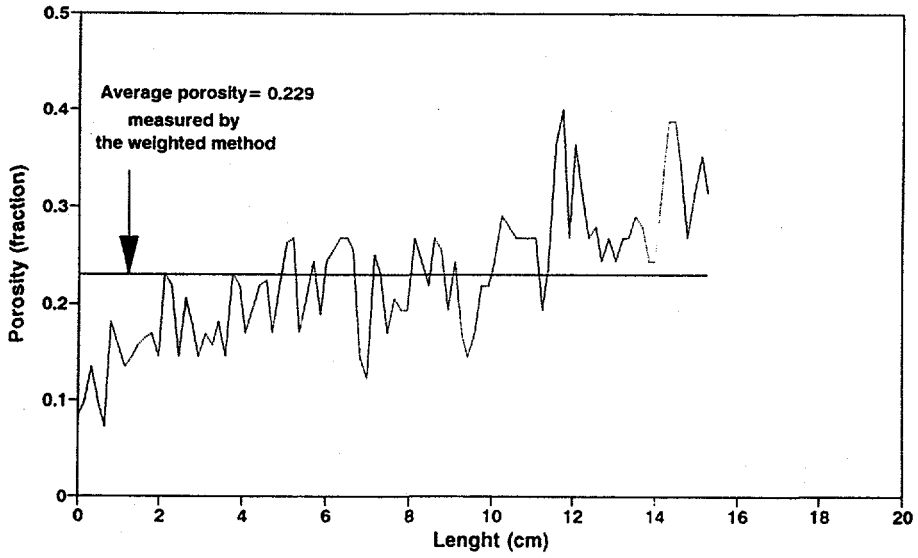

Figure 4.3.19 Porosity Profile Measured on YH1 Berea Core Using X-Ray Linear Core Scanning System

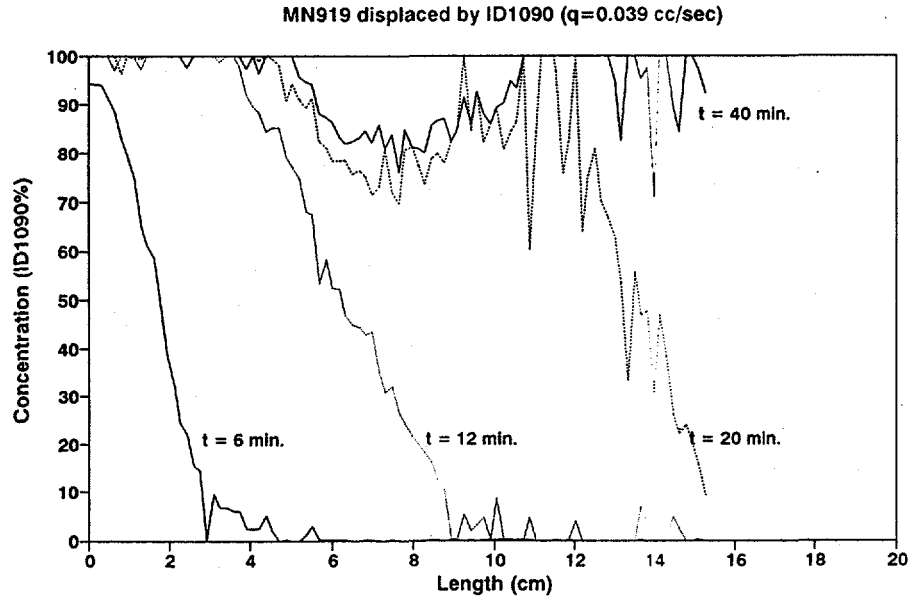

Figure 4.3.20 Concentration Curves Measured on YH1 Berea Core

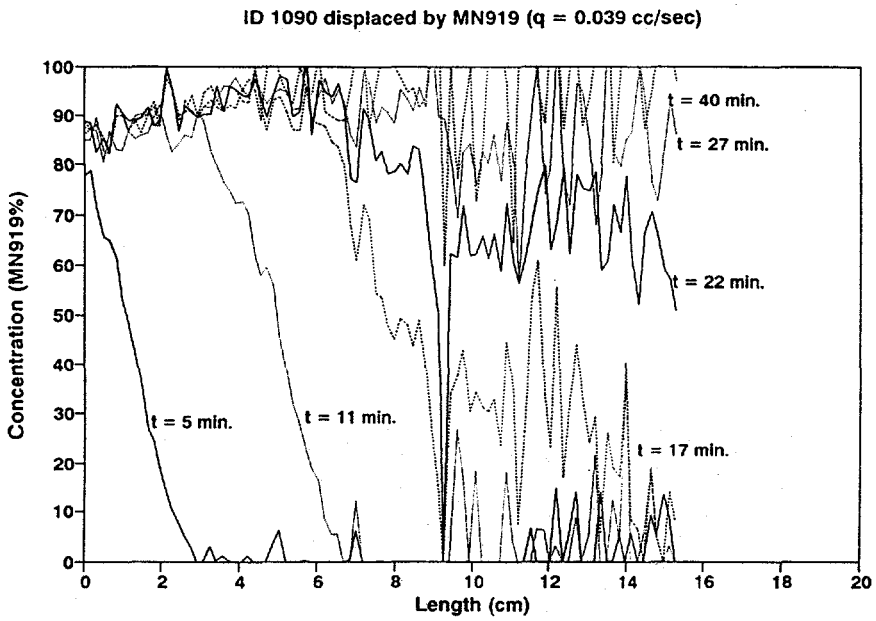

Figure 4.3.21 Concentration Curves Measured on YH1 Berea Core

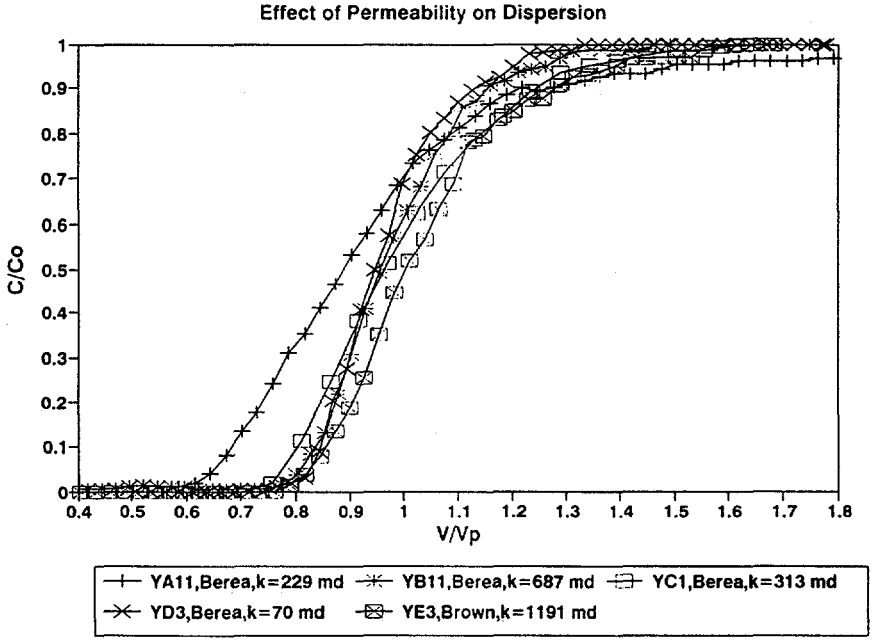

Figure 4.3.22 Concentration Curves Measured on 15.2 cm Cores

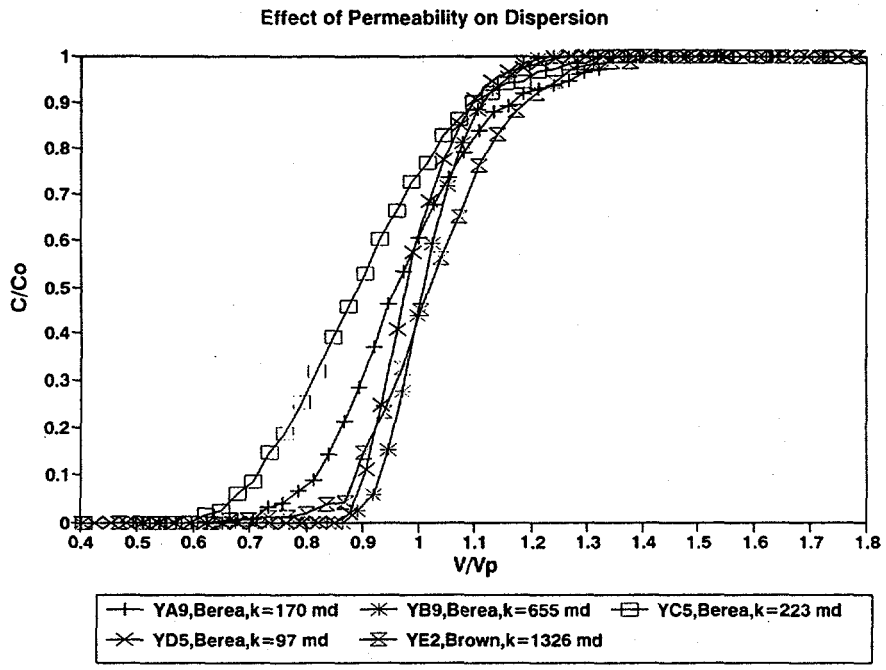

Figure 4.3.23 Concentration Curves Measured on 30.5 cm Cores

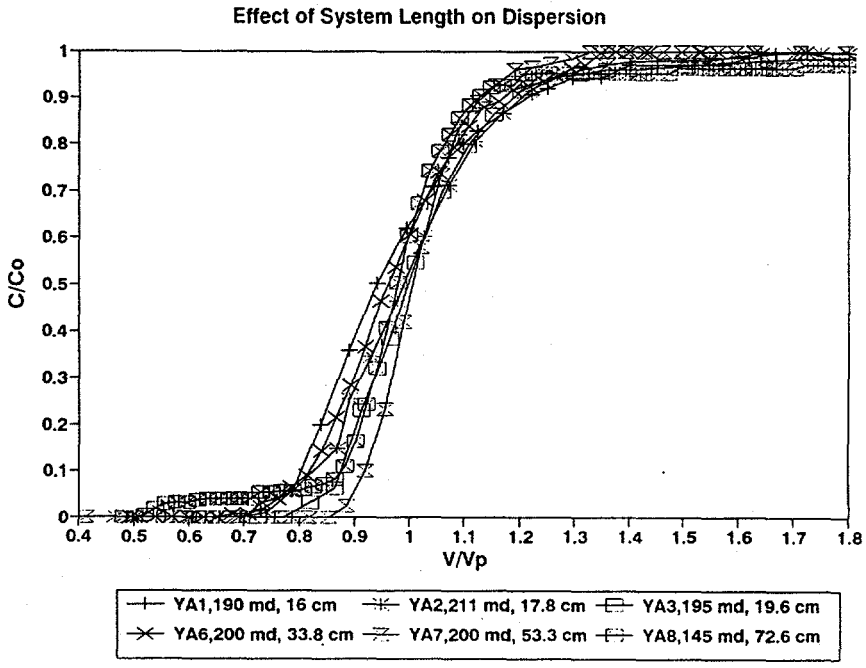

Figure 4.3.24 Concentration Curves Measured on YA Berea Core (Set 1)

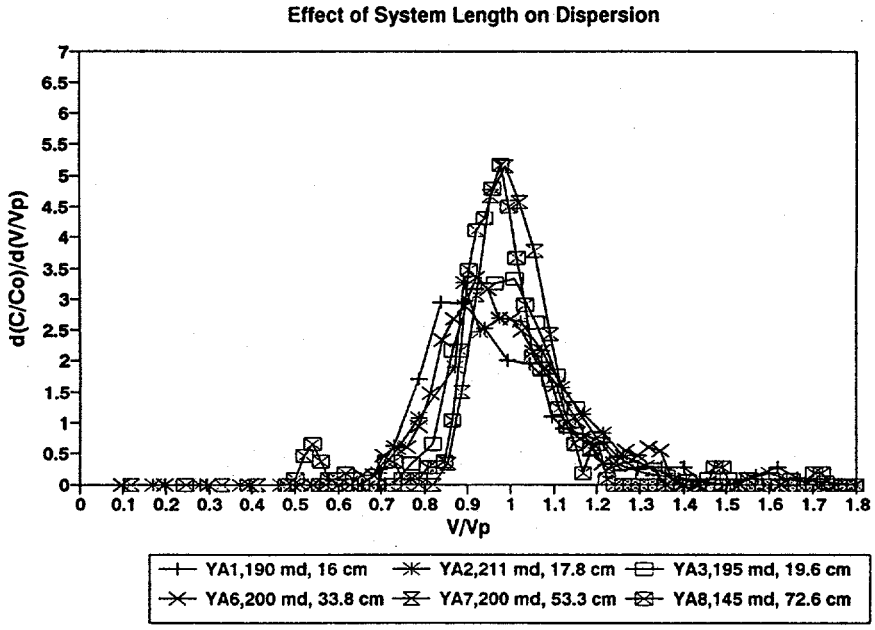

Figure 4.3.25 Derivative Curves Measured on YA Berea Cores (Set 1)

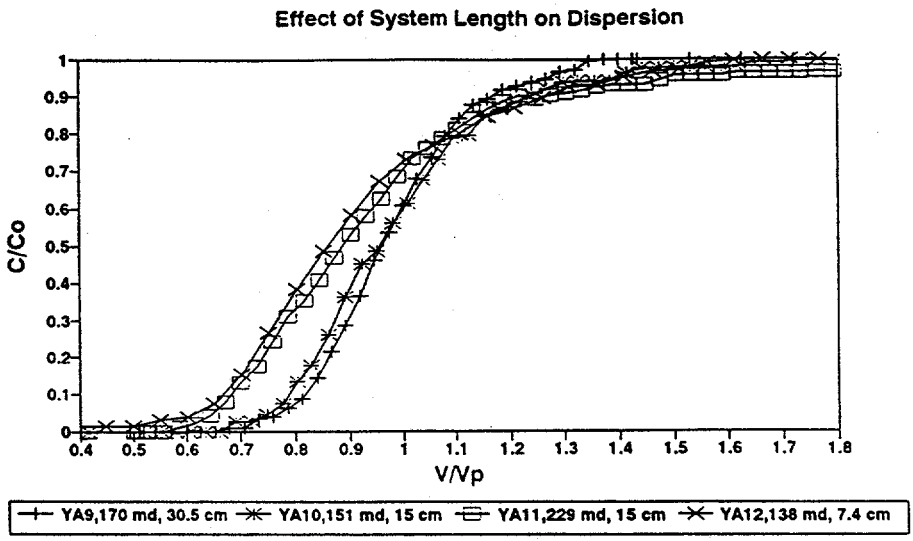

Figure 4.3.26 Concentration Curves Measured on YA Berea Core (Set 2)

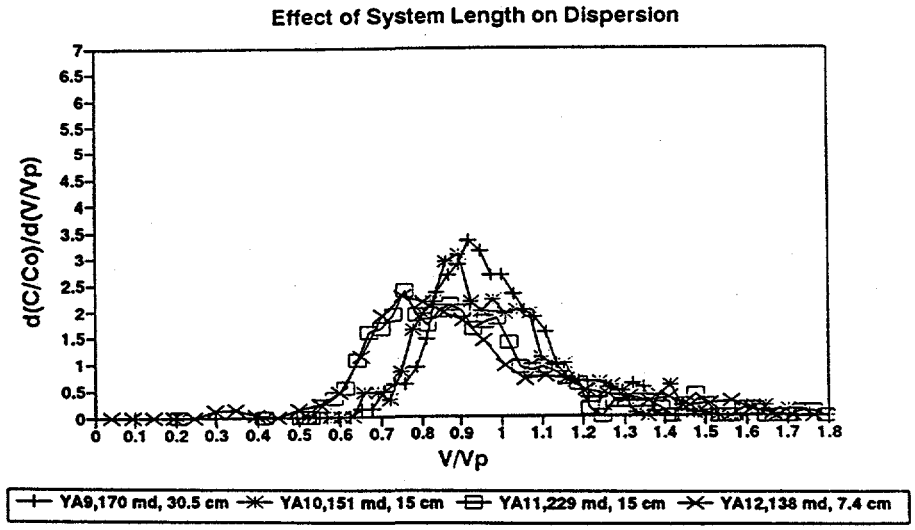

Figure 4.3.27 Derivative Curves Measured on YA Berea Core (Set 2)

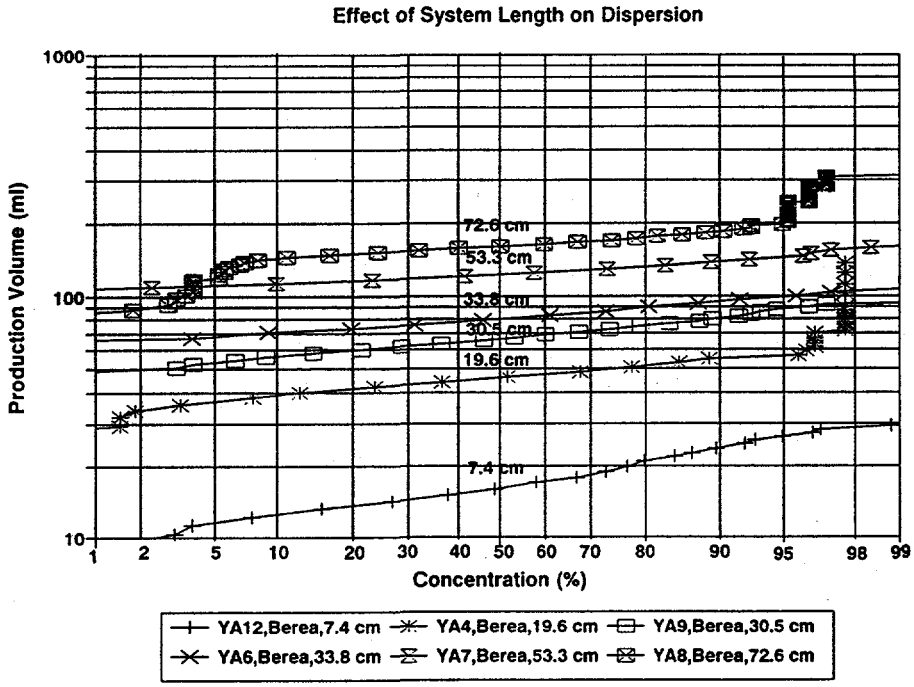

Figure 4.4.1 Lognormal Distribution Curves Measured on YA Berea Cores

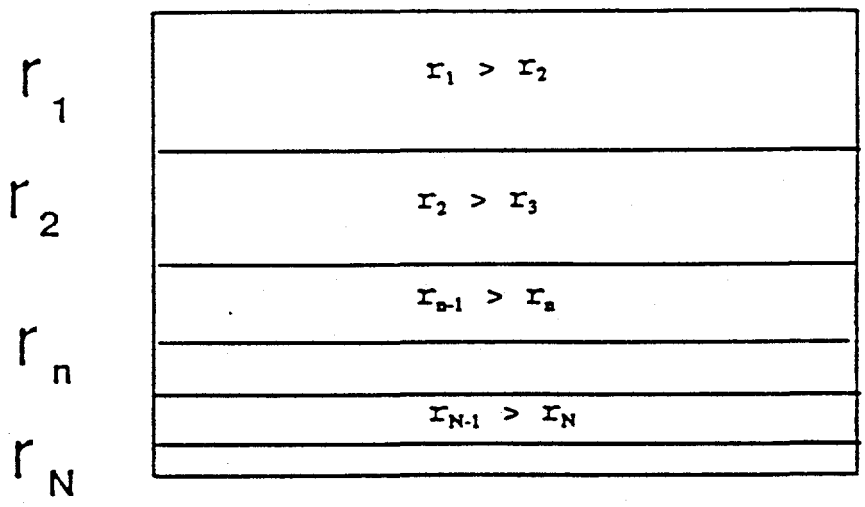

Figure 4.5.1 Capillary Tube Model

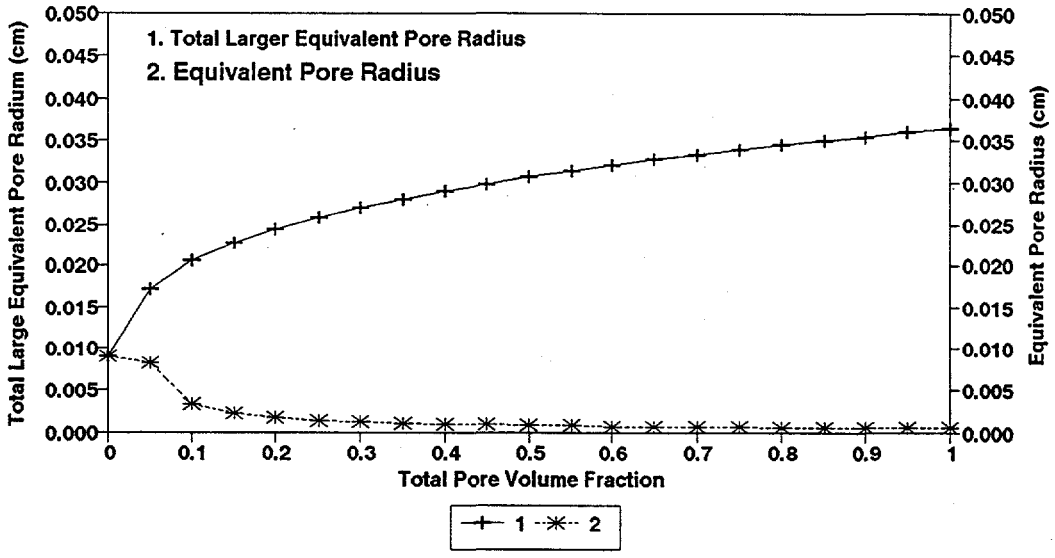

Figure 4.5.2 Equivalent Pore Size Distribution of YA9 Berea Core Calculated from the Concentration Profile

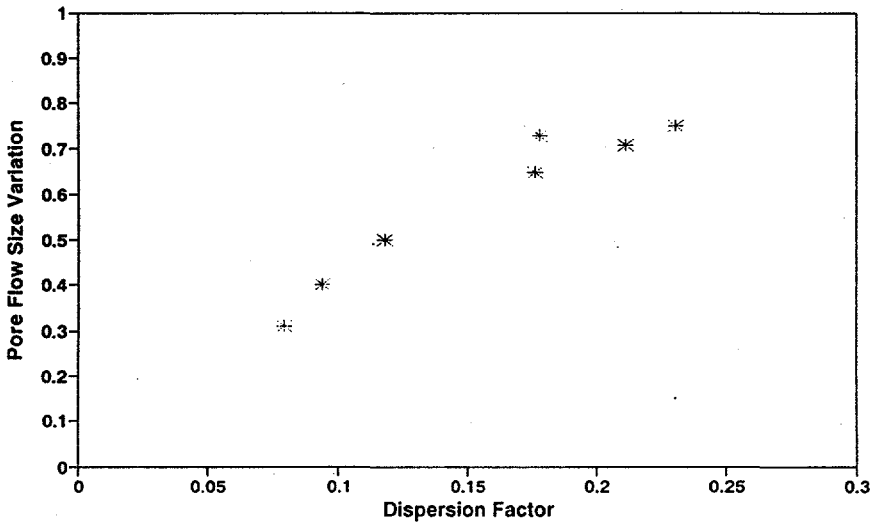

Figure 4.5.3 Dispersion Factor versus Pore Flow Size Variation of Berea and Brown Cores

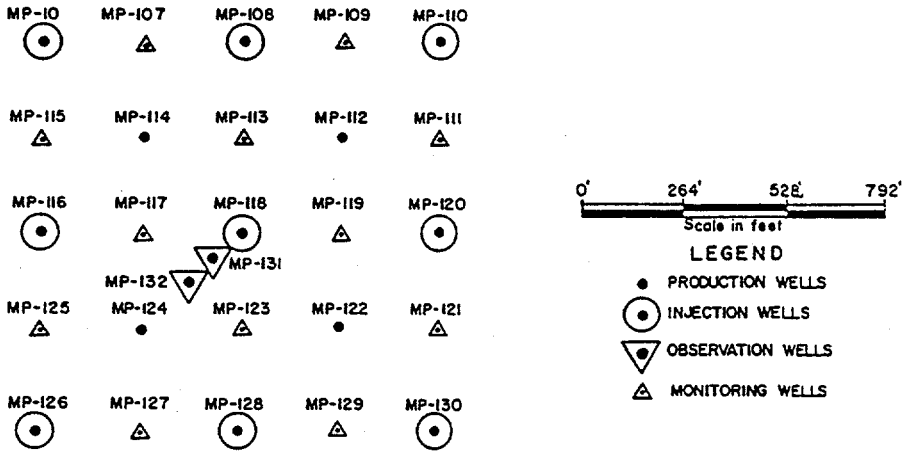

Figure 4.5.4 Location of the Observation Wells in El Dorado Field (Ravnaas, 1981)

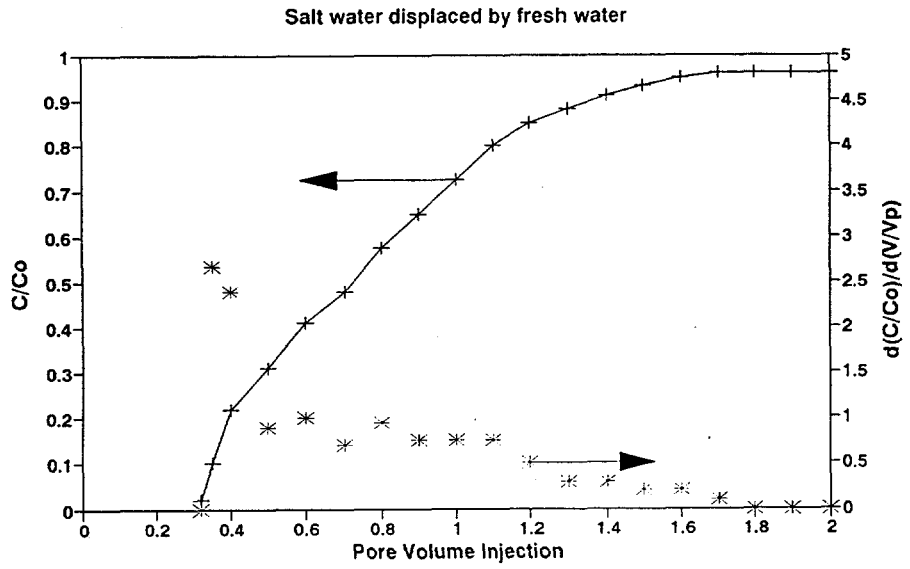

Figure 4.5.5 Concentration Profile and Derivative Curve Measured from MP131 Well in El Dorado Field

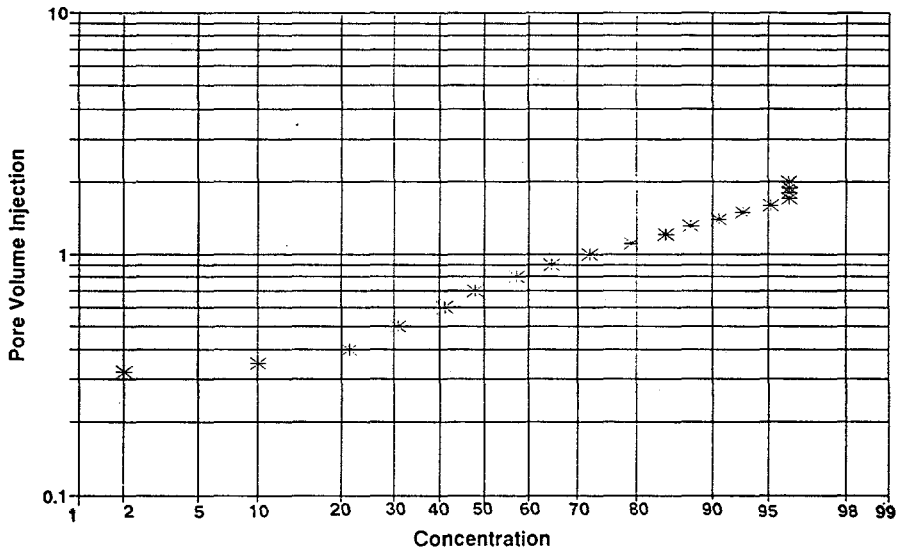

Figure 4.5.6 Lognormal Distribution Curve of the Concentration Profile Measured from MP131 Well in El Dorado Field

CHAPTER 5

Dispersivities of Reservoir Rocks From Well Logging Data

5.1 Introduction

To characterize the dispersion process, a parameter, called dispersivity, was defined as the hydrodynamic dispersion coefficient divided by fluid flow velocity[21]. This parameter is also called the characteristic length by some physicists such as Charlaix et al.[50] and Hulin et al.[117]. They believe the characteristic length is a controlling factor of the dispersion process and the structure of the pore space.

Currently the dispersivity of a reservoir rock is usually determined by tests performed on core samples (plugs) in the laboratory because the field tracer tests are often precluded due to the expense and time involved. As a very important tool in oil exploration and development, well logging provides continuous, extensive, and cost-effective in-situ information about the reservoir rocks. If this information can be fully utilized to estimate dispersivity, time and expenses involved with the coring process can be reduced. Extensive, continuous and in-situ dispersivity values about the reservoir rocks could be provided. At the same time, the pivotal role of well logging in reservoir characterization will be greatly enhanced.

The objective of this research is to develop a method of estimating the in-situ dispersivities of reservoir rocks from well logging data. This result will be then applied to the characterization of pore structures, fluid flow systems, and heterogeneities of the reservoir rocks. The determination of dispersivity from well logs would also help to interpret the current suite of logs to add additional characterization of the producing zone.

5.2 Theoretical Analysis

5.2.1 Tortuous Capillary Model

When the matrix of a porous medium can be considered as a non-conductor, the fluid flow and electrical current flow are usually assumed to follow an identical and tortuous path in the porous medium. This may be the case in clean oilfield sandstones. To describe this tortuous path, Carman[45] defined a parameter, called tortuosity, as the ratio of the actual length of the path followed by a particle or ion in passing through the porous medium, L_e, to the geometrical length of the medium, L. Mathematically it is expressed as:

$$\tau = \frac{L_e}{L} \tag{5.2.1}$$

However, in most cases the tortuosity enters equations as its square. Therefore, another parameter, called the tortuosity factor, is defined as follows:

$$T = \tau^2 = (\frac{L_e}{L})^2 \qquad (5.2.2)$$

Both the fluid flow property and the electrical conductivity of a porous medium are linked to the tortuosity or tortuosity factor. These properties are conditioned by the geometrical properties of the pore system. The physical complexity of a porous medium makes it virtually mandatory that some simplified model be assumed if qualitative, particularly, quantitative predictions are to be made of flow behavior in the medium[221]. For this purpose, a simple but effective model, called the tortuous-capillary model[193,250], was adapted for the present study. This model is illustrated in Figure 5.2.1.

5.2.2 Electrical Formation Factor of Porous Rocks

The most fundamental concept in considering electrical properties of porous media is that of the formation factor. As defined by Archie[8], the formation factor is:

$$F = \frac{R_o}{R_w} \qquad (5.2.3)$$

where R_o is the resistivity of the rock when saturated fully with brine having a resistivity of R_w.

Applying Ohm's law to the porous medium shown in Figure 5.2.1 and assuming the matrix to be non-conductive, the formation factor can be expressed as:

$$F = \frac{(\frac{L_e}{L})}{(\frac{A_e}{A})} \qquad (5.2.4)$$

where A_e is the area available to fluid flow and A is the cross-sectional area of the porous medium.

In regard to the area available for flow (A_e), Wyllie and Rose[269] assumed:

$$A_e = \phi * A \qquad (5.2.5)$$

where ϕ is the average porosity of the porous medium.

However, Cornell and Katz[63], followed the Slawinski[231] concept and assumed:

$$A_e = \phi(\frac{L}{L_e})A \tag{5.2.6}$$

Wyllie and Rose[269], and Wyllie and Spangler[270] did not differentiate between A_x and A_e (see Figure 5.2.1b), leading to variations in their expressions and in some subsequent analyses[268]. Cornell and Katz[269] by differentiating between A_x and A_e arrived at the expression for the formation factor as below:

$$F = \frac{(\frac{L_e}{L})^2}{\phi} = \frac{\tau^2}{\phi} = \frac{T}{\phi} \tag{5.2.7}$$

where τ is tortuosity and T is the tortuosity factor.

By measuring the electrical formation factor and porosity, the tortuosity and tortuosity factor can be calculated from Equation 5.2.7.

5.2.3 Fluid Permeability of Porous Rocks

According to Poiseuille's law, Kozeny[140] derived the average velocity along a tortuous path as:

$$v_e = -(\frac{r_h^2}{k_o \mu})\frac{dp}{dx_e} \tag{5.2.8}$$

where r_h, the hydraulic radius, is the ratio of the volume of the tortuous path to its wetted area; k_o is the Kozeny constant which depends on pore shape; μ is the fluid viscosity; and dp/dx_e is the pressure gradient along the tortuous path.

As illustrated in Figure 5.2.1b, therefore:

$$\frac{dp}{dx_e} = \frac{1}{\tau}\frac{dp}{dx} \tag{5.2.9}$$

where dp/dx is the pressure gradient along the porous medium.

According to Darcy's law, the fluid permeability of the porous rock is defined as:

$$K = -\frac{(\frac{Q}{A})\mu}{(\frac{dp}{dx})} \tag{5.2.10}$$

where K is the rock permeability and Q is the flow rate.

Substituting Equation 5.2.8 and 5.2.9 into 5.2.10, and also considering the difference between A_x and A_e, we obtain:

$$K = \frac{r_h^2}{k_o F} \tag{5.2.11}$$

Further, considering the definition of mean hydraulic radius (r_h) given by Carman[46]:

$$r_h = \frac{\phi}{S} \tag{5.2.12}$$

where S is the particle surface area per unit volume which is defined as:

$$S = S_o(1 - \phi) = \frac{6(1 - \phi)}{d_p} \tag{5.2.13}$$

where S_o is the specific surface of the particles and d_p is the average diameter of particles. Then:

$$K = \frac{1}{36k_o}\left(\frac{\phi}{1-\phi}\right)^2 \frac{d_p^2}{F} \tag{5.2.14}$$

This equation shows the relationship between fluid flow property (K) and electrical property (F). It also indicates that the permeability of a rock decreases with an increase in the formation factor and an increase in the particle diameter. When Equation 5.2.7 is substituted into Equation 5.2.14, it can be seen that permeability decreases as tortuosity increases.

5.2.4 Dispersion-Convection Model

The general 1-D equation which describes the transport and mixing of fluids through a porous rock is expressed as:

$$D_L \frac{\partial^2 C}{\partial x^2} - V\frac{\partial C}{\partial x} = \phi \frac{\partial C}{\partial t} \tag{5.2.15}$$

where D_L is the longitudinal dispersion coefficient in a porous medium, including the effects of both molecular diffusion and convective dispersion, V is the Darcy velocity, and C is the concentration.

Applying this equation to the model illustrated in Figure 5.2.1, Equation 5.2.15 can be rewritten as:

$$D'_L \frac{\partial^2 C}{\partial x_e^2} - V' \frac{\partial C}{\partial x_e} = \frac{\partial C}{\partial t} \qquad (5.2.16)$$

where,

$$D'_L = D_L * \frac{\tau^2}{\phi} \qquad (5.2.17)$$

$$V' = V \frac{\tau}{\phi} \qquad (5.2.18)$$

where D'_L is the effective dispersion coefficient in the tortuous capillary and V' is the Carman's modified pore velocity[46].

When solved with different boundary conditions, Equation 5.2.16 yields slightly different solutions for the effluent concentration. Kreft and Zuber[141] compared in detail all different boundary conditions and the corresponding solutions in their paper and concluded that the differences between the solutions for different injection-detection modes are essential in cases of low Peclet numbers. In systems having high Peclet numbers, the numerical differences between the solutions become negligible and the injection-detection mode is not as important.

The simplest case is to assume that the porous medium extends infinitely in both the +x and -x directions when the porous medium is long compared with the length of the mixed zone, i.e.,

$$\text{as } x \text{ ------} > 0 \qquad C(x,t) \text{ ------} > 0$$

and (5.2.19)

$$\text{at } x = V't, \qquad C(x,t) \text{ ------} > 1/2$$

The resulting solution is:

$$C = \frac{1}{2} erfc\left(\frac{x_e - V't}{\sqrt{4D'_L t}}\right) \qquad (5.2.20)$$

where

$$erfc(x) = 1 - erf(x) = 1 - \frac{2}{\sqrt{\pi}} \int_0^x e^{-\zeta^2} d\zeta \qquad (5.2.21)$$

By substituting Equations 5.2.17 and 5.2.18 into 5.2.20:

$$C = \frac{1}{2} erfc\left(\frac{x-(\frac{V}{\phi})t}{\sqrt{4(\frac{D_L}{\phi})t}}\right) \tag{5.2.22}$$

By writing:

$$U = \frac{V}{\phi} \tag{5.2.23}$$

$$K_L = \frac{D_L}{\phi} \tag{5.2.24}$$

Equation 5.2.22 then becomes the same expression as given in the literature:

$$C = \frac{1}{2} erfc\left(\frac{x-Ut}{\sqrt{4K_L t}}\right) \tag{5.2.25}$$

where U is called the Dupuit's pore velocity[80] and K_L is the effective dispersion coefficient in a porous medium.

In the laboratory the effluent concentration is often measured at the outlet of the core. To compare the equation with the experiment, it has been the practice to set x equal to L in Equation 5.2.25 and calculate the concentration for various values of injected pore volume[35]. The resulting equation is:

$$C = \frac{1}{2} erfc\left(\frac{1-I}{\sqrt{\frac{4I}{\gamma}}}\right) \tag{5.2.26}$$

where $I = V_i/V_p$ is the pore volume number of the displacing fluid injected, V_i is the displacing fluid volume injected, V_p is the pore volume of the medium which includes the effective pore volume of the sample and the endplate volume, and $\gamma = V^*L/D_L$ is the dimensionless dispersivity.

In addition, Brigham[35] also noted that Equations 5.2.19 and 5.2.20 define the fluid concentration in situ, while the measured fluid concentration at the outlet of the core is the average flowing concentration. From material balance, the relationship between the in-situ concentration and the average flowing concentration is derived as:

$$C_f = C - \frac{K_L}{U}\left(\frac{\partial C}{\partial x}\right) \tag{5.2.27}$$

Since dC/dx is negative, Equation 5.2.27 states that the average concentration flowing across a plane is always greater than the concentration in place.

Substituting Equation 5.2.26 into 5.2.27:

$$C_f = \frac{1}{2}erfc\left(\frac{1-I}{\sqrt{\frac{4I}{\gamma}}}\right) + \frac{1}{\sqrt{4\pi\gamma I}}e^{-\left(\frac{1-I}{\sqrt{\frac{4I}{\gamma}}}\right)^2} \tag{5.2.28}$$

To match experimental data Equation 5.2.28, rather than Equation 5.2.26 should be applied.

Concentration at I= 1 PV, and therefore,

$$C_{f@I=1} = \frac{1}{2} + \frac{1}{\sqrt{4\pi\gamma}} \tag{5.2.29}$$

is always greater than 0.5. This is consistent with the experimental data on consolidated rocks.

Then the dispersivity can be evaluated from the 1 PV concentration point:

$$\alpha_D = \frac{L}{\gamma} = 4\pi L\left(C_{f@I=1} - \frac{1}{2}\right)^2 \tag{5.2.30}$$

Further, taking the first derivative to pore volume (I) on both sides of Equation 5.2.28, the concentration derivative is:

$$\frac{\partial C_f}{\partial I} = \frac{\left(1+\frac{1}{I}\right)}{4\sqrt{\frac{\pi I}{\gamma}}}e^{-\frac{(1-I)^2}{\frac{4I}{\gamma}}} - \frac{e^{-\frac{(1-I)^2}{\frac{4I}{\gamma}}}}{4\sqrt{\pi I\gamma}}\left[\frac{1}{I}+\frac{\gamma}{I}\left(1-\frac{1}{I^2}\right)\right] \tag{5.2.31}$$

It is apparent that the peak of the concentration derivative is:

$$\left(\frac{\partial C_f}{\partial I}\right)_{max} = \frac{\left(1+\frac{1}{I_{max}}\right)}{4\sqrt{\frac{\pi I_{max}}{\gamma}}} e^{-\frac{(1-I_{max})^2}{4I_{max}/\gamma}} \tag{5.2.32}$$

where,

$$I_{max} = \frac{\sqrt{\gamma^2+1} - 1}{\gamma} \tag{5.2.33}$$

is the pore volume where dynamic miscible displacement efficiency reaches the maximum. Equation 5.2.33 states that I_{max} is always less than 1.0, which means the peak of the concentration derivative will occur prior to the injection of one pore volume of fluid.

Again, the dispersivity can be then evaluated from the maximum miscible displacement pore volume, I_{max}:

$$\alpha_D = \frac{L}{\gamma} = L\left(\frac{1 - I_{max}^2}{2I_{max}}\right) \tag{5.2.34}$$

C_f at I =1 and I_{max} are related to each other. From Equation 5.2.30 and 5.2.34, the following may be obtained:

$$C_{f@I=1} = \frac{1}{2} + \sqrt{\frac{1 - I_{max}^2}{8\pi I_{max}}} \tag{5.2.35}$$

This relationship indicates that the less the I_{max}, the larger the C_f at I=1. This conclusion is consistent with the material balance. The normal range of I_{max} is usually from 0.70 to slightly less than 1.0, and correspondingly C_f at I=1 ranges from 0.67 to slightly greater than 0.50.

The usual method of plotting the effluent concentration profile in miscible displacement is to use probability paper and a volume modifying function. Brigham[36] defined this volume modifying function as:

$$\lambda = \frac{\left(\frac{V_i}{V_p}-1\right)}{\sqrt{\frac{V_i}{V_p}}} = \frac{I-1}{\sqrt{I}} \tag{5.2.36}$$

If this plotting gives a straight line on probability paper, the dimensionless dispersivity can be then calculated from the slope of the line:

$$\gamma = \left(\frac{2.380}{\lambda_{80} - \lambda_{20}}\right)^2 = \left(\frac{3.625}{\lambda_{90} - \lambda_{10}}\right)^2 \qquad (5.2.37)$$

where λ_{10}, λ_{20}, λ_{80}, and λ_{90} are λ values at 10%, 20%, 80%, and 90% concentration of the displacing fluid, respectively.

Then the dispersivity of the rock is calculated by the following equation:

$$\alpha_D = L\left(\frac{\lambda_{80} - \lambda_{20}}{2.380}\right)^2 = L\left(\frac{\lambda_{90} - \lambda_{10}}{3.625}\right)^2 \qquad (5.2.38)$$

If the plotting on probability paper does not yield a straight line, the above equations are no longer valid. In these cases, the following more complex model should be used.

5.2.5 Dispersion-Capacitance Model

Although most laboratory tests using sandpacks resulted in a symmetrical effluent concentration profile, as predicted by Equation 5.2.30, many tests carried out on actual reservoir rocks showed a marked deviation from this ideal behavior. These tests were characterized by (1) breakthrough of the 50 percent concentration prior to the injection of one pore volume of displacing fluid, and (2) an asymmetrical effluent concentration profile[222,54]. It was postulated by Deans[74] that such results might be due to capacitance effects. That is, the porous rocks in these tests must contain stagnant or dead-end pores which contribute to the total pore volume but which do not contribute to flow. Based on this postulation, Coats and Smith[58] developed a mathematical model, called the dispersion-capacitance model, to take into account of the effect of a stagnant pore volume on the growth of the mixing zone. The modified equations are:

$$K_L\frac{\partial^2 C}{\partial x^2} - U\frac{\partial C}{\partial x} = f\frac{\partial C}{\partial t} + (1-f)\frac{\partial C^*}{\partial t} \qquad (5.2.39)$$

$$(1-f)\frac{\partial C^*}{\partial t} = M(C - C^*) \qquad (5.2.40)$$

where f is the flow fraction of pore volume, M is the mass transfer coefficient, C is the in-situ concentration of flowing fluid, and C* is the concentration of stagnant fluid.

Coats and Smith[58] gave the resulting solution as a complex integral, evaluated at x=L. This same equation is given by Brigham[35] for any x, as shown below:

$$C(J,y) = \frac{2e^{J}}{\pi}\int_{0}^{\infty}\frac{e^{\frac{w}{2}(1-\frac{\gamma v}{4w})}}{a_1^2+a_2^2}[a_1\cos(\beta J-wy)+a_2\sin(\beta J-wy)]d\beta \qquad (5.2.41)$$

where J=I/f = U*t/L*f and y=x/L. Other terms are defined in the Nomenclature.

Again, by considering the difference between in-situ concentration and flowing concentration indicated by Equation 5.2.27, the above solution may be modified as follows:

$$C_f(J,y) = \frac{2e^{J}}{\pi}\int_{0}^{\infty}\frac{e^{\frac{w}{2}(1-\frac{\gamma v}{4w})}}{a_1^2+a_2^2}[\Gamma_1\cos(\beta J-wy)+\Gamma_2\sin(\beta J-wy)]d\beta \qquad (5.2.42)$$

where,

$$\Gamma_1 = \frac{a_1}{2}(1+\frac{\gamma v}{4w})+\frac{a_2 w}{\gamma} \qquad (5.2.43)$$

$$\Gamma_2 = \frac{a_2}{2}(1+\frac{\gamma v}{4w})-\frac{a_1 w}{\gamma} \qquad (5.2.44)$$

Equation 5.2.42 rather than Equation 5.2.41, should be used when matching laboratory data to the capacitance model.

Ordinarily, the capacitance model can match any effluent concentration profiles observed in the laboratory by adjusting three parameters: f, M, and K_L. Because of the multiple adjustable parameters, multiple solutions can be obtained. To obtain a unique value for dispersivity, the other two parameters (f and M) must be independently predetermined prior to using the capacitance model.

Using the concept of dead-end pore volume employed by Goodknight et al.[94], Coats and Smith[58] derived the following expression of the mass transfer coefficient:

$$M = \frac{(1-f)A_s}{V_s l_s}D_o \qquad (5.2.45)$$

where V_s is the volume of the stagnant space, and A_s and l_s are the cross-sectional area and length, respectively, of the neck leading to it, and D_o is the molecular diffusivity of the two miscible fluids. Equation 5.2.45 indicates that the mass transfer coefficient is proportional to the diffusivity of the two miscible fluids. Jasti et al.[123] have proved this fact experimentally. Therefore, when the same fluids and flow rate are used for all experimental runs, the mass transfer coefficient should only be

adjusted for flow fraction. If lower flow fraction is used, a higher mass transfer coefficient should be used.

Flow fraction was conceptually defined as the pore volume that contributes to the dynamic fluid flow. However, no practical method is currently available to measure directly its value in the laboratory or field. An attempt was made to use I_{max} as the flow fraction. Physically the value of I_{max} is the pore volume at which the dynamic miscible displacement efficiency reaches maximum. By definition, this point corresponds to the peak of the concentration derivative.

After the mass transfer coefficient (M) and flow fraction (f) parameters are predetermined for the system of interest, a unique value of dispersivity could be obtained by matching the laboratory measured concentration profile with the capacitance model solution as indicated by Equation 5.2.42.

5.2.6 Relating Dispersivity to Petrophysical Parameter of Porous Rocks

Nearly all literature data shows that the longitudinal dispersivity for unconsolidated sand or bead packs is proportional to particle size, d_p, as shown in the following equation[189]:

$$\alpha_D = 1.75\, d_p \qquad (2 < P_e < 50) \tag{5.2.46}$$

where P_e is the Peclet number ($P_e = L^*U/D_o$).

Raimondi et al.[202] have given a more general equation as below:

$$\alpha_D = c_1 \sigma d_p \tag{5.2.47}$$

where c_1 is a constant and σ is a measure of the heterogeneity of the pack. Aris and Amundson[10], Carberry[42], and Prausnitz[201] have shown that the mixing-cell theory leads to a value of $c_1 = 0.5$. This would then give a value of about $\sigma = 3.5$ for the typical random pack. However, it is expected that σ should be larger than 3.5 for consolidated sandstones.

Since the heterogeneity of a rock is only a conceptual parameter, the only way to determine its value is to calculate back through Equation 5.2.47. Therefore, it is more convenient to report the value of ($c_1^*\sigma$).

Substituting Equation 5.2.14 into 5.2.47, the following is obtained

$$\alpha_D = 6 c_1 \sigma \left(\frac{1-\phi}{\phi}\right)\sqrt{k_o K F} \tag{5.2.48}$$

This is the relationship between fluid flow and electrical conductance properties. Since the porosity and formation factor can be obtained directly from logs, and permeability can also be estimated from logging data using empirical correlations, the rock dispersivity is then determined

using the above equation. However, the method of determination of the heterogeneity factor from logs is still not developed.

5.3 Experimental Apparatus and Procedures

5.3.1 Experimental Preparation

Two sets of core samples, one Berea sandstone and the other Brown sandstone, were used for the preliminary study on the correlation between dispersivity and log-derivable parameters. The Berea and Brown sandstones were selected mainly because they are relatively clean (clay-free). The shapes of samples were typically right cylinders with a diameter of 2.5 cm and with the length ranging from 6.38 to 9.60 cm (see Table 5.3.1).

Table 5.3.1 Dimensions of Berea and Brown Sandstone Core Samples

Core sample #	Diameter (cm)	Length (cm)
Berea sandstone		
B#1	2.50	9.60
B#2	2.50	9.45
B#3	2.50	9.16
B#4	2.50	9.41
B#5	2.50	9.30
B#6	2.50	7.20
B#10	2.50	9.34
B#11	2.50	9.30
B#12	2.50	7.08
Brown sandstone		
BN#1	2.50	9.32
BN#2	2.50	9.52
BN#3	2.50	9.46
BN#4	2.50	6.38

The porosities of the cores were measured by the weight method. The resistivity of brine solution and core samples were measured using a conducting bridge apparatus. The formation factor of the sample was calculated by Archie's equation. Liquid permeabilities of the cores were measured using the injection method.

5.3.2 Miscible Displacement

To run miscible displacement tests, two fluids were selected. These two fluids met the following requirements:

(1) completely miscible,
(2) equal or close viscosities,
(3) equal or close densities,
(4) wide range of refractive indices,
(5) no chemical reactions with rock matrix,
(6) no adsorption to rock matrix,
(7) available and cost effective,
(8) easy to clean for repeat runs.

Methanol and toluene were selected as the testing fluids for the present research (Table 5.3.2). Since the tests are run horizontally, the effect of the small density difference can be considered negligible.

Table 5.3.2 Physical Properties of Methanol and Toluene (at room conditions: 24 °C and 1 atm)

Properties	Methanol	Toluene
Formula	CH_3OH	$C_6H_6CH_3$
Molecular Weight	32.04	92.13
Density	0.81	0.88
Viscosity	0.600	0.5980
Refractive Index	1.3290	1.4890

The following three points are crucial for the system setup of a miscible displacement test.

(a) Since two different types of fluids will be used in this experiment, two separate flow systems should be established to avoid flushing the flow system after injecting one fluid. Further, if the flushing is not complete, the effluent concentration will be in error.

(b) In addition, because relatively low pressure (less than 5 psi) is usually applied in this experiment, Manometers, rather than pressure gauges, should be used to record pressures. In this way, accurate permeability values can be obtained.

(c) As indicated in the theoretical analysis, a constant flow rate is assumed. To ensure a constant flow rate, a constant injection pressure should be maintained during the whole process of displacement. However, even though the pump flow rate is usually kept constant, inlet pressure increases initially from zero to a stabilized value. This pressure variation will cause the fluctuation

of flow rate inside the core sample. Therefore, establishing a constant injection pressure prior to the beginning of the displacement will be critical to the accuracy of the experimental data.

Based on these considerations, the apparatus used for miscible displacement was set up as shown in Figure 5.3.1.

The general procedure to run a miscible displacement is described below:

(a) With three-way valve open to the resident fluid injection line, pump resident fluid (methanol) at the pre-determined flow rate until pressure drop stabilizes. This step can be done during the permeability measurement process;

(b) Close the three-way valve and switch the pump to the displacing fluid (toluene);

(c) Establish a constant injection pressure by pumping displacing fluid with three-way valve closed until the same pressure drop as established in step (a) is reached;

(d) Open the three-way valve to the displacing fluid injection line. At the same time, start the timer.

(e) Record the time when switching the fluid sample collecting tubes;

(f) Read the volume of effluent and refractive index for each fluid sample. If this step can not be done immediately, the tubes must be capped to prevent vaporization of the fluid sample;

(g) Continue steps (e) and (f) until more than 99 percent displacing fluid is reached in the effluent.

5.4 Data Analysis and Discussion

5.4.1 Experimental Data

Figs.5.4.1 and 5.4.2 are typical concentration profiles and the first derivative curves for Berea and Brown sandstones, respectively. Tables 5.4.1 and 5.4.2 list the experimental data on Berea and Brown core samples, respectively.

5.4.2 Correlation and Discussion

Formation Factor vs Porosity

As shown in Figs.5.4.3 and 5.4.4, good correlations are observed between the measured formation factor and porosity for both Berea and Brown sandstone core samples. These correlations indicate the reliability of the measured resistivity and porosity values.

From the straight lines, the cementation factor as defined in Archie's equation is obtained as: $m=1.56$ for Berea sandstone and $m=1.66$ for Brown sandstone.

Table 5.4.1 Experimental Data of Berea Sandstone Cores

Core #	ϕ (%)	K (md)	F	T	C_f @I=1	$c^*\sigma$	α_D/L	α_D
B#1	18.76	137	13.32	2.50	55	33	0.020	0.19
B#2	19.72	187	12.99	2.56	54	55	0.031	0.30
B#3	19.08	144	13.40	2.56	56	75	0.045	0.41
B#4	19.24	172	12.77	2.46	54	32	0.020	0.19
B#5	18.77	144	13.47	2.53	53.5	25	0.015	0.14
B#6	18.72	136	13.49	2.53	56	59	0.045	0.33
B#10	21.40	440	10.46	2.24	60	158	0.126	1.17
B#11	21.45	780	10.70	2.29	61.5	155	0.166	1.55
B#12	21.15	460	10.95	2.32	61	137	0.152	1.08

Table 5.4.2 Experimental Data of Brown Sandstone Cores

Core #	ϕ (%)	K (md)	F	T	C_f @I=1	$c^*\sigma$	α_D/L	α_D
BN#1	22.80	2543	11.54	2.63	64	103	0.246	2.30
BN#2	22.50	390	12.20	2.75	60	157	0.126	1.20
BN#3	22.65	1945	11.67	2.64	63	100	0.212	2.01
BN#4	22.60	827	12.11	2.74	62	98	0.181	1.15

Permeability vs Formation Factor

As expected, permeability decreases with the increase of the formation factor (Figs.5.4.5 and 5.4.6). The exponential factor in the relationship between permeability and the formation factor is found to be 5.85 for Berea sandstone and 30.0 for Brown sandstone. The exponential factor for Brown sandstone is so high because it is not well consolidated, and also may be not homogeneous. Since all four Brown core samples were drilled from the same block, their widespread range of permeability indicates the heterogeneity of the sandstone.

Dependence of S-Shaped Curve on Fluid Viscosity

Considering the immiscible displacement, a similar effect of the viscosity or mobility ratio on displacement efficiency is also expected for miscible displacement. Therefore, when the viscosity ratio is unity, the same results are expected regardless of the absolute value of viscosity. If different

results are observed, this difference is usually attributed to the fluid composition. The effect of the absolute value of viscosity is neglected.

Shown in Figs.5.4.7 and 5.4.8 are effluent concentration profiles for Berea and Rock Creek sandstones, respectively, given by Bretz et al.[34]. On the left side of each figure is the water phase dispersion curve, and on the right side is the oil phase dispersion curve. Apparently, both figures indicate that rock dispersivity of the oil phase is larger than that of the water phase because of the longer tail on the oil-phase dispersion curve. Similar curves can also be found in the paper by Wang et al.[251]. However in a case of single phase fluid displacement, a different dispersion curve was also obtained when fluids with different viscosity were used. Generally, the larger the absolute viscosity of fluid, the longer the tail of the s-shaped curve and the larger the dispersivity. This observation is contrary to the statement in the literature that dispersivity is a fluid-independent rock property when the viscosity ratio is unity.

Equation 5.2.45 indicates that the mass transfer coefficient is proportional to the fluid diffusivity. According to the Coats-Smith model, the longer tail of the s-shaped curve means a lower mass transfer coefficient and flow fraction. However, fluid diffusivity is proportional to the reverse of fluid viscosity[68]. Therefore, the tail of the s-shaped curve will be proportional to the absolute value of the miscible fluid, even though the viscosity ratio is unity. More experiments need to be run to substantiate this statement.

Dispersivity vs Permeability

The relationship between dispersivity and permeability has been studied by several investigators[105,159]. As expected, dispersivity increases with an increase in permeability as shown in Figures 5.4.9 and 5.4.10.

Dispersivity vs Tortuosity

The relationship between dispersivity and tortuosity was different from the initial expectation. As shown in Figures 5.4.11 and 5.4.12, dispersivity decreases with an increase in tortuosity. An explanation for this fact is below.

For a homogeneous rock, higher tortuosity does not mean higher heterogeneity but rather lower permeability. Due to the more even pore size distribution and capillary pressure, rock with lower permeability has higher dynamic miscible displacement efficiency (I_{max}). Further, based on the Coats-Smith model, lower permeability rock has lower dispersivity. Permeability of a rock dominates its dispersivity value. This is consistent with the theoretical analysis as shown in Equation 5.2.48.

Matching Experimental Data with Theoretical Model

The dispersivity values listed in Tables 5.4.1 and 5.4.2 were used in theoretical models to study laboratory measured S-shaped curves. The matching results are satisfactory. See Figures 5.4.13 and 5.4.14.

Effect of Micro-Heterogeneity Factor

The micro-heterogeneity of Berea and Brown sandstones have been back calculated from Equation 5.2.48. As shown in Table 5.4.1, two groups of Berea sandstone samples have two significant values of the heterogeneity factor: the low permeability group has an average value of 55, while the high permeability group has an average value of 120. This fact might be attributed to the samples being drilled from two Berea sandstone blocks having different permeabilities.

5.5 Conclusions and Future work

Through the above theoretical analyses and experimental studies on Berea and Brown sandstone samples, the following conclusions have been obtained:

(1) Tortuosity is an essential pore structure in relating fluid flow and electrical conduction properties of a porous rock.
(2) Both the diffusion-type model and the capacitance model for dispersion phenomena apply to the tortuous capillary model for a porous rock.
(3) Rock dispersivity increases as its permeability and tortuosity increases. Permeability dominates its value.
(4) The literature review reveals that rock permeability can be effectively estimated from either a single log or a combination of several logs, including porosielectric, geochemical, and acoustic logs.
(5) The effect of clay in a shaly sandstone can be modified based on its type of distribution in the rock.
(6) Potentially the in-situ dispersivity of a reservoir rock can be estimated from well logs based on Equation 5.2.48.

The results presented here are only a start for the research on this subject. The continuing studies should focus on the following topics:

(1) Interpretation of the laboratory-measured S-shaped dispersion curve.
(2) Relationship between the S-shaped curve and the pore structure of the porous medium. Emphases are placed on several critical points on the curve such as C at $I=1$, PV at $C=0.5$, PV at breakthrough, peak of the first derivative, and length of the tail.
(3) Development of an effective technique to determine the dispersivity value from the S-shaped curve or its derivative.
(4) Computer simulation of the dispersion phenomena to match capacitance model with experimental data by fixing mass transfer coefficient (M) and flow fraction (f) based on the fluids used and the derivative curve.
(5) Determination of the heterogeneity factor from well logs.
(6) Application to field logs of the approach developed here.

5.6 Nomenclature

A	cross-sectional area of the core sample, cm^2
A_e	cross-sectional area available to fluid flow defined by Cornell and Katz, cm^2
A_s	cross-sectional area of the neck leading to the stagnant pore space, cm^2
A_x	cross-sectional area available to fluid flow defined by Wyllie and Rose, cm^2
C	in-situ concentration of flowing fluid
C_f	flowing concentration of displacing fluid
C^*	in-situ concentration of stagnant fluid
d	diameter of the sample, cm
D_L	longitudinal dispersion coefficient in a porous medium, cm^2/s
D_L'	longitudinal dispersion coefficient in a tortuous capillary, cm^2/s
D_o	molecular diffusivity of fluid, cm^2/s
d_p	particle diameter, cm
f	flow fraction
F	electrical formation factor
I	pore volume number (=Vi/Vp)
I_{max}	number of pore volume corresponding to the peak of the concentration derivative curve
J	I/f
K	permeability, md
K_L	effective longitudinal dispersion coefficient in a porous medium, cm^2/sec
k_o	Kozeny shape constant
L	length of the sample, cm
L_e	length of the tortuous path in a porous medium, cm
l_s	length of the neck leading to the stagnant volume, cm
M	mass transfer coefficient, cm^2/s
p	pressure, atm
P_e	Peclet number ($=L*U/D_o$)
PV	pore volume of a rock, cc
Q	flow rate, cc/s
r_h	hydraulic radius, cm
R_o	resistivity of the rock that is fully saturated rock with brine, ohm-m
R_w	resistivity of the brine, ohm-m
S	particle surface area per unit volume, cm^2
S_o	specific surface area of the particles
t	time, sec
T	tortuosity factor ($=\tau^2$)
U	Dupuit's pore velocity, cm/s
V	Darcy velocity, cm/s
V'	pore velocity modified by Carman, cm/s
V_e	average velocity along a tortuous path, cm/s
V_i	volume of displacing fluid injected, cc
V_p	pore volume of the medium, cc

V_s	volume of the stagnant volume, cc
x	length of porous medium, cm
x_e	length of tortuous path, cm
y	x/L

Greek Letters

α_D	dispersivity, cm
γ	dimensionless dispersivity ($=V^*L/D_L$)
λ	volume modifying function
μ	fluid viscosity, cp
ϕ	porosity of the rock, %
σ	heterogeneity factor
τ	tortuosity

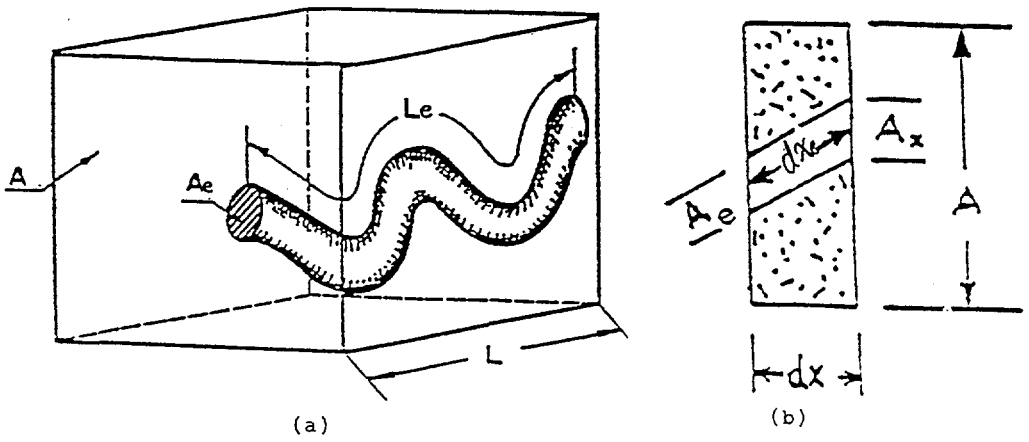

Figure 5.2.1 A Tortuous Capillary Model for a Porous Medium

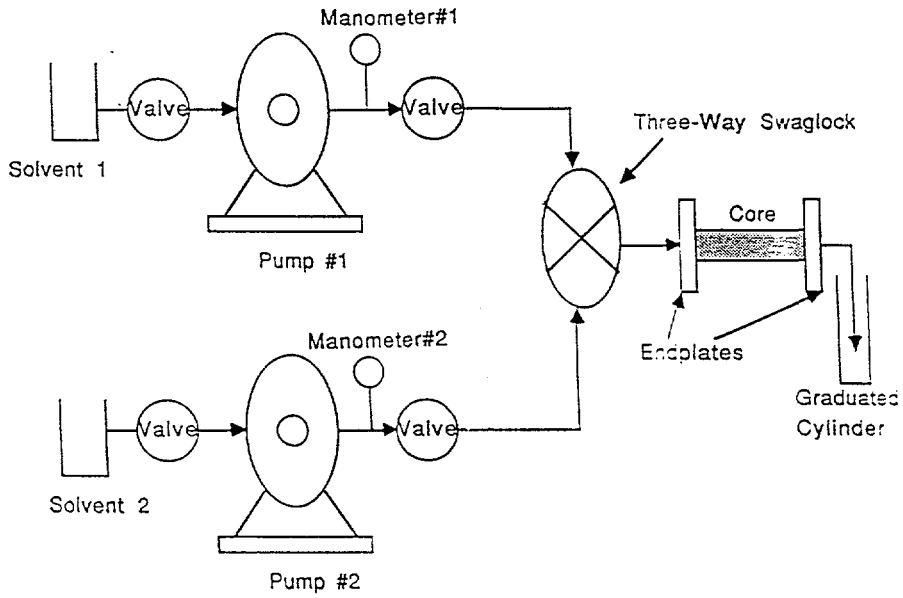

Figure 5.3.1 System Setup for Permeability Measurement and Miscible Displacement Test

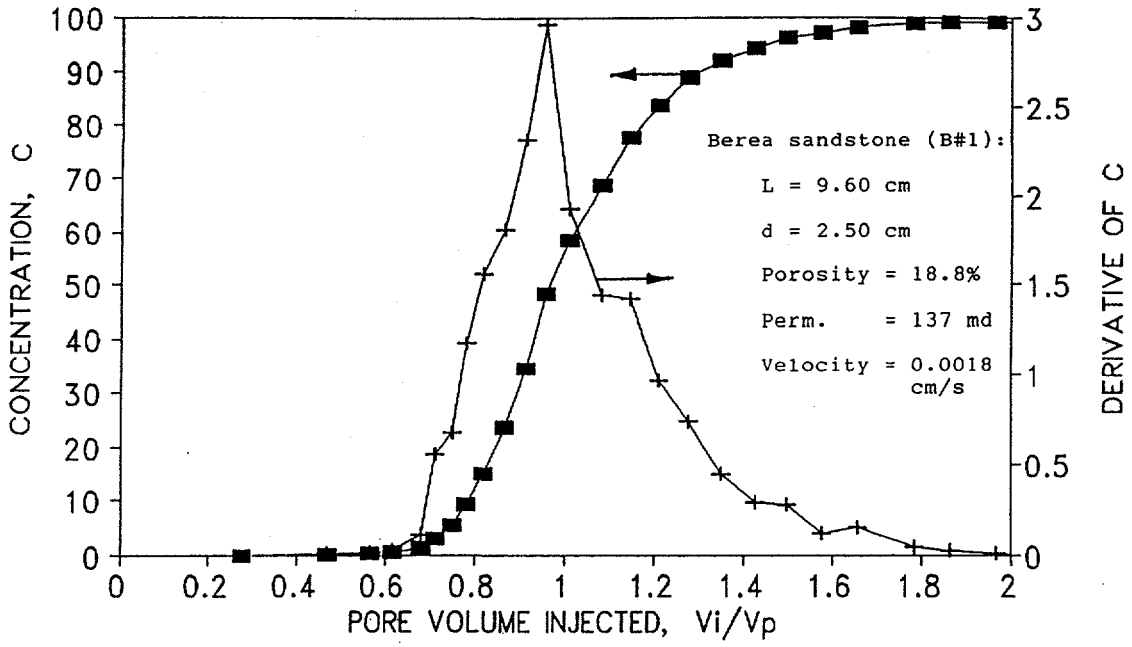

Figure 5.4.1 Concentration Profile (Core B#1)

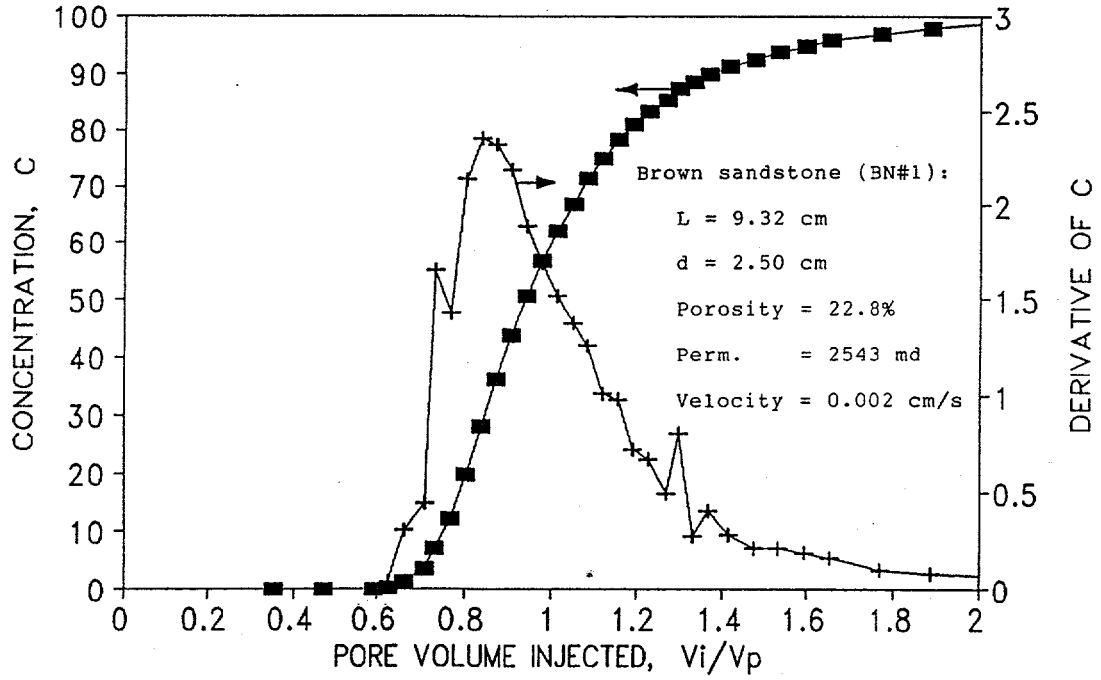

Figure 5.4.2 Concentration Profile (Core BN #1)
(Dimensionally Homogeneous Model for Berea Sandstone Plugs)

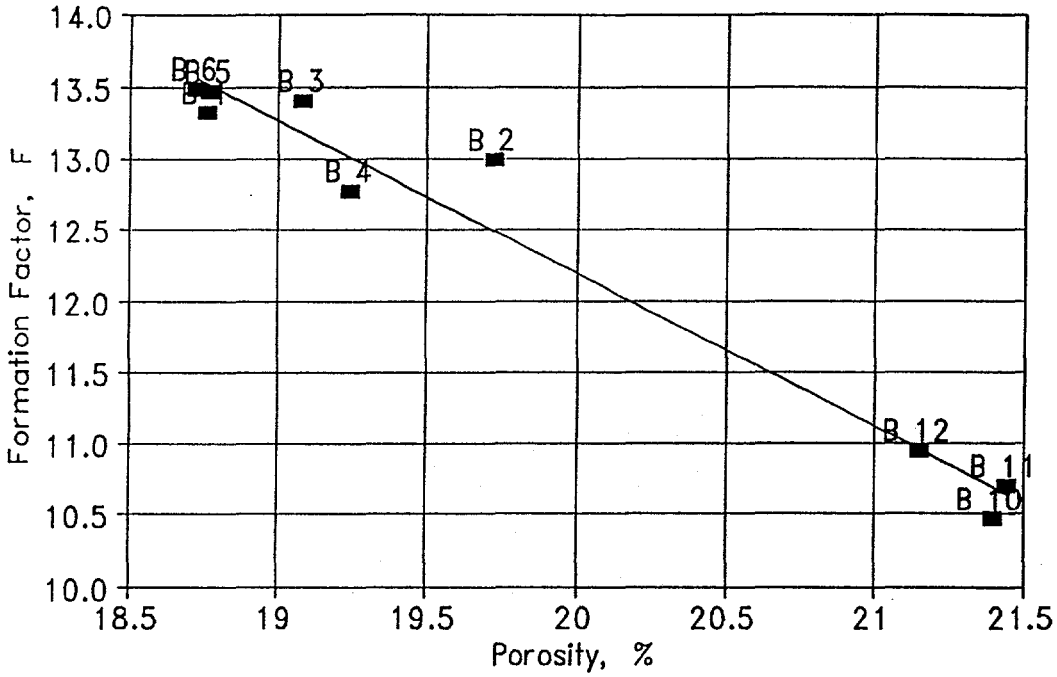

Figure 5.4.3 Formation Factor vs Porosity (Berea Sandstone)

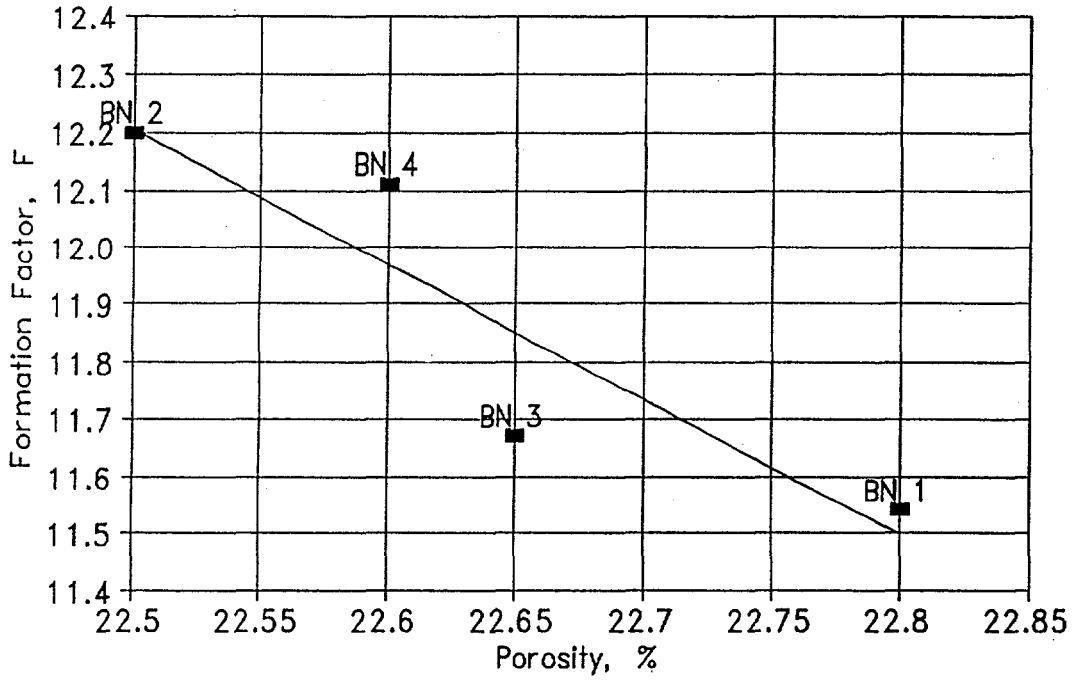

Figure 5.4.4 Formation Factor vs Porosity (Brown Sandstone)

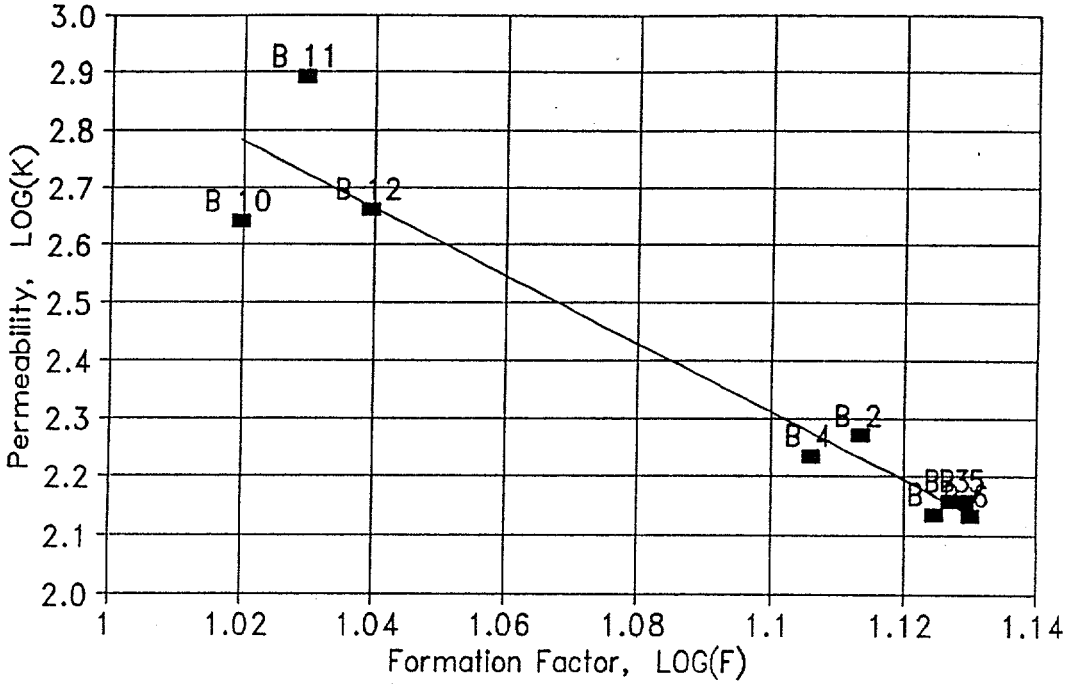

Figure 5.4.5 Permeability vs Formation Factor (Berea Sandstone)

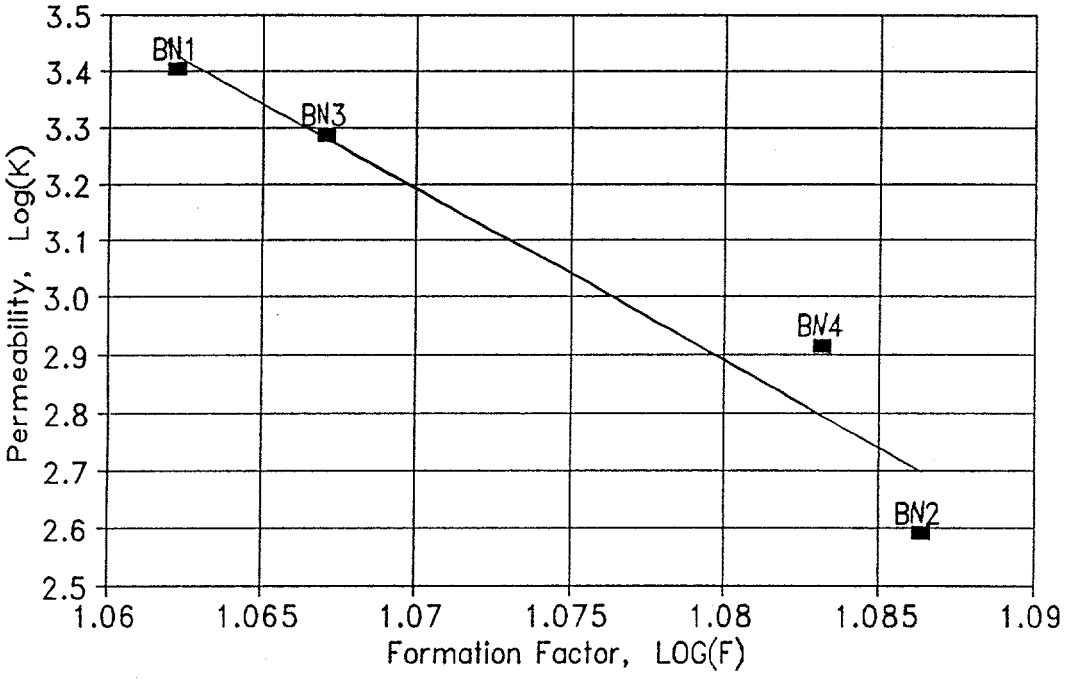

Figure 5.4.6 Permeability vs Formation Factor (Brown Sandstone)

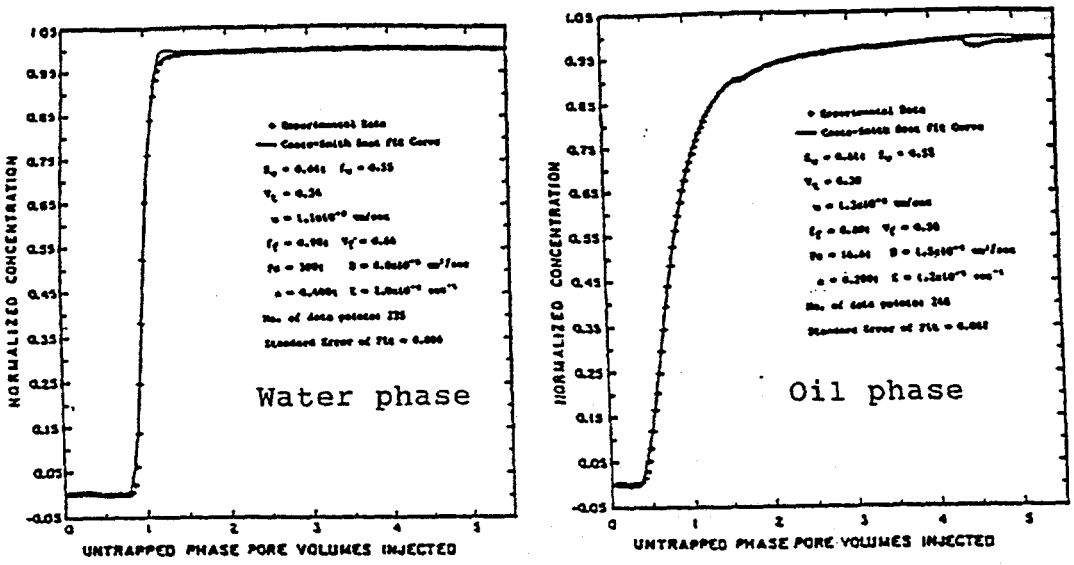

Figure 5.4.7 Concentration Profiles of Water and Oil Phases in Berea Sandstone

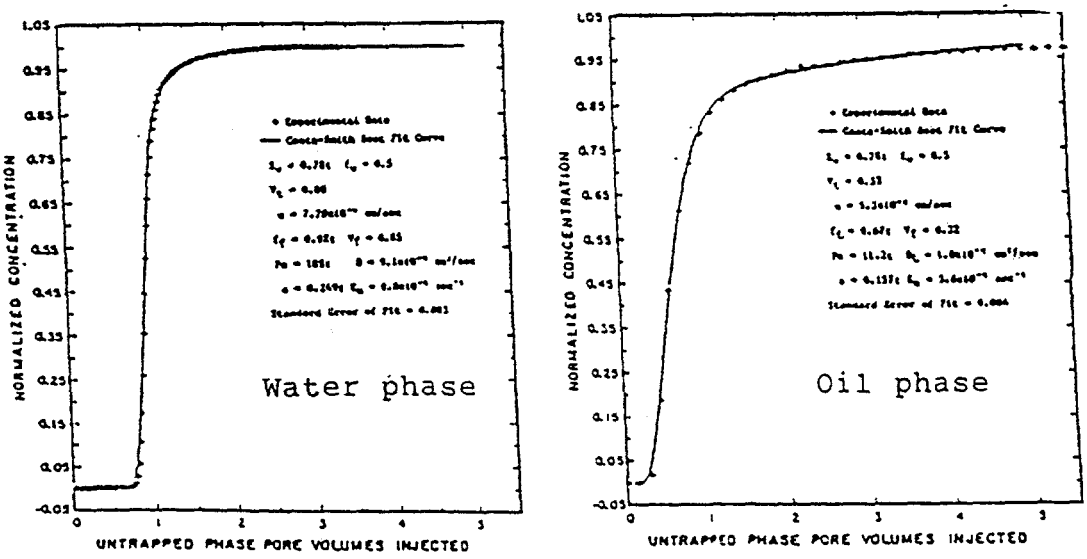

Figure 5.4.8 Concentration Profiles of Water and Oil Phases in Rock Creek Sandstone

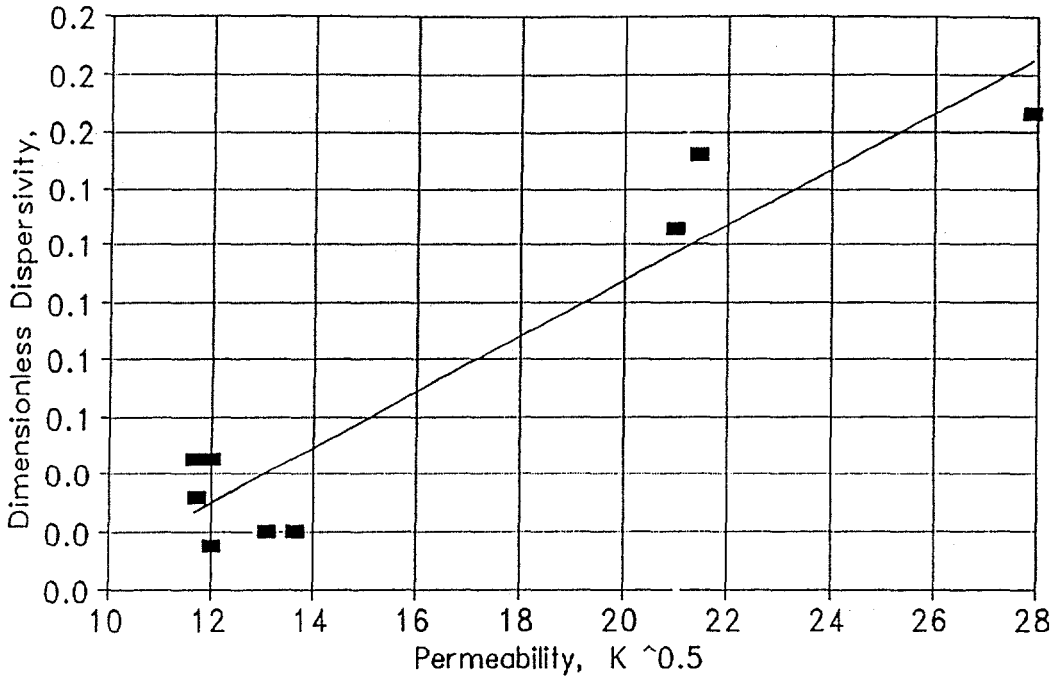

Figure 5.4.9 Dispersivity vs Permeability (Berea Sandstone)

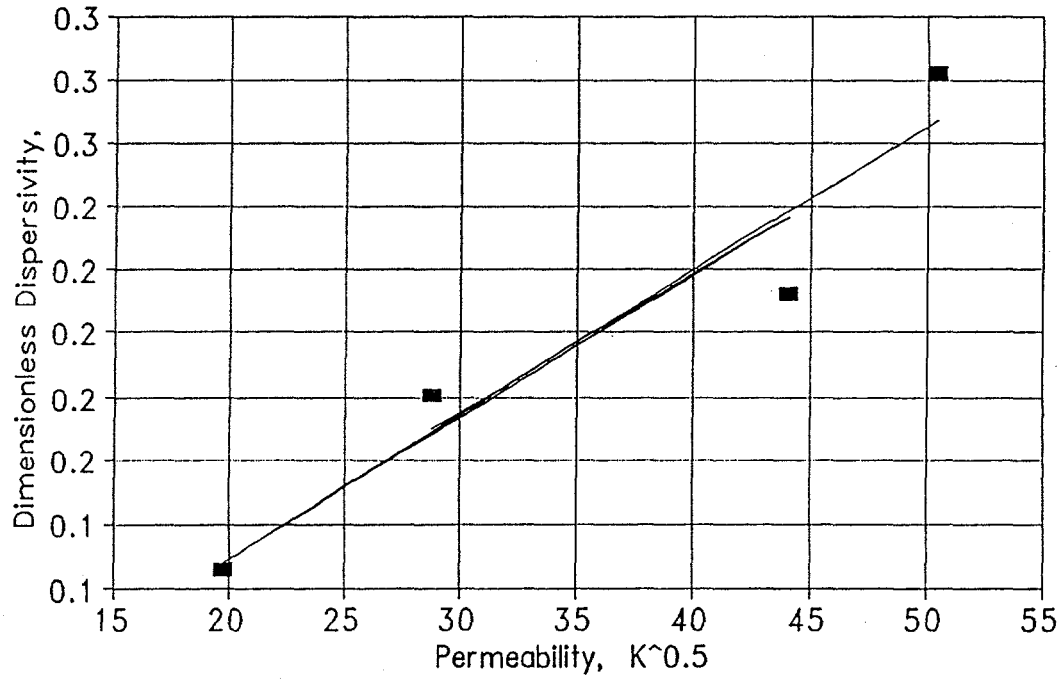

Figure 5.4.10 Dispersivity vs Permeability (Brown Sandstone)

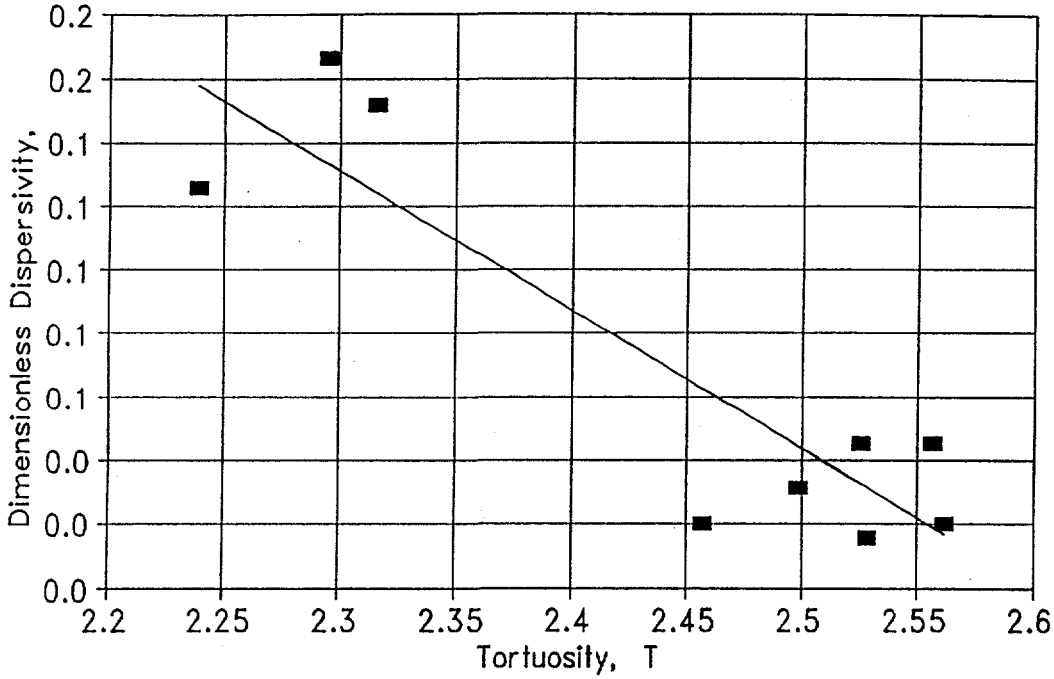

Figure 5.4.11 Dispersivity vs Tortuosity (Berea Sandstone)

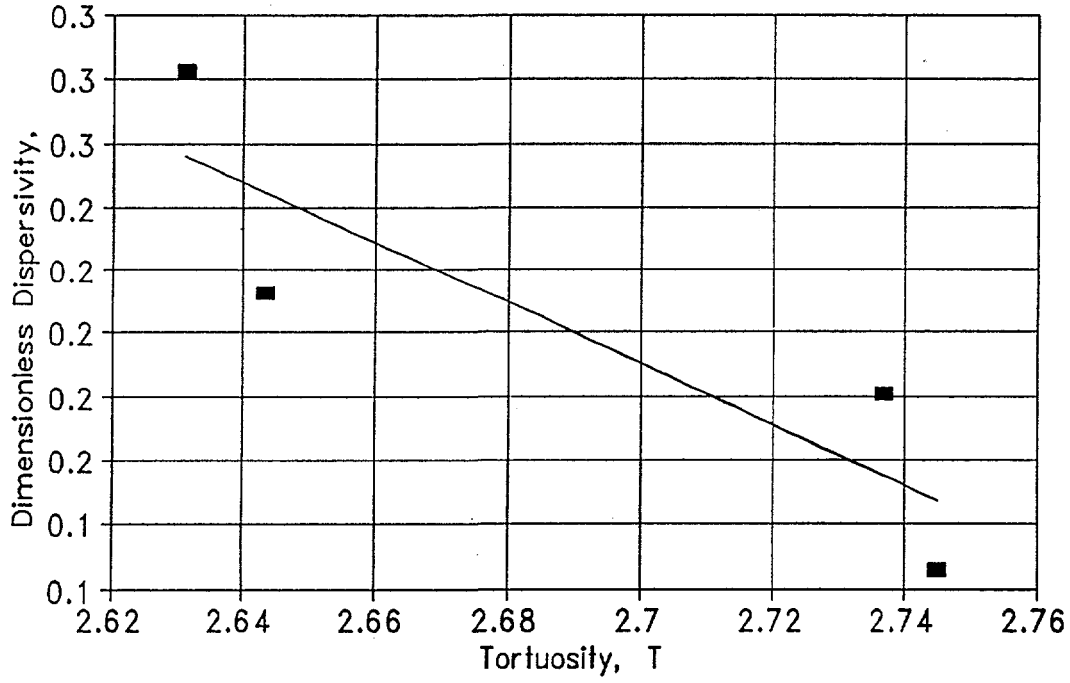

Figure 5.4.12 Dispersivity vs Tortuosity (Brown Sandstone)

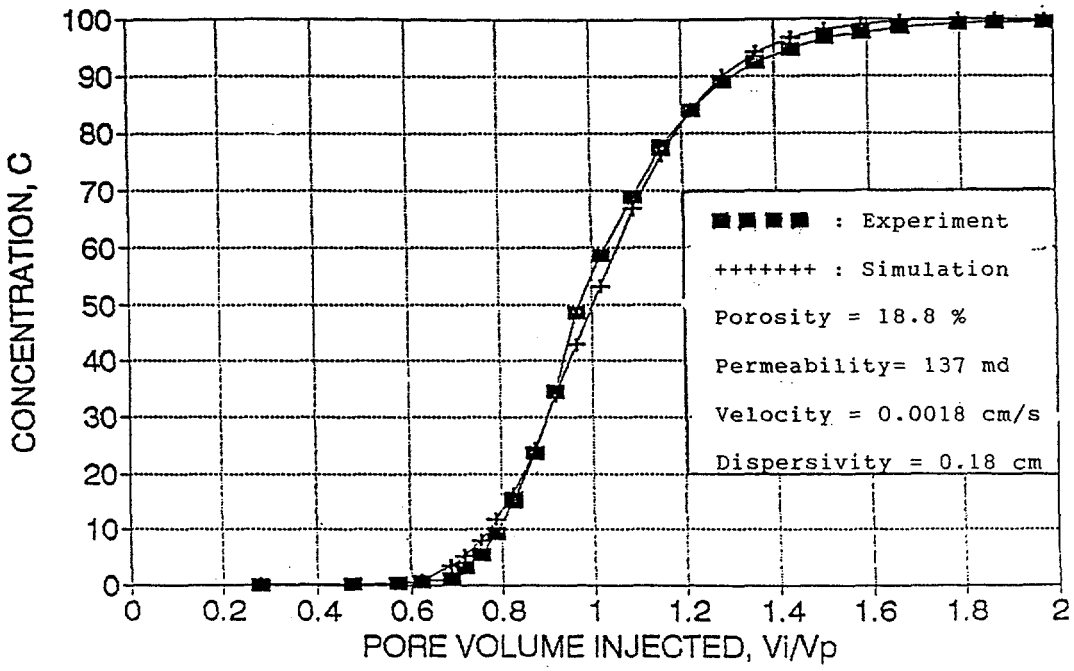

Figure 5.4.13 Concentration Profile (Core B #1)

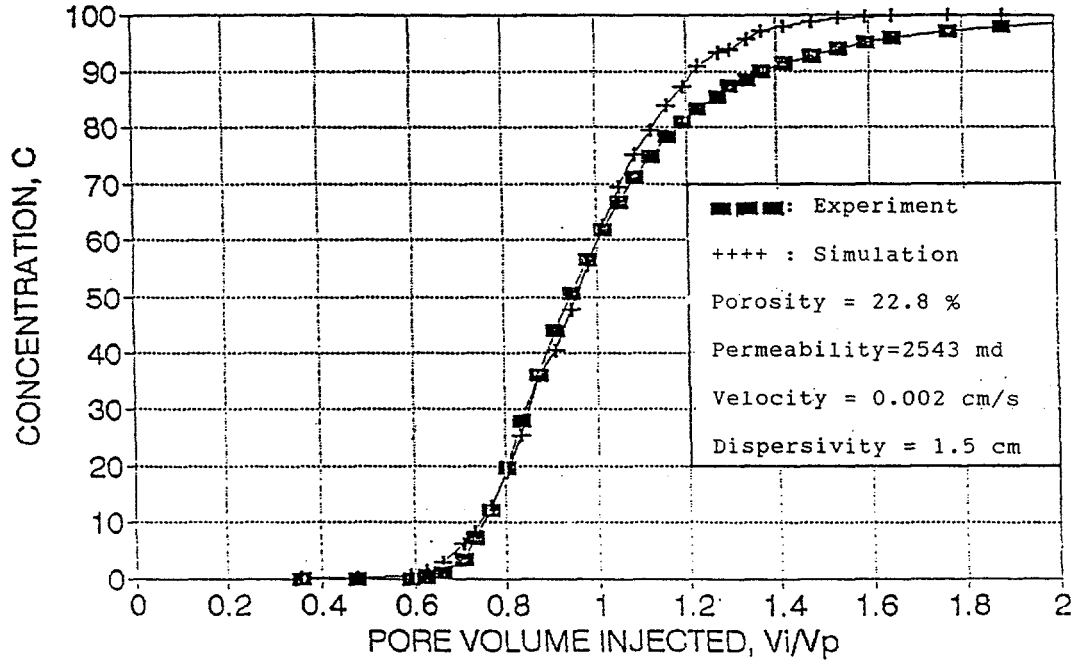

Figure 5.4.14 Concentration vs Vi/Vp (Core BN #1)

CHAPTER 6

Transverse Dispersivity in Porous Media

A new experimental apparatus has been developed to evaluate the transverse dispersivity of a consolidated porous media. Determination of transverse dispersivity involves the simultaneous injection of two miscible matched-viscosity fluids into the porous media and the subsequent measurements of the lateral effluent concentration gradients. The longitudinal and transverse dispersion coefficients of a miscible fluid system flowing through a Berea sandstone block of dimensions 12" x 12" x 2" were determined for a range of laminar Reynolds numbers. Vertical experimental runs were also conducted to examine the effect of gravity on transverse dispersion coefficients. In an effort to examine the propagation of miscible plumes in consolidated media, tracer pulses were injected into the block via a carrier fluid. The propagation of the tracer plumes were monitored at the effluent face by measuring tracer concentrations at various effluent outlets as a function of time. Flow rate measurements at various lateral locations on the effluent face provided a quantitative description of the porous media heterogeneity.

The longitudinal dispersivity of the Berea block was two orders of magnitude greater than the transverse dispersivity. This ratio has been determined to be higher than the corresponding values for unconsolidated packed bed media.

6.1 Introduction

The transverse dispersion phenomena has been studied in various engineering and scientific fields. An understanding of the mechanisms of transverse diffusion and dispersion is essential in characterization of many physical processes.

In petroleum engineering, dispersion coefficients are used to model chemical enhanced oil recovery (EOR) processes such as miscible floods and viscosity graded polymer floods, and are often the input parameters of simulators. Dispersion coefficients also play a significant role in several other areas including heat transfer, determination of the extent of groundwater contamination plumes, contaminant transport in porous media, radioactive waste injection, porous catalysts and chemical reactors.

Dispersion of fluids in a porous media flow has two components: longitudinal (in the direction of flow) and transverse (perpendicular to the direction of flow). Transverse dispersion is therefore an indication of mass transport perpendicular to a uni-directional flow in porous media. Transverse dispersion can occur perpendicular to the mean flow path horizontally and/or vertically. The horizontal component of transverse dispersion (also referred to as lateral or radial dispersion) is the focus of this study. The combined effects of gravity and vertical transverse dispersion are also investigated in this research project.

There are three factors contributing to transverse dispersion of miscible fluids in a porous media: transverse molecular motion, porous media heterogeneity, and structural and mechanical effects.

The intertwining or wandering of the flow paths in a porous medium is the major contributor to transverse dispersion. The streamlines in an interconnected pore space merge and separate (i.e., tangle) creating a kinematic mechanism of dispersion perpendicular to the flow direction. A dynamic mechanism also exists: when a flow passage divides into two or more flow paths, the velocity of the fluid in each path will be dependent on the local pressure gradients and the hydraulic conductivity of each flow path. A porous media under the above two mechanisms (tangling of the pore space and local velocity variations within the media) may be thought of as a static mixer; fluids mix, due to mechanical and structural effects, when they flow simultaneously in a porous media. Intuitively one expects porous media with higher coordination numbers (the number of pore throats emanating from a pore body) to exhibit greater transverse dispersion since at high coordination numbers, stream splitting becomes more significant.

The mechanism of transverse dispersion at high flow rates is dominated by the flow parameters and the structure of the porous media and influenced slightly, if at all, by molecular diffusion. At low flow rates, on the other hand, the mechanism is entirely due to molecular motion. At low velocities the longitudinal and transverse dispersion coefficients merge; at zero velocity they converge to the molecular diffusivity and mixing will be exclusively dominated by molecular diffusion. At high Reynolds numbers the transverse dispersion coefficient exhibits a linear relationship with flow velocity [see results].

The dispersion process can have both beneficial and detrimental effects in engineering process designs. In chemical EOR, slugs of solvents are injected to improve oil recovery. Transverse dispersion of a solvent slug in the resident fluid will increase the areal domain of influence of the slug, improving oil recovery. However, if the slug disperses too much, its concentration falls below what is required for mobilization of residual oil. Knowledge of dispersion coefficients then becomes a crucial tool in designing optimum slug sizes. Another process in which transverse dispersion has a detrimental effect is mixing of contaminants in groundwater. Dispersion coefficients are used in computer programs to predict contaminant concentrations in groundwater at distances away from contamination sources. Transverse dispersion is also instrumental in suppression of viscous fingers in viscosity graded polymer floods providing more efficient displacements. Also, when oil is displaced by a fluid of lesser density, the displacing fluid may override the oil phase and create a gravity tongue. Transverse dispersion at the interface of the bulk fluid and the gravity tongue will result in a more efficient displacement.

6.2 Experimental Procedures

The miscible fluid system used in this study consisted of naphtha and a mixture of 53% iso-octane and 47% o-xylene (from here on referred to as "isoxy"). Isoxy has viscosity similar to naphtha; their densities are within 7% of each other. There is also a wide difference in the refractive indices of the two fluids, making them an excellent fluid system choice for unit mobility ratio miscible displacements. Table 6.2.1 provides a summary of the fluid properties.

Table 6.2.1. Fluid Properties at 73°F.

FLUID	DENSITY	VISCOSITY	REFRACTIVE
O-xylene	0.889	0.71	1.5042
Iso-octane	0.699	0.45	1.3906
Isoxy	0.789	0.53	1.4451
Naphtha	0.736	0.53	1.4150

The porous media in this experiment was a block of consolidated Berea sandstone with dimensions of 1 ft x 1 ft x 2 in. The block was coated with J B Weld. Two 2 in x 1 ft sides were designated as inlet and outlet sides and were mounted by reducer fittings prior to coating with J B Weld. The block and the inlet and outlet fitting assemblies were subsequently leak tested under CO_2 pressures of up to 5.5 psi. Table 6.2.2 is a summary of the porous media properties.

Table 6.2.2. Summary of the Rock Properties.

Permeability	541 md
Porosity	23%
Pore Volume	1109.2 cc
Bulk Volume	4816.5 cc
Bulk Density	2.02 g/cc

Measurement of the transverse dispersion coefficients involves the co-injection of the two fluids. For the vertical transverse dispersion runs the apparatus was set up vertically with the denser fluid (isoxy) injected from the top. Longitudinal dispersion runs were conducted using one fluid to displace the other through all inlets. To obtain a measure of plume propagation, fluid pulses were injected into the middle inlet using a syringe with the other fluid acting as carrier. The concentration profiles were measured at the outlets. To obtain outlet samples, three different methodologies were incorporated: (1) the outlet fitting assembly, (2) fluid collection system (trough), and (3) sample collection rack. Figures 6.2.1 through 6.2.4 are schematic diagrams of the apparatus.

6.3 Experimental Results

The apparatus was used to conduct a total of forty five (45) experimental runs. An identification of the 5 categories of runs follows:

L longitudinal dispersion run

P pulse injection run

T transverse dispersion run
V vertical transverse dispersion run
R outlet rate determination run

The experimental runs were conducted at nine (9) different flow rates. All runs were conducted at laminar flow.

Figures 6.3.1 and 6.3.2 are typical longitudinal dispersion runs. Figures 6.3.3 and 6.3.4 summarize the outlet flow rate data, and Figures 6.3.5 and 6.3.6 are pulse injection runs. Figures 6.3.7 and 6.3.8 are horizontal transverse dispersion runs, and Figures 6.3.9 and 6.3.10 are typical vertical transverse dispersion runs where the effect of density on transverse dispersion coefficients is quantified.

The calculated dispersion coefficients for each Reynolds number are presented in Table 6.3.1. The subscripts l, t, and v refer to longitudinal, transverse, and vertical dispersion coefficients, respectively. The reported values are in 100 cm^2/sec.

Table 6.3.1 The Calculated Dispersion Coefficients.

Re * 100	D_l * 100	D_t * 100	D_v * 100
0.280	0.211	0.0024	0.0037
0.517	0.327	0.0034	0.0040
0.805	0.776	0.0045	0.0055
0.987	0.808	0.0057	0.0071
1.210	0.940	0.0081	0.0082
1.380	1.163	0.0101	0.0090
1.551	1.205	0.0106	0.0108
1.674	1.240	0.0128	0.0127
1.857	1.310	0.0148	0.0125

Figure 6.3.11 is a plot of the mixing zone length as a function of flow rate. Figure 6.3.12 is a plot of the longitudinal and transverse dispersion coefficients, and Figure 6.3.13, the ratio of these coefficients versus Reynolds Number. Figures 6.3.14 and 6.3.15 are the plots of the horizontal and vertical transverse dispersion coefficients and their ratios as a function of Reynolds Number. Figures 6.3.16 through 6.3.17 are the longitudinal, transverse, and vertical transverse dispersivity plots, respectively.

The following is a summary of the results:
Longitudinal dispersion coefficients, D_l: 2.11×10^{-3} - 1.31×10^{-2} cm^2/sec
Transverse dispersion coefficients, D_t: 2.37×10^{-5} - 1.48×10^{-4} cm^2/sec
Longitudinal dispersivity, α_l: 0.31 cm
Transverse dispersivity, α_t: 3.4×10^{-3} cm
Dispersion coefficient ratio, D_l / D_t: 88 - 172
Dispersivity ratio, α_l/α_t: 91

The magnitudes of the measured transverse dispersion coefficients in this study are in general agreement with the literature regardless of whether a consolidated porous media or a packed bed was used. There does not appear to be any significant differences between the consolidated and unconsolidated media transverse dispersion coefficients. This study's measured transverse dispersion values, however, are smaller than the field measurement ranges. Also, the measured transverse dispersivity is much smaller than the field values. This is probably due to large scale heterogeneities in the field.

The measured D_l/D_t range of 88-172 is higher than the presented values in the literature. This is probably due to the clusters of small diameter pores that exist in the consolidated porous media but are absent in packed beds of uniformly distributed grains. The steady state determinations of transverse dispersion coefficients are less likely to be affected by these heterogeneities (including dead end pores) than the longitudinal component of dispersion. Longitudinal dispersion is governed by the local pore velocities, and are highly dependent on the clusters of fine pores and dead end pores. Therefore, the Berea block's heterogeneities probably caused the elevation of the measured D_l/D_t ratios.

6.4 Impact on the Industry

The findings of this study can potentially impact the practices of the industry in several ways. The following is a brief outline of how the results of this study can further our understanding of the involved physical phenomena, improve the designs of EOR processes, and enhance flow modeling.

The measured dispersion coefficients can impact the design of miscible EOR processes. In a large scale oil recovery project, even the smallest changes in the input design parameters can translate into significant financial gains or losses. The presented dispersion coefficients in this study, represent the most accurate and reliable values for Berea sandstones of similar permeability; incorporating them in the design process can greatly improve the overall performance of miscible floods.

The qualitative findings of the pulse injection experiments can help model the mixing and dilution of miscible slugs. The fact that the slugs in the experimental runs did not travel significant transverse distances from the axis of injection, can provide some insight into the expected areal sweeps of the slugs and their subsequent dilution as a result of this slight transverse dissipation. This would in turn aid the engineers in determining the optimum slug sizes.

Packed bed correlations for dispersion coefficients have been used in the literature for the design of viscosity graded polymer floods. These correlations can provide erroneous criteria for

suppression of viscous fingers. The sandstone dispersion coefficients measured in this study can enhance the quality of these designs by providing more realistic values for the dispersion coefficients.

In processes where oil is displaced by a fluid of lesser density, and a gravity tongue has been created, the measured dispersion coefficients can provide a more accurate description of mass transfer across the interface of the two fluids and help predict the system's behavior.

Dispersion coefficients are often the input of simulators and various computer flow models. The presented values can potentially have an impact on the performance of these models.

The presented longitudinal to transverse dispersivities ratio is an order of magnitude greater than the value used most commonly in groundwater contamination models. For consolidated media, the presented α_l/α_t ratio will provide a more realistic contamination plume boundary in the transverse direction of flow.

The presented data for the vertical transverse dispersion coefficients for fluids of different densities (D_v /D_t of 1.5 for the low velocity range) can help model the movement of DNAPLs (dense non aqueous phase liquids) in moving groundwater.

6.5 Conclusions

(1) An experimental apparatus and protocol capable of measuring the transverse dispersion coefficients of consolidated porous media has been developed.

(2) Longitudinal and transverse dispersion coefficients for a Berea sandstone block were measured for a range of Reynolds numbers. The dispersion coefficients were linear functions of Reynolds numbers. The straight line relationship suggests that for the experimental flow range, the effect of molecular diffusion was negligible. The longitudinal and transverse dispersivities were also determined.

(3) Although the longitudinal and transverse dispersion coefficients and the mixing profiles are functions of flow rate, the boundaries of the mixing zones are not. For longitudinal dispersion, in other words, for a given pore volume of injection, the length of the mixed zone is independent of flow rate. For transverse dispersion, the average transverse mixing zone is estimated to be $\sim$7 cm wide, independent of flow rate.

(4) Gravity shifts the transverse s-shaped curve downward. The mixing zone length, however, is unaffected. At high flow rates inertia becomes more significant and the effect of gravity is diminished. The dispersion coefficients, hence, approach the horizontal values. At high flow rates the system responds more closely to the ideal behavior.

(5) The peak concentrations of the plumes do not deviate from the slug injection axis. Also, dissipation of slugs in the transverse direction is small.

(6) It is postulated that dispersivity is not only a function of media characteristics, but also depends on flow parameters. This postulate, however, was not validated by the results in the experimental flow range.

(7) The stepwise secondary response of the longitudinal runs, the trailing edges of the pulse injection curves, and the obtained transverse profiles indicate the presence of non-random distribution of clusters of small diameter pores. However, the porous media used in this study is only mildly heterogeneous with respect to layering.

6.6 Nomenclature

C	concentration, mg/liter
C_i	injection concentration, mg/liter
D_l	longitudinal dispersion coefficient, cm^2/sec
D_t	transverse dispersion coefficient, cm^2/sec
D_v	vertical transverse dispersion coefficient, cm^2/sec
k	permeability, md
PV	pore volume, cm^3
Q	total flow rate, cm^3/sec
u	interstitial velocity, cm/sec

Greek Letters

α_l	longitudinal dispersivity, cm
α_t	transverse dispersivity, cm
ϕ	porosity, %

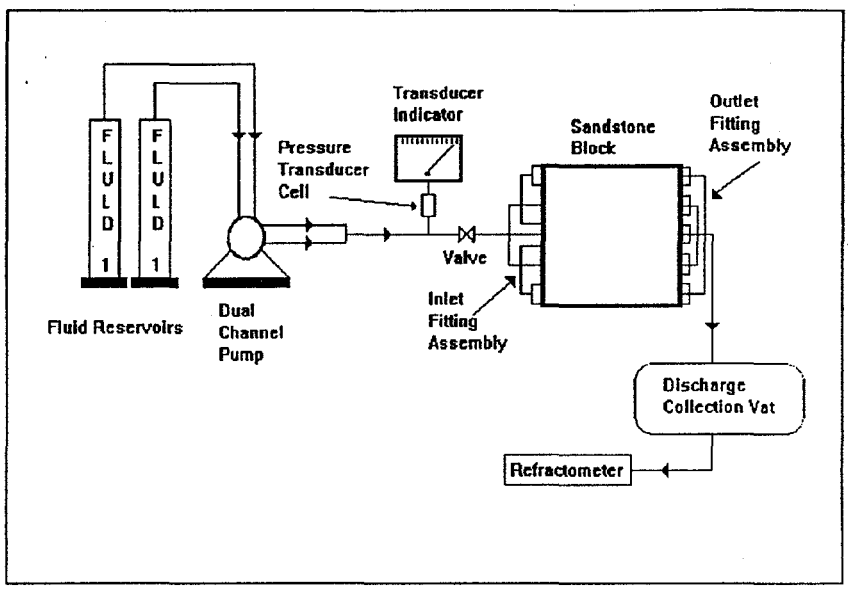

Figure 6.2.1 Schematic Diagram of the Apparatus with the Fitting Assemblies/Longitudinal Dispersion

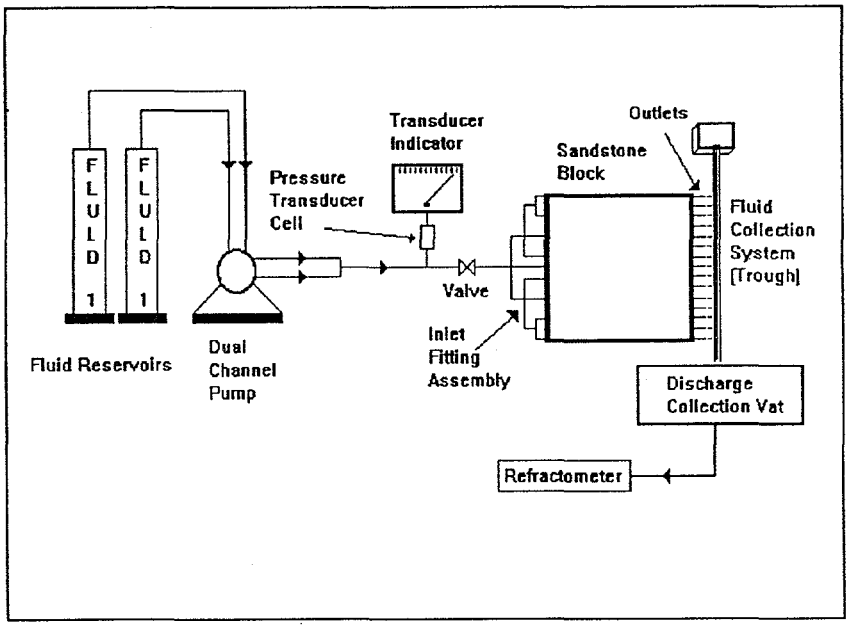

Figure 6.2.2 Schematic Diagram of the Apparatus with the Fluid Collection System

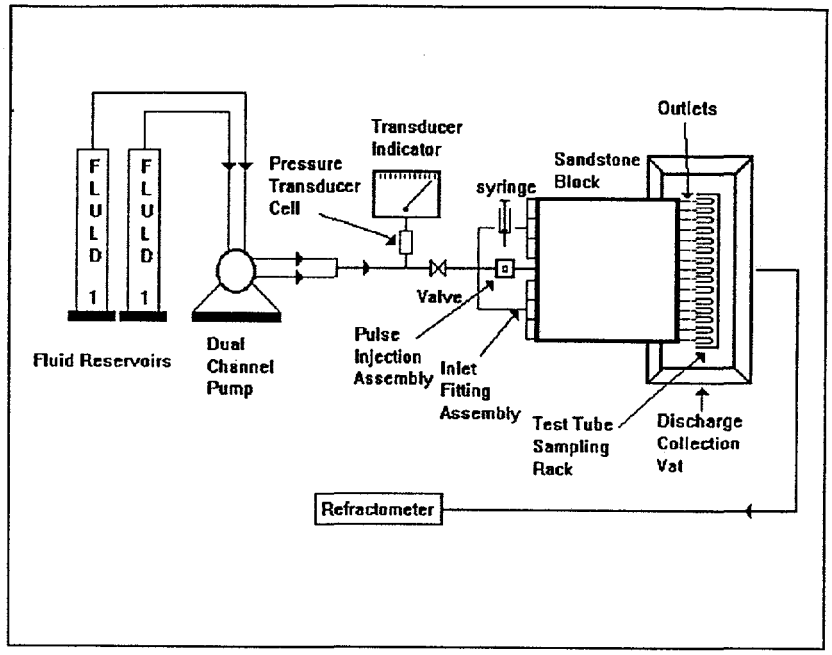

Figure 6.2.3 Schematic Diagram of the Apparatus with Pulse Injection Assemblies/Sample Collection Rack

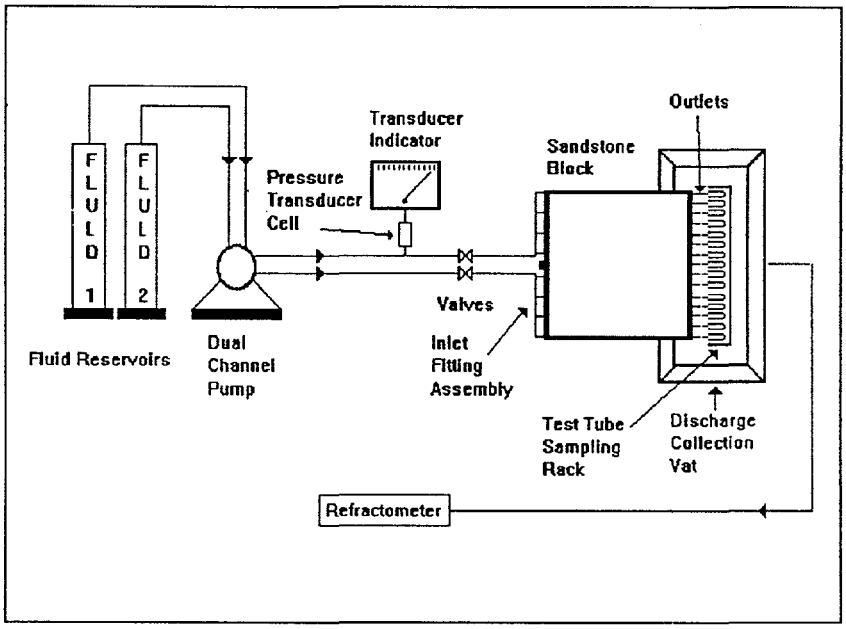

Figure 6.2.4 Schematic Diagram of the Apparatus/Transverse Dispersion Runs

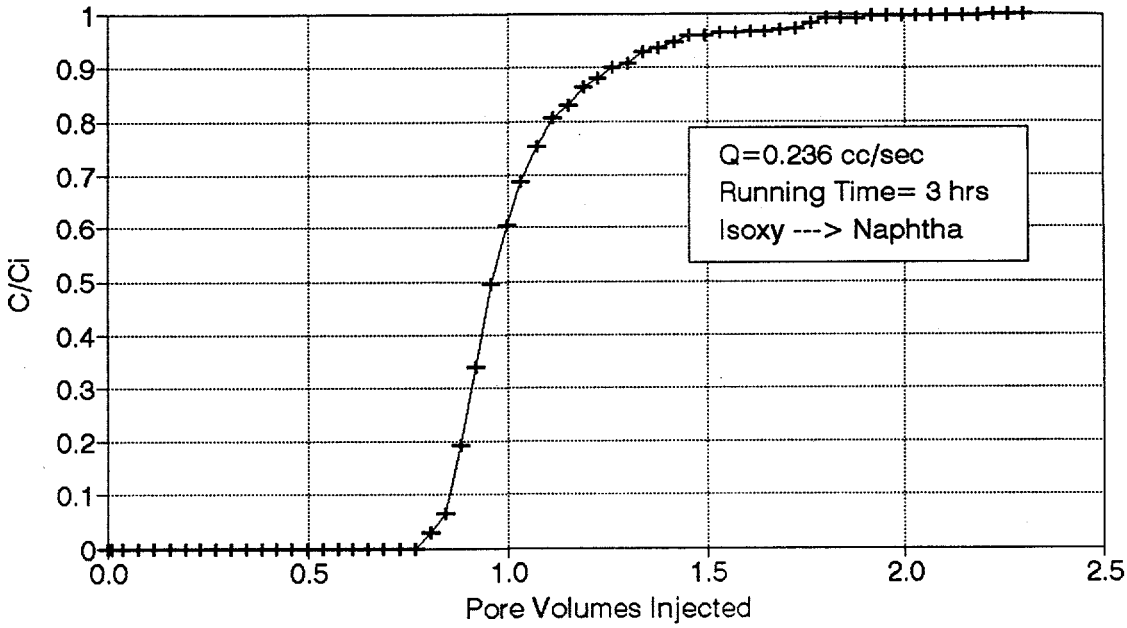

Figure 6.3.1 Longitudinal Dispersion (Run -1L)
K=541 md; ϕ =23%; PV=1109.2 cc

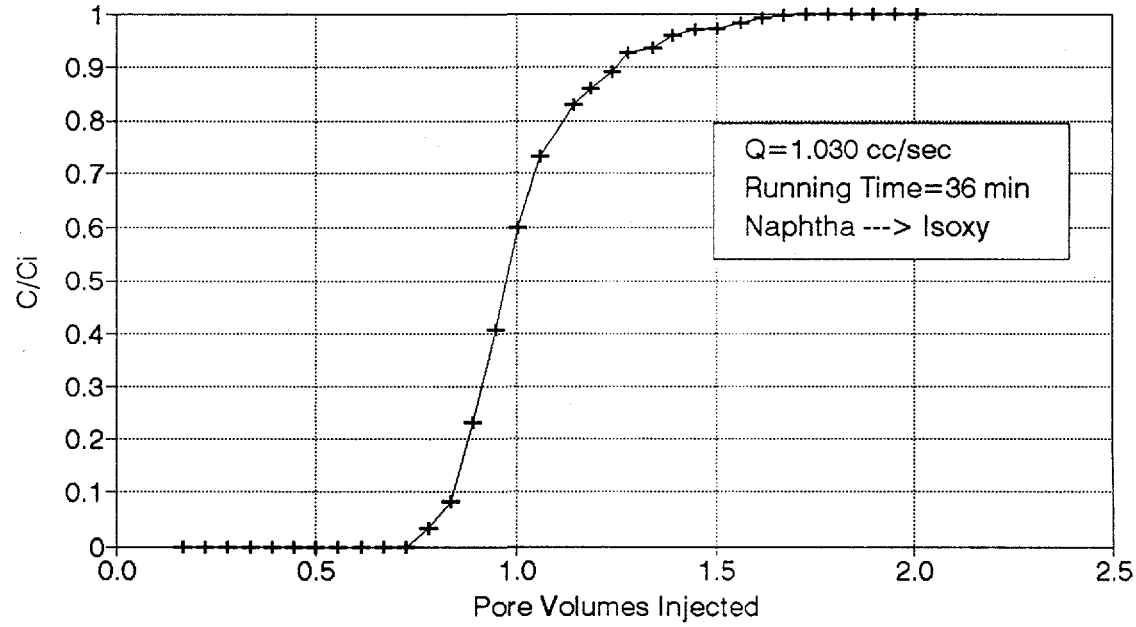

Figure 6.3.2 Longitudinal Dispersion (Run-5L)
k = 541 md; ϕ = 23%; PV = 1109.2 cc

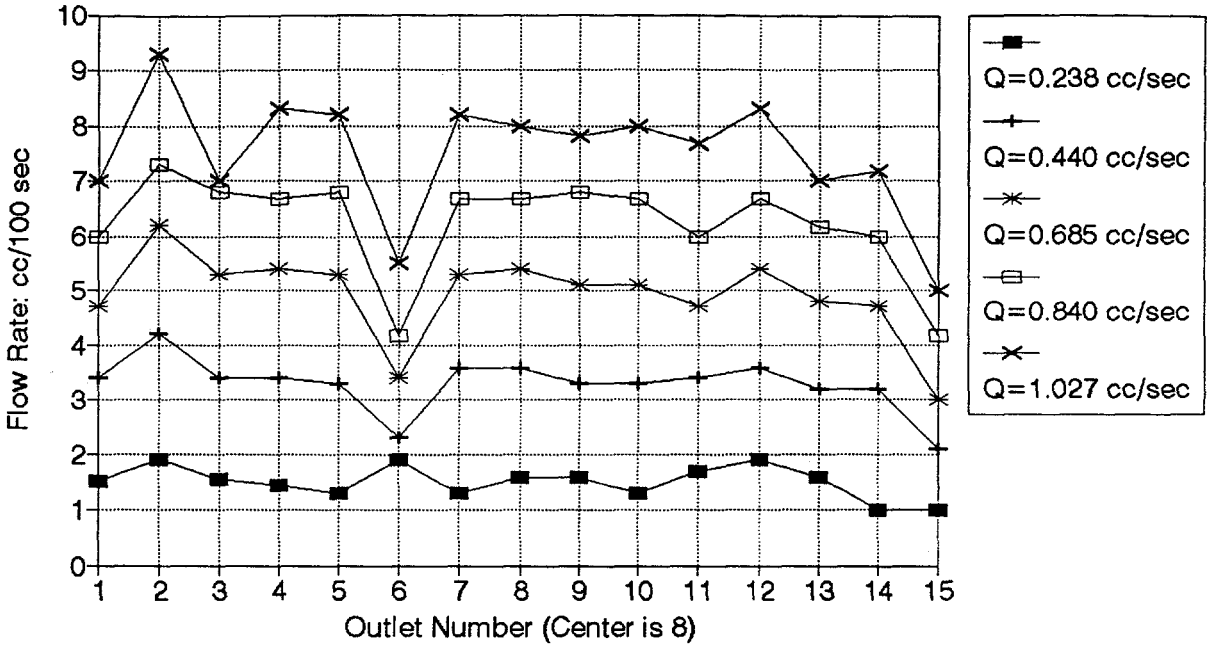

Figure 6.3.3 Outlet Flow Rates
K=541 md; ϕ =23%; PV=1109 cc

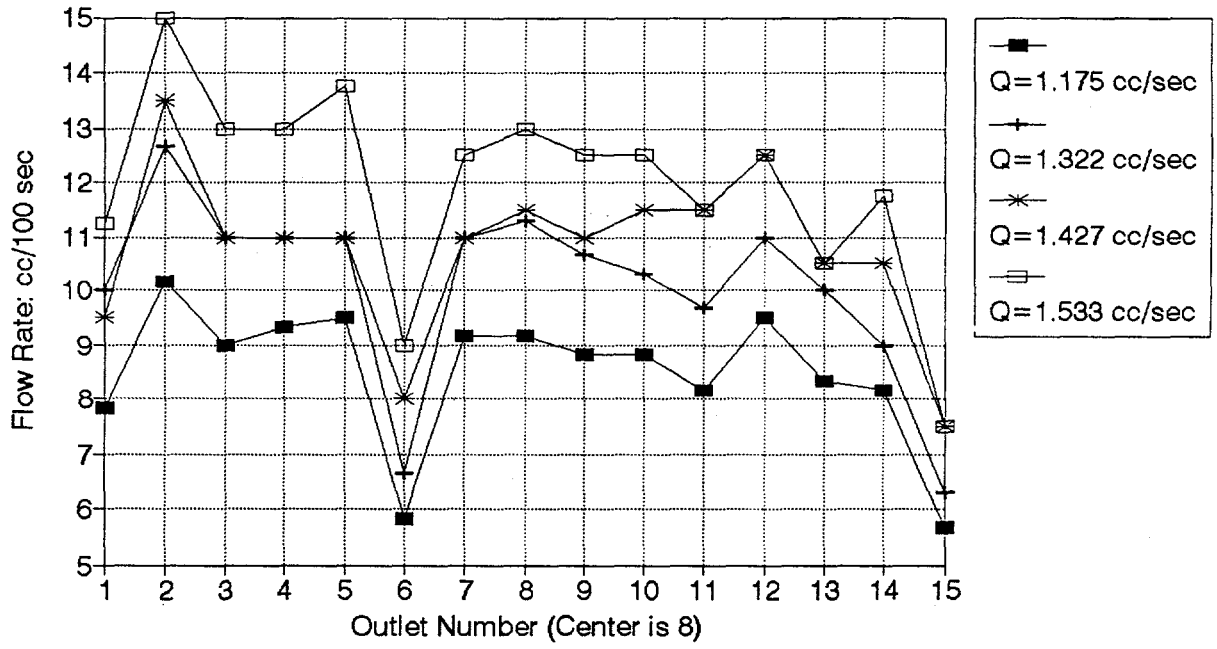

Figure 6.3.4 Outlet Flow Rates
k = 541 md; ϕ = 23%; PV = 1109 cc

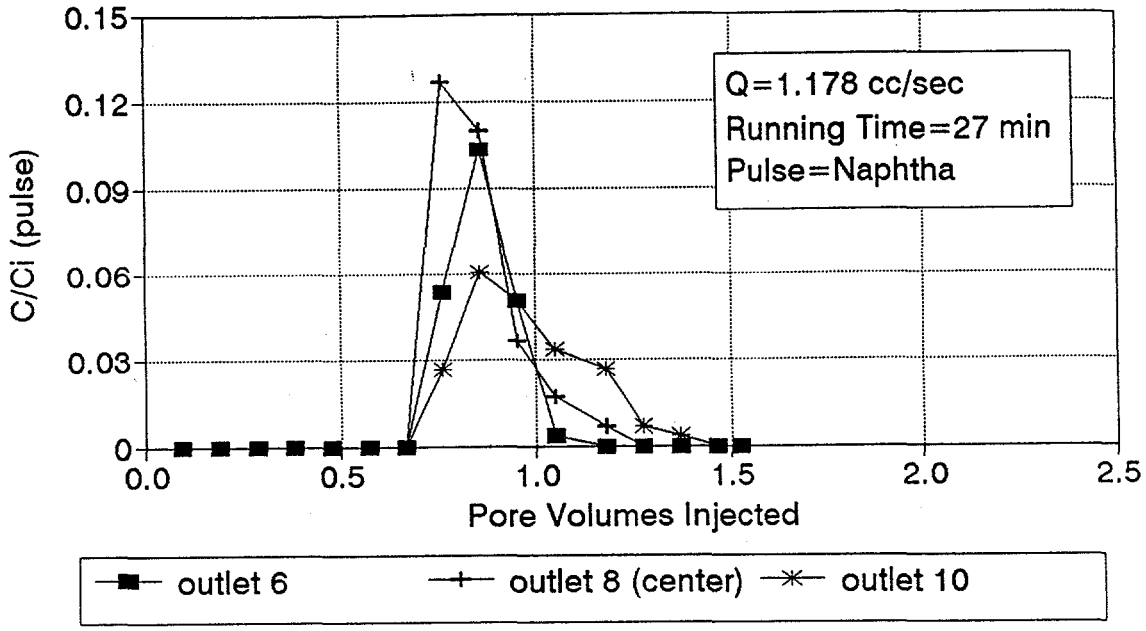

Figure 6.3.5 Pulse Injection (Run-6P)
K=541 md; ϕ =23%; PV=1109.2 cc

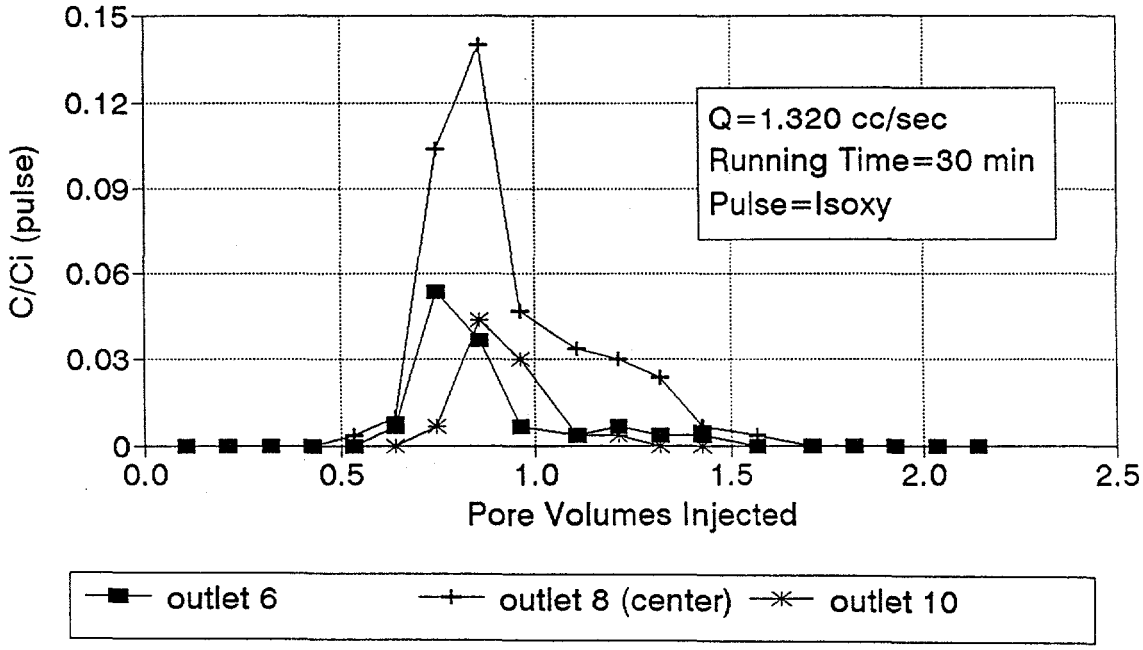

Figure 6.3.6 Pulse Injection (Run-7P)
k = 541 md; ϕ = 23%; PV = 1109.2 cc

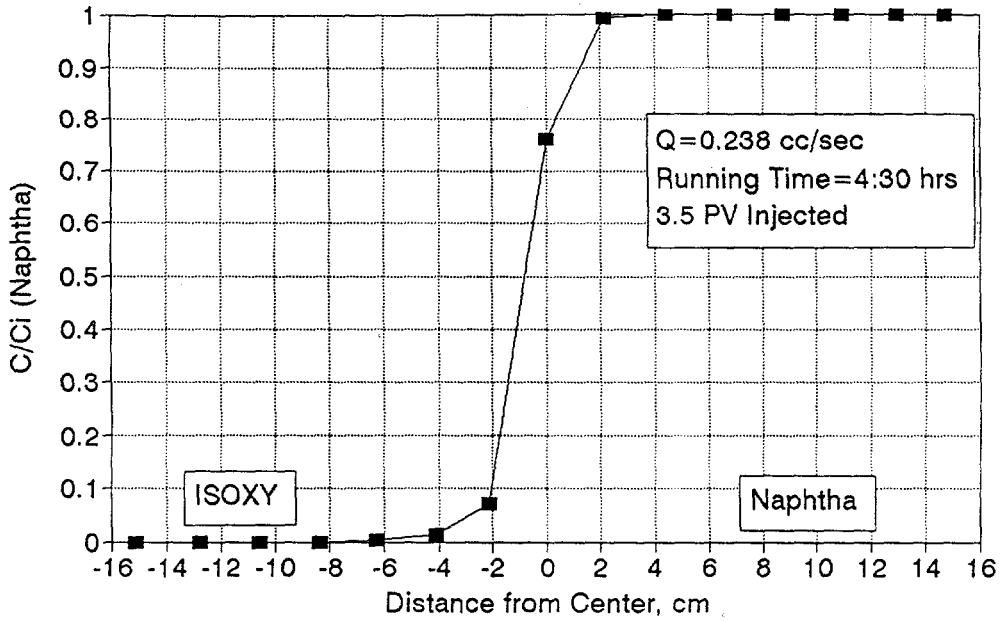

Figure 6.3.7 Transverse Dispersion (Run-1T)
K=541 md; ϕ =23%; PV=1109 cc

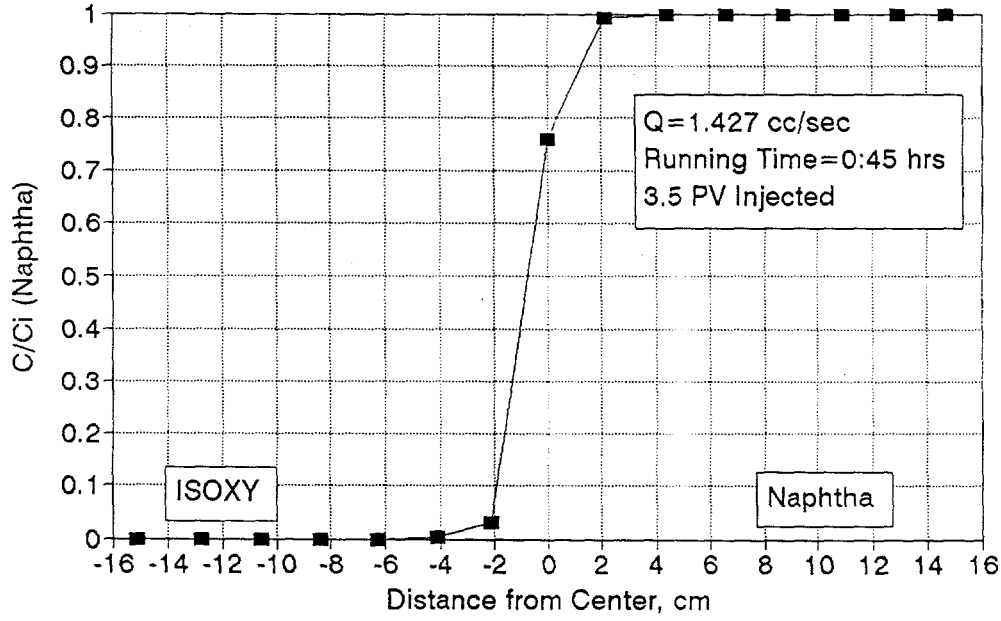

Figure 6.3.8 Transverse Dispersion (Run-8T)
k = 541 md; ϕ = 23%; PV = 1109 cc

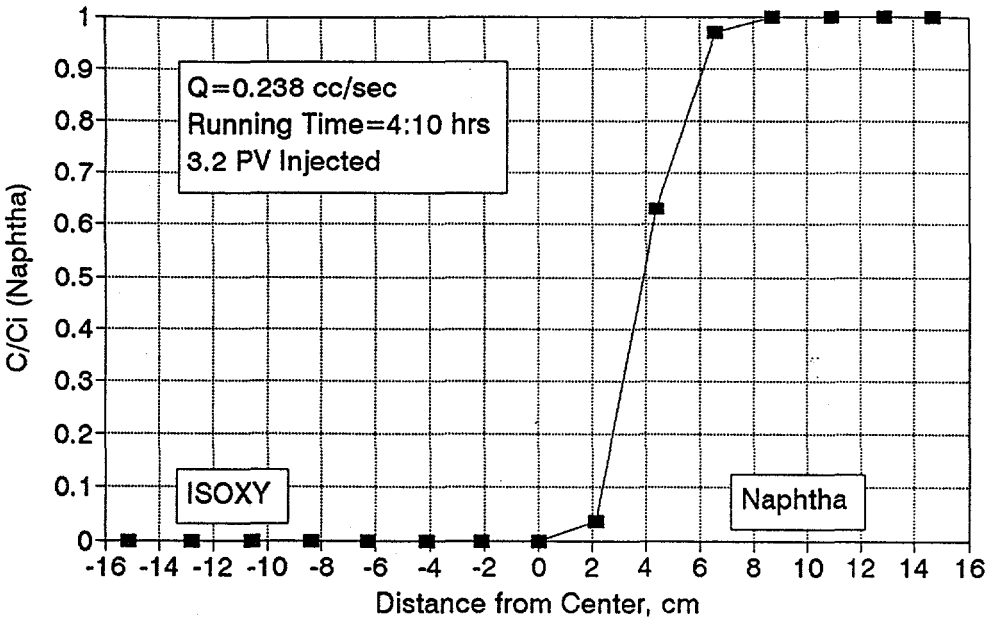

Figure 6.3.9 Vert X-Verse Dispersion (Run-1V)
K=541 md; ϕ =23%; PV=1109 cc

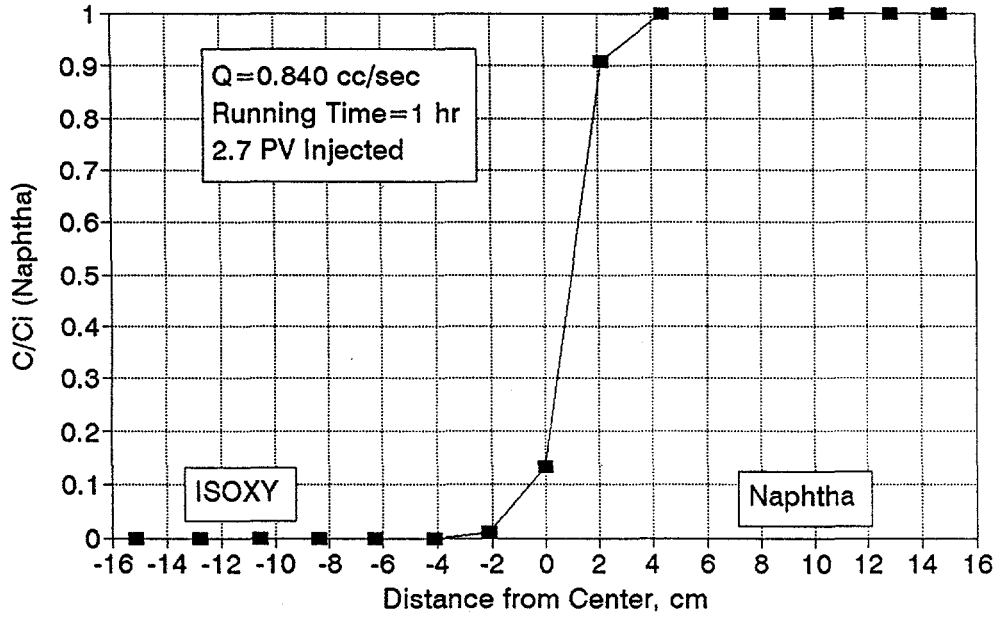

Figure 6.3.10 Vert X-Verse Dispersion (Run-4V)
k = 541 md; ϕ = 23%; PV = 1109 cc

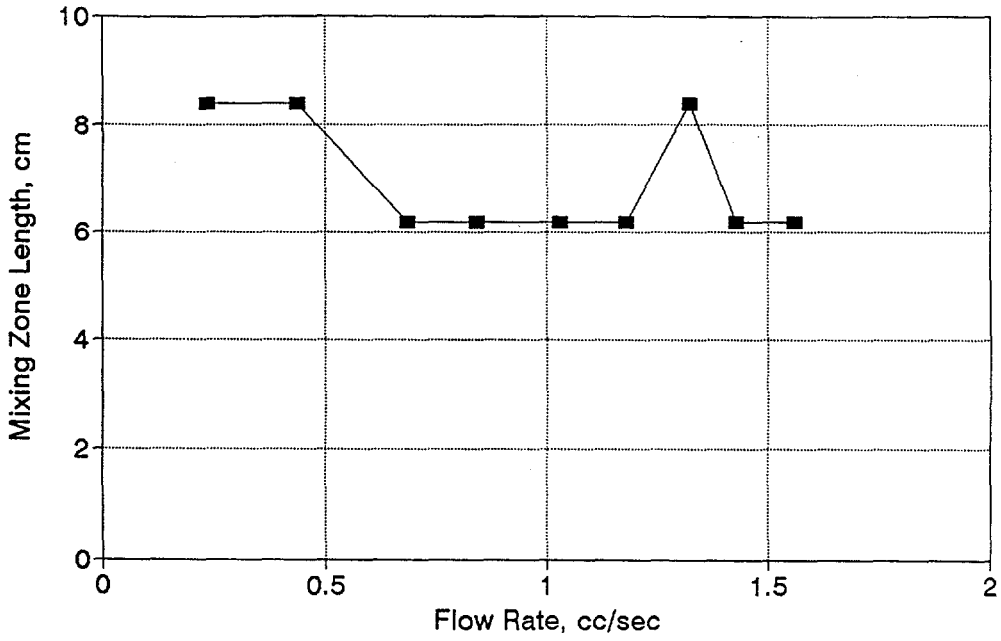

Figure 6.3.11 Transverse Dispersion Mixing Zone Length vs Flow Rate

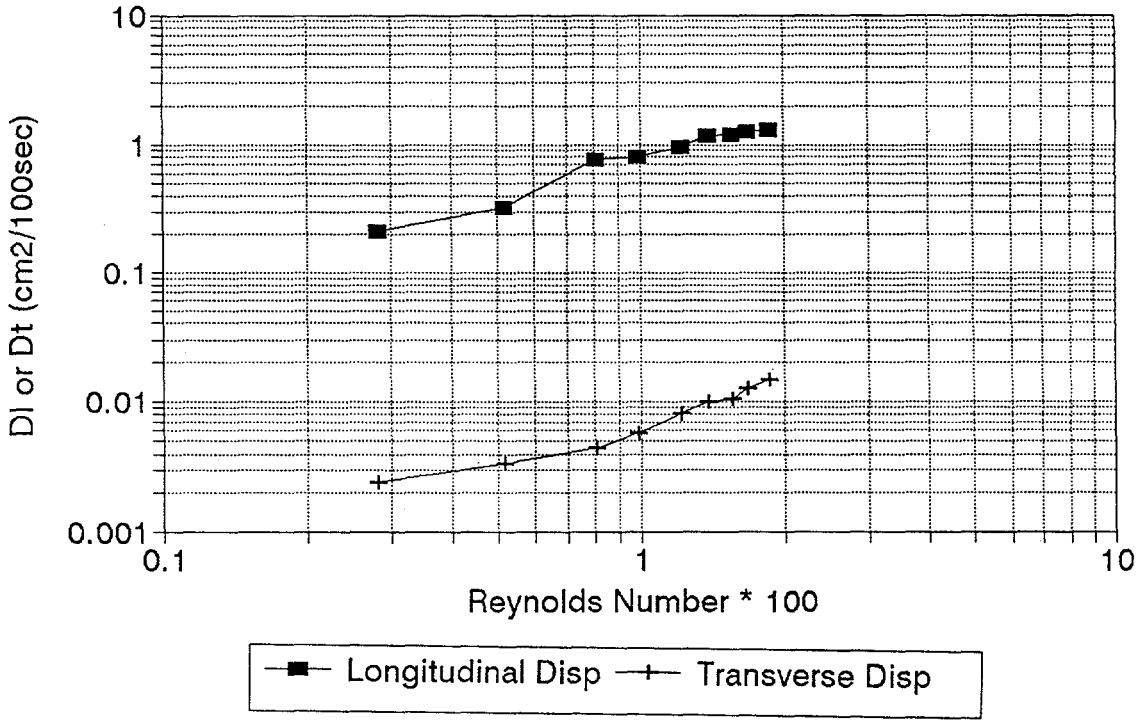

Figure 6.3.12 Transverse & Logitudinal Dispersion Coefficients D_l and D_t vs Reynolds Number

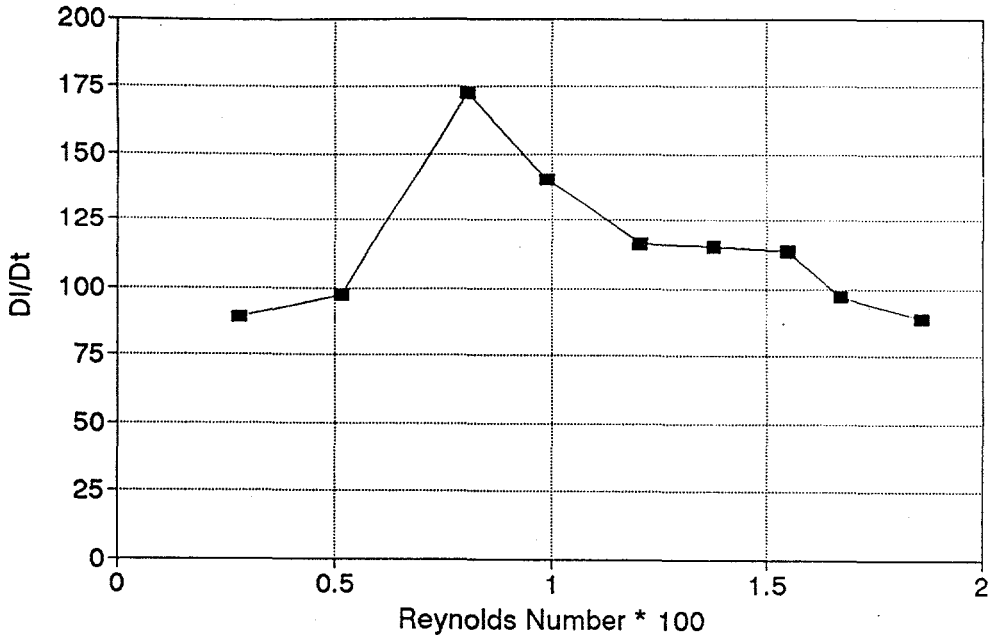

Figure 6.3.13 Ratio of Dispersion Coefficients D_l/D_t vs Reynolds Number

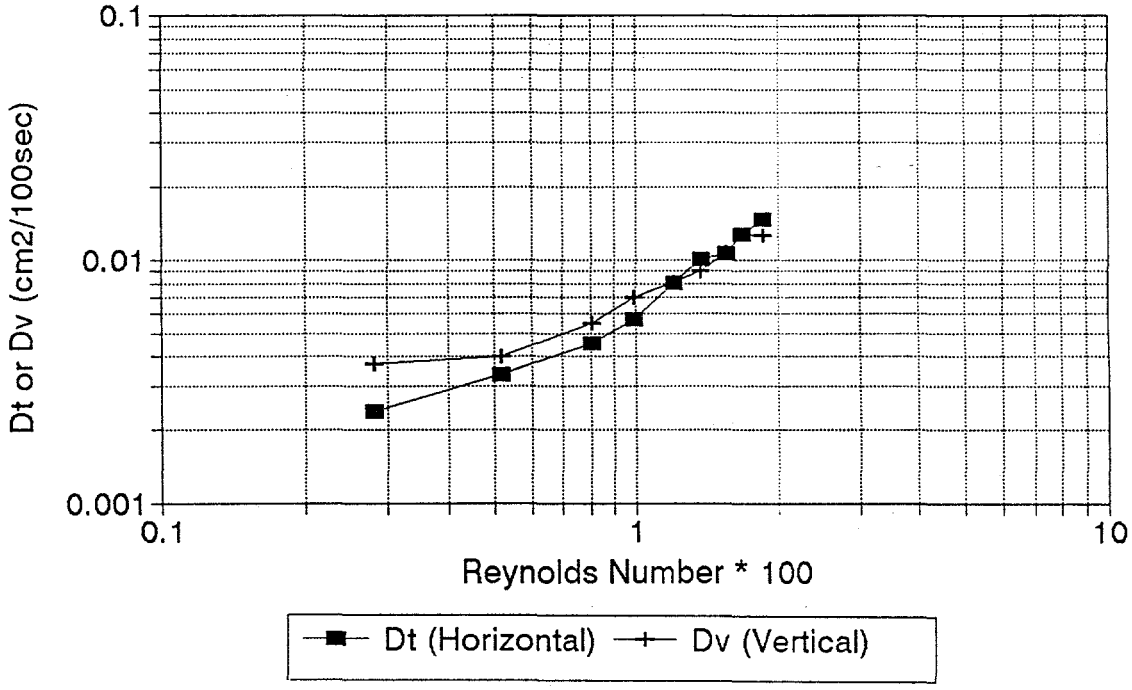

Figure 6.3.14 Transverse Dispersion Coefficients D_t and D_v vs Reynolds Number

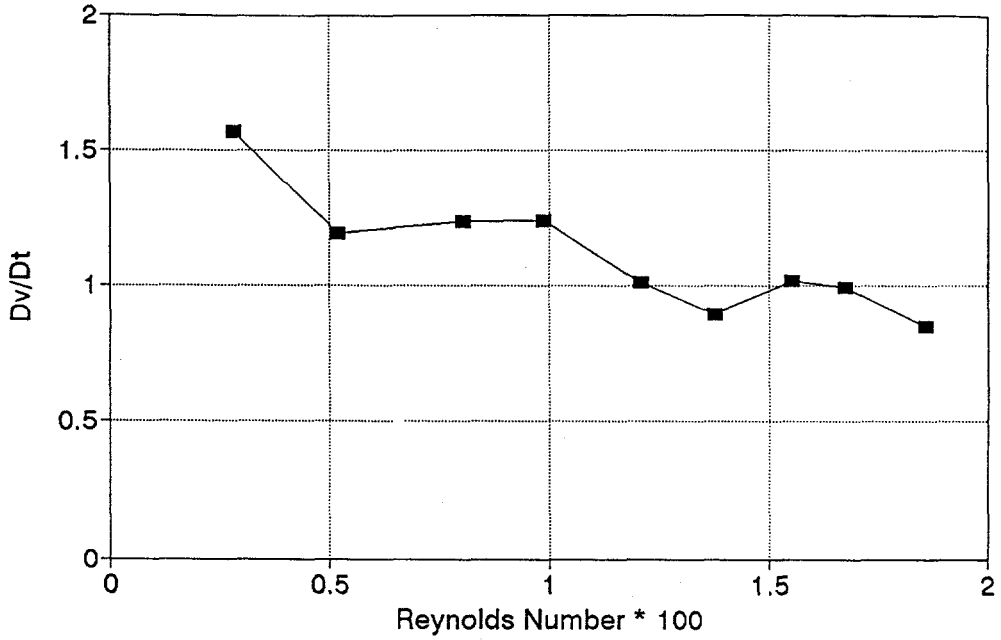

Figure 6.3.15 Ratio of Dispersion Coefficients D_v/D_t vs Reynolds Number

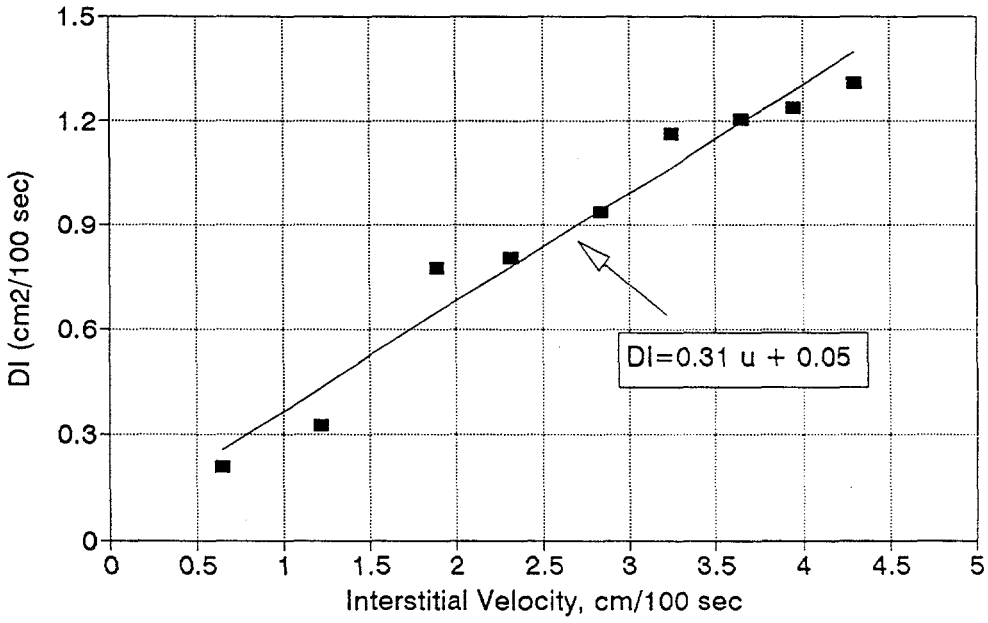

Figure 6.3.16 Longitudinal Dispersion Coefficient vs Interstitial Velocity

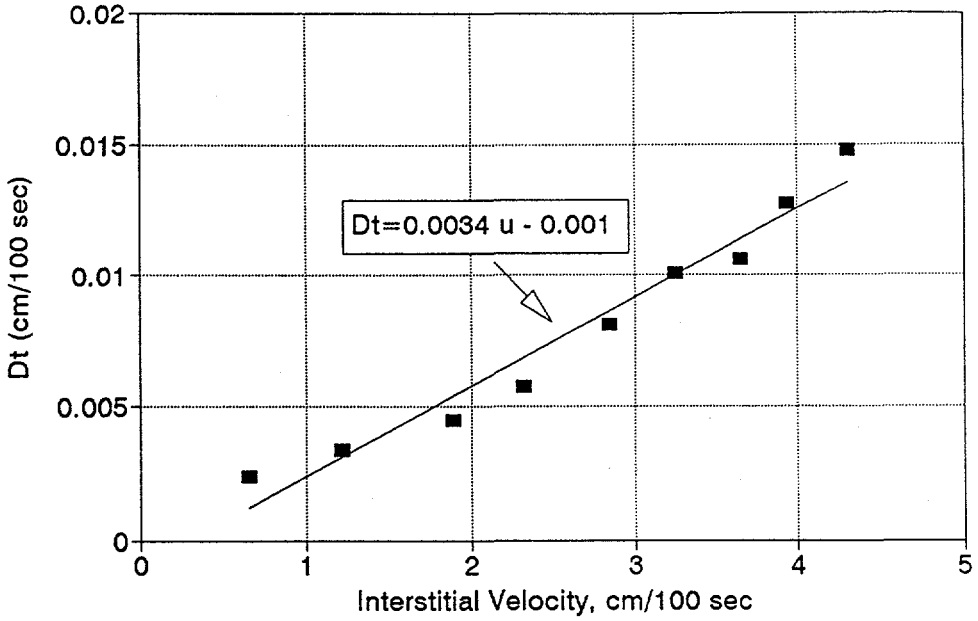

Figure 6.3.17 Horizontal Transverse Dispersion Coefficient D_t vs Interstitial Velocity

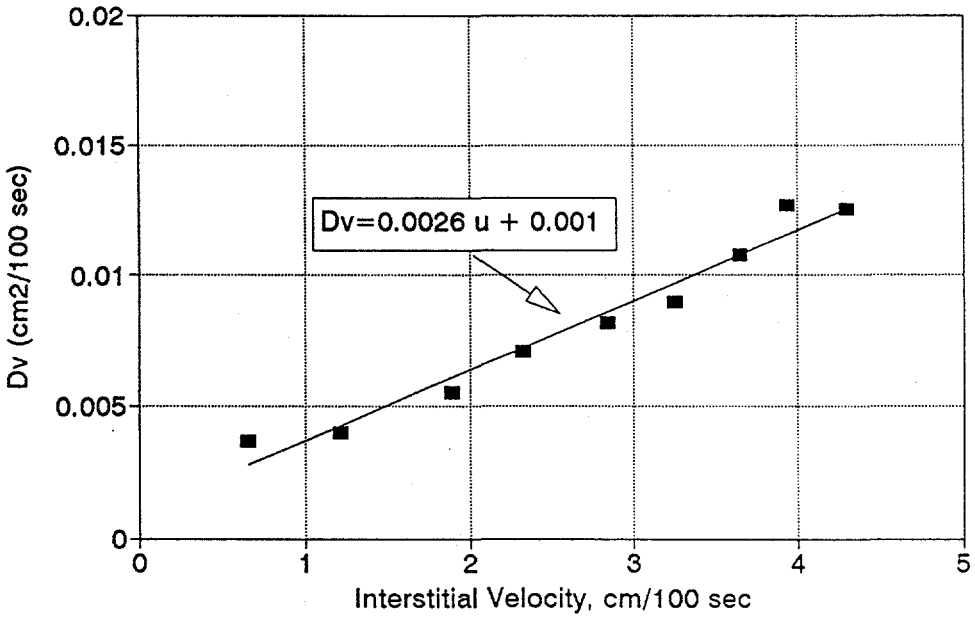

Figure 6.3.18 Vertical Transverse Dispersion Coefficient D_v vs Interstitial Velocity

Chapter 7

Gas-Gas Dispersion and Characterization of Reservoir Rocks

7.1 Introduction

Almost all research in the area of dispersion has focused on the flow of liquids through porous media. Menzie, *et al*, (1989) have been conducting the study of dispersivity as a reservoir rock property for several years. A significant amount of experimental work has been conducted in this area. The effects of scale, velocity and rock properties on liquid-liquid dispersion have been studied. The objective of previous research was to characterize and define reservoir heterogeneities by measuring liquid-liquid dispersion in porous media. The measurement of dispersion with gases should significantly contribute to the overall understanding of flow systems in reservoir rocks.

The objectives of this study are:

(1) To develop a method and set up an experimental apparatus to measure gas-gas dispersion in consolidated rocks.
(2) To study the effect of displacement velocity and pressure on gas-gas dispersion and dispersivity.
(3) To study the heterogeneity of reservoir rocks and investigate the relationship between dispersivity and rock properties in order to characterize the flow system using gas-gas dispersion measurements.

Twenty eight gas-gas dispersion measurements with different velocities and pressures were conducted on three Berea sandstone cores in this study. The effects of velocity and pressure on gas-gas dispersion were thoroughly investigated. The characterization of the rocks through dispersion measurement was studied.

7.2 Experimental Apparatus and Procedures

A schematic diagram of the equipment used for gas-gas dispersion is shown in Figure 7.2.1. The system included (1) two bottles of pure helium, one used as the displaced gas, the another used as the carrier gas in the gas chromatograph; (2) one bottle of nitrogen used as the displacing gas; (3) three precise pressure and flowrate regulators on the top of each gas cylinder; (4) a core holder; (5) a vacuum pump; (6) a pressure gauge; (7) a gas flow meter; (8) a bubble gas flow meter; (9) a gas chromatograph; and (10) some needle valves. To get accurate and continuous smooth S-shaped breakthrough curves, the gas chromatograph was modified to let the tested gas bypass the column and flow directly into the gas detector.

Figure 7.2.2 shows the flow chart of the experimental procedures used in the measurement of gas-gas dispersion in this study.

7.3 Experimental Results and Analysis

Twenty eight experimental measurements of gas-gas dispersion were conducted on three Berea sandstone cores. The three cores have the same cross section diameters but different lengths. The three cores were labeled as YF1, YD6 and YA8, which are identical to the labeling used in the liquid-liquid displacement experiments (Li, 1992).

The geometries and properties of the cores are summarized in Table 7.3.1. The properties of helium and nitrogen are listed in Table 7.3.2.

Table 7.3.1 Physical Properties of the Tested Cores

Core	Type	d (cm)	L (cm)	PV (cm^3)	Φ (%)	K (md)
YF1	Berea	3.8	29.1	67	20.0	300
YD6	Berea	3.8	45.6	93	17.89	97
YA8	Berea	3.8	72.6	160.5	19.39	185

Table 7.3.2 Physical Properties of Gases Used in The Study (at T = 23°C and P = 1 atm)

Gas	ρ (g/cm^3)	μ (cp)	Molecular Weight
Nitrogen	0.001154	0.0177	28.02
Helium	0.000163	0.0186	4.0

7.3.1 Experimental Results

To study the effect of velocity and pressure on gas-gas dispersion, twenty eight runs were conducted on three cores under different flowrates and pressures. Figure 7.3.1 and 7.3.2 are typical experimental results measured on core YD6 and YA8.

7.3.2 Effect of Flowrate and Pressure on Gas-Gas Dispersion

The effect of flowrate on gas-gas dispersion was observed by plotting the effluent breakthrough curves under the same displacing pressure but different flowrates on the same cartesian plot as in Figure 7.3.1 and 7.3.2. The runs performed on all three cores produced data that infer

that lower flowrates led to earlier breakthrough and higher dispersion and higher flowrates led to later breakthrough and less dispersion.

In liquid-liquid dispersion, molecular diffusion is assumed to be negligible as compared to the effect of convection on dispersion. However, molecular diffusion plays a significant role in gas-gas dispersion.

It is presumed that in a porous media for a specific displacement, there is a critical velocity at which the least dispersion will take place. Below the critical velocity, an increase of velocity will lead to less dispersion. However, above the critical velocity, the increase of velocity will lead to more dispersion. To determine the critical velocity, experiments were conducted at high velocities under displacing pressures of 15 psig and 40 psig with core YA8. Because the coating of the tested cores can not stand pressure higher than 70 psia, the pressures used in the experiments were too low to obtain the critical velocity.

Figure 7.3.3 shows the effect of pressure on gas-gas dispersion. Three experimental runs were conducted on the same core at similar velocities but different displacement pressures (15, 30 and 40 psig). It was observed that the increase of displacement pressure led to less dispersion in gas-gas displacement. The velocities used in the three runs were not exactly the same. The effect of pressure would be seen more clearly if exactly the same velocity had been used on each run.

If the displacement pressure is increased continually and the gas is liquefiable, the extreme situation will be liquefaction and gas-gas dispersion will transform into liquid-liquid dispersion. As expected, less dispersion should take place because the effect of diffusion reduces to zero in liquid-liquid dispersion. Figure 7.3.4 is the comparison of gas-gas dispersion with liquid-liquid dispersion for core YD6. It can be observed that much less dispersion took place in the liquid-liquid dispersions.

7.3.3 Dispersion Coefficient and Dispersivity

Because of the compressibility of gases, the Convection-Dispersion Equation can not be used to fully describe gas-gas dispersion in porous media. In this study, the pressure difference between the inlet and outlet ranged from 0.2 to 3.8 psia, allowing the compressibility of gases to be assumed negligible. Therefore, two methods for liquid-liquid dispersion were used in this study to calculate the gas-gas dispersion coefficients.

The first method used in this study was the curve matching method, which utilizes the convection-dispersion transport model to match the experimental data to obtain the dispersion coefficients. The computer program used in this study is called CXTFIT (Parker & Van Genuchten, 1984). It combines the one-dimensional analytical solution of the C-D Equation along with the non-linear least square numerical method to match the experimental data.

The second method used to calculate the dispersion coefficients was the Analytical Solution Method (ASM) proposed by Greenkorn (1983). It is expressed by the following equation:

$$D_l = \frac{V_p L}{4\pi \left[\frac{dC/C_0}{dV/V_p}\right]^2_{\frac{V}{V_p}=1}} \qquad (7.3.1)$$

In this equation, the slope of the effluent breakthrough curve at one pore volume injected should be used. Under ideal displacing conditions, the slope at one pore volume injected should be the maximum slope on the effluent breakthrough curve. Only material balance was considered when the C-D Equation was derived. In reality, many other factors could affect the dispersion of fluids in porous media. Hence, the S-shaped effluent breakthrough curves obtained from these experiments always shifted up or down. Therefore, the maximum slope on the effluent breakthrough curve was used to calculate the dispersion coefficients.

Figures 7.3.5 and 7.3.6 show the relationship between the dispersion coefficient and displacement velocity for core YD6 and YA8. It was observed from these plots that dispersion coefficients obtained from the curve matching method do not correlate well with velocities. One reason probably is because the consideration of the flow and boundary conditions for porous media in deriving the C-D Equation and its solution was based on an infinite boundary system but applied to a finite system. Another reason probably is because of the mathematical problem in the program; big differences were observed between the experimental curves and the fitted curves in some matching results. The analytical solution method worked better than the curve matching method, as the dispersion coefficients obtained by this method had better correlations with velocities.

In liquid-liquid dispersion, a higher dispersion coefficient corresponds to higher dispersion, while in gas-gas dispersion, a higher dispersion coefficient corresponds to less dispersion. By observing the equation 7.3.1, it was realized that the dispersion coefficient is a function of velocity and the square of maximum slope of the S-shaped breakthrough curve. For liquid-liquid dispersion, the slope of the S-shaped curve decreases with velocity, hence the dispersion coefficient increases with velocity. For gas-gas dispersion, the slope of the S-shaped breakthrough curve increases with velocity. The increase of velocity overrides the increase of slope; hence the dispersion coefficient increases with velocity.

Dispersivity is considered to be a property of porous media. The following is the relationship between dispersivity, diffusion, and dispersion:

$$D_l = D_e + \alpha v \qquad (7.3.2)$$

where, D_l = longitudinal dispersion coefficient (cm^2/sec)
D_e = effective molecular diffusion coefficient (cm^2/sec),
α = dispersivity (cm).

For liquid-liquid dispersion, the molecular diffusion is assumed to be negligible or D_e is set equal to zero. Hence, the dispersivity value for liquids is proportional to the dispersion coefficient and inversely proportional to velocity. In gas-gas dispersion, the effect of molecular diffusion is

significant and assumed to be constant. In reality, it is a function of pressure and rock properties. The increase in pressure will decrease the diffusion of gases and the effective molecular diffusion coefficients. Rock heterogeneity will increase the diffusion of gases in porous media.

The effective molecular diffusion coefficients can be obtained experimentally. However, an experimental apparatus different from the gas-gas dispersion experimental apparatus used in this study has to be developed. Hence, a graphical method was proposed in this study. By plotting the first three dispersion coefficients under low velocities for each core as shown in Figures 7.3.7 and 7.3.8, it was observed that the gas-gas dispersion coefficient is proportional to velocity at low velocities. The effective molecular diffusion coefficients were obtained by linear regression and extrapolation of the velocity to zero. The effective molecular diffusion coefficients are listed in Table 7.3.3.

Table 7.3.3 Effective Molecular Diffusion Coefficients Obtained in the Study

Core	Φ (%)	K (md)	P (psig)	D_e (cm^2/sec)
YF1	20.00	300	15	0.003409
YD6	17.89	97	15	0.007296
YA8	19.39	185	15	0.02804
			30	0.01831
			40	0.001535

Ali (1989) conducted gas-gas diffusion experiments on four types of sandstone outcrop and calculated the effective diffusion coefficients. The effective diffusion coefficient obtained from Ali's experiments on Berea sandstone was 0.0225 cm^2/sec. It is close to the value of core YA8 at 15 psig, which is 0.02804 cm^2/sec.

Using the effective molecular diffusion coefficients obtained above, and dispersion coefficients obtained by the analytical solution method, dispersivities were calculated. By plotting the dispersivities versus velocity as in Figures 7.3.9 and 7.3.10, it was concluded that dispersivity decreases with velocity for gas-gas dispersion under the experimental conditions in this study. It decreases more rapidly at low velocity than at high velocity. Due to the small difference in pressures, all of the points for three different pressures (15, 30 and 40 psig) follow almost the same curve in Figures 7.3.10 for core YA8 . By plotting the dispersivity versus velocity on log-log plot as in Figures 7.3.11 and 7.3.12, three approximately straight lines were obtained. The correlations between dispersivity and displacing velocity were obtained by using regression analysis.

Observing equation 7.3.2, dispersivity is a function of the maximum slope on the S-shaped effluent breakthrough curve. The slope on the S-shaped breakthrough curve is a function of velocity; therefore dispersivity is also a function of velocity. It is presumed that for gas-gas dispersion under a certain pressure there will be a critical velocity above which dispersivity increases with velocity,

under which dispersivity decreases with velocity. When pressure is high enough, gas-gas dispersion will transform into liquid-liquid dispersion, and dispersivity will increase with velocity only.

7.3.4 Dispersion Factor

Li (1992) proposed a method to calculate dispersion factors in the study of the effect of scale on liquid-liquid dispersion. The dispersion factor was defined by the following equation:

$$DF_{ML} = \frac{(\frac{V}{V_p})_{50\%} - (\frac{V}{V_p})_{15.9\%}}{(\frac{V}{V_p})_{50\%}} \qquad (7.3.3)$$

where, DF_{ML} = dispersion factor (dimensionless),
V = volume injected (cm^3),
V_P= one pore volume (cm^3),
$(V/V_p)_{50\%}$ = pore volume injected at 50% concentration (dimensionless),
$(V/V_p)_{15.9\%}$ = pore volume injected at 15.9% concentration (dimensionless).

By plotting dispersion factors versus the velocity on cartesian plots as in Figures 7.3.13 and 7.3.14, it was observed that the dispersion factor decreases with velocity just as dispersivity does. The correlations of dispersion factor and velocity in these figures were obtained by using regression analysis.

7.4 Rock Characterization

7.4.1 Determination of the Pore Volume of Resident Fluid Displaced

S-shaped breakthrough curves obtained from dispersion measurements can provide another approach to investigate the heterogeneity of reservoir rock. In an absolutely homogeneous reservoir, the effluent concentration curve should appear as a sharp-step change. However, smearing occurs at the breakthrough point due to mixing caused by non-uniform flow velocities within individual pores, which occurs during displacement. The concentration profile is strongly dependent upon the heterogeneity of reservoir rock. The earlier portion of the S-shaped curve represents the flow in pores with high conductivity, or the larger pores. The later portion of the curve represents the flow in pores with low conductivity, or the smaller pores. The slope in the middle portion of the curve is indicative of the theoretical considerations related to the heterogeneity of reservoir rock, or the pore size distribution.

Li (1992) proposed a capillary tube model to determine the pore size distribution using S-shaped breakthrough curves. The pore size distribution was modeled as a bundle of straight cylinder tubes with different radii. The flow in each tube was quantitatively evaluated using Poiseuille's equation:

$$Q_i = \frac{\pi r_i^4 \Delta p}{8 \mu L} \qquad (7.4.1)$$

where,

Q_i = flowrate in a single tube (cm^3/sec),
r_i = radius of a flow tube (cm),
Δp = pressure drop between the inlet and outlet of core (atm),
μ = viscosity of fluid (cp),
L = length of flow tube (cm).

The total flowrate of a bundle of tubes is:

$$Q_T = \sum_{i=1}^{N} \frac{\pi r_i^4 \Delta p}{8 \mu L} \qquad (7.4.2)$$

where, Q_T = total flowrate of the core (cm^3/sec),
N = total number of tubes in the porous media

It was assumed that the injection fluid breakthrough occurs first from the flow channel that has the largest flow radius. After the initial breakthrough, the tubes produce injection fluid only. Poiseuille's equation was applied to the miscible displacement of the injection fluid as:

$$Q_T C_n = \frac{\pi \Delta p}{8 \mu L} \sum_{i=1}^{n} r_i^4 \qquad (7.4.3)$$

and for the displaced fluid:

$$Q_T (1 - C_n) = \frac{\pi \Delta p}{8 \mu L} \sum_{i=n+1}^{N} r_i^4 \qquad (7.4.4)$$

where,

C_n = concentration of the injection fluid measured at outlet (%),
n = number of tubes which are full of injection fluid,
N = total number of flow tubes in porous media.

In dispersion measurement, the flowrate, Q_T, and pressure drop, Δp, are considered constant. If the viscosity of fluid and the length of core are known, the following calculation can be conducted:

$$\sum_{i=1}^{n} r_i^4 = \frac{8 \mu L Q_T C_n}{\pi \Delta p} \qquad (7.4.5)$$

The left side of equation 7.4.5 represents the sum of r_i^4 of the tubes that are full of injection fluid. It was assumed that for every increment of concentration, there is only one more tube, R_i,

that contributes to the increment of flow of injection fluid through the porous media. In actuality, the tube R_i consists of many small tubes, but the number and the size of the tubes are not readily identifiable. The R_i, in fact, is the equivalent radius of a single tube, whose sectional area is equal to the sum of the sectional areas of many small tubes. The R_i can be calculated using the following equation:

$$R_i^4 = \sum_{i=1}^{n} r_i^4 - \sum_{i=1}^{n-1} r_i^4 = \frac{8\mu L Q_T (C_n - C_{n-1})}{\pi \Delta p} \qquad (7.4.6)$$

Therefore, the pore volume of resident fluid displaced by injection fluid between every concentration increment can be calculated as:

$$(PV)_i = \pi R_i^2 * L \qquad (7.4.7)$$

The cumulative pore volume of resident fluid displaced by injection fluid at concentration C_n is:

$$\sum_{i=1}^{n} (PV)_i = \sum_{i=1}^{n} \pi R_i^2 * L \qquad (7.4.8)$$

The concentration C_n can be read from the S-shaped breakthrough curves for each pore volume injected. If the cumulative pore volume displaced by injection fluid versus the concentration of displaced fluid at the outlet of the core is plotted on a cartesian plot, the slope of the curve can indicate the degree of heterogeneity of the core. A core associated with a large slope is considered more homogeneous than a core with a small slope. The difference in slope refers to more pore volumes of resident fluid being displaced between the same concentration increment. Therefore, the heterogeneity of the rock can be evaluated qualitatively with this method.

By plotting the pore volume of resident fluid displaced versus the effluent relative concentration for the three cores as in Figure 7.4.1, it was observed that only part of the pore volume contributes to the flow. For core YA8, the contribution was calculated to be 53%. For core YF1, the contribution was 41%. For core YD6, the contribution was only 27%. The difference in contribution explains why the three cores have similar porosities, but very different air permeabilities.

The heterogeneity of the cores was analyzed using Figure 7.4.1. The higher slope at the earlier part of the curve indicates that the core has a higher percentage of large pores. A higher percentage of small pores is indicated if the later part of the curve has a higher slope. In Figure 7.4.1, core YD6 has a low slope at both the earlier and later portion of the curve. The total flowing pore volume is also the smallest. This indicates that core YD6 has a poor flowing system with both high heterogeneity and low conductivity. Both the highest slope and the highest total flowing pore volume are observed for core YA8, which means that the core was more homogeneous than the other

two cores and has a higher conductivity. For core YF1, a lower slope at the earlier portion of the curve was observed, but a higher slope occurred at the later portion of the curve. This indicates that the core has a small percentage of big pores and a high percentage of small pores in the total pore volume. It was observed that core YF1 has the highest permeability, which was attributed to the heterogeneity of the porous media. Another reason for the high permeability observed may be due to the higher pressures used during the permeability measurements. Core YF1 has a fine flowing system or a system composed of many small pores. Under higher pressure, gas had less freedom of movement and was compelled to flow through the small pores, resulting in a large total flowing pore volume and a high permeability as observed.

7.4.2 Correlations of Dispersivity and Dispersion Factor

Part two presented the exponential correlations between dispersivity (α), the dispersion factor (DF_{ML}) and velocity. These correlations are of the form $Y=b.v^n$. The values of the correlation coefficients and exponents are provided in Table 7.4.1. It appears that these coefficients and exponents are related to the effective diffusion coefficients, D_e.

Table 7.4.1 Correlation Coefficients and Exponents of α and DF_{ML}

Core	D_e	α		DF_{ML}	
	(cm^2/sec)	Coefficient	Exponent	Coefficient	Exponent
YF1	0.003409	1.1621	-0.1546	0.1141	-0.2854
YD6	0.007296	0.5234	-0.256	0.09627	-0.2905
YA8	0.02804	0.0777	-0.6658	0.03607	-0.4641

It can be observed from Table 7.4.1 that the coefficients in the correlations for both dispersivity and the dispersion factor are positive values; however, the correlation exponents are negative.

The effective diffusion coefficient for gas is a function of the geometry and physical properties of the core. Heterogeneity is conducive to high molecular diffusion; hence, the effective diffusion coefficients increase.

From the analysis of the presented data, it can be concluded that cores with high effective diffusion coefficients will have low correlation coefficients and exponents. These parameters are possible effective tools in characterization of reservoir rocks.

7.5 Conclusions and Recommendations

7.5.1 Conclusions

The following conclusions were obtained from this study:

(1) The experimental method and apparatus developed in this study for gas-gas dispersion measurement provides a simple and accurate way to study the dispersion phenomenon in porous media.
(2) Under low pressures (15, 30, and 40 psig), increasing displacing velocity will decrease the dispersion of gases. Although not verified experimentally, it appears that a critical velocity exists below which the increase of velocity will decrease the dispersion and above which the dispersion of gas increases.
(3) The increase in pressure will decrease the dispersion of gases.
(4) Dispersivity is a function of rock properties, displacing velocity and displacing pressure in gas-gas dispersion.
(5) The dispersion factor, DF_{ML}, is a reliable parameter for describing the dispersion of gas in porous media. It has a behavior similar to that of dispersivity.
(6) The total flowing pore volume for a core can be determined by the method proposed in this study. In gas-gas displacement, only part of the total pore volume contributes to the fluid flow in porous media.
(7) The flow system and heterogeneity of a reservoir can be analyzed qualitatively by dispersion measurements.

7.5.2 Recommendations

Based on this study, future research work should be continued in the following areas:

(1) The analytical model and theory of gas-gas dispersion needs to be developed further.
(2) Gas-gas dispersion experiments with consolidated porous media under high pressures and velocities should be conducted to investigate the existence of the critical velocity.
(3) Experiments should be conducted on several cores in order to characterize reservoir rocks by gas-gas dispersion measurements. To eliminate the effect of scale, the tested cores should have the same lengths and diameters .
(4) The effect of gravity on gas-gas dispersion should be considered. Vertical displacement experiments can be conducted to study this effect.
(5) The experimental procedure can be improved by using a better and more accurate method to measure the flow rates of gas. A computer program should be developed to process the experimental results.

7.6 Nomenclature

C	concentration (mg/liter)
C_O	injected concentration (fraction)
d	diameter of the core (cm)
D_e	effective molecular diffusion coefficient (cm^2/sec)
D_l	longitudinal dispersion coefficient (cm^2/sec)
DF_{ML}	dispersion factor (dimensionless)
K	air permeability (darcy)
L	core length (cm)
N	total number of the tubes in porous media
P_i	inlet pressure (atm)
PV	pore volume, (cm^3)
Q_i	flowrate in a single tube (cm^3/sec)
Q_T	total flowrate of the core (cm^3/sec)
r_i	radius of a flow tube (cm)
R_i	equivalent radius of tube for a concentration increment (cm)
υ	interstitial velocity (cm/sec)
V	pore volume injected (cm^3)
V_p	one pore volume of the core (cm^3)

Greek Letters

α	dispersivity (cm)
μ	viscosity of fluid (cp)
ρ	density of fluid (gm/cm^3)
ϕ	porosity (fraction)

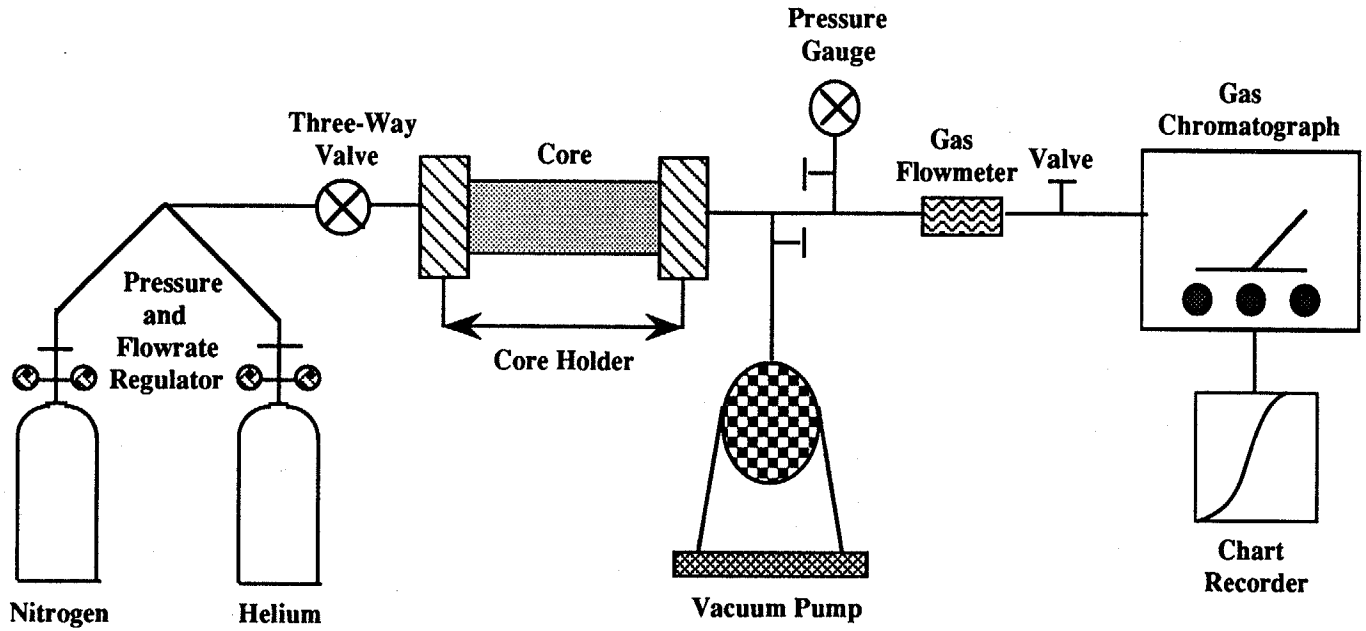

Figure 7.2.1 Experimental Apparatus for the Measurement of Gas-Gas Dispersion

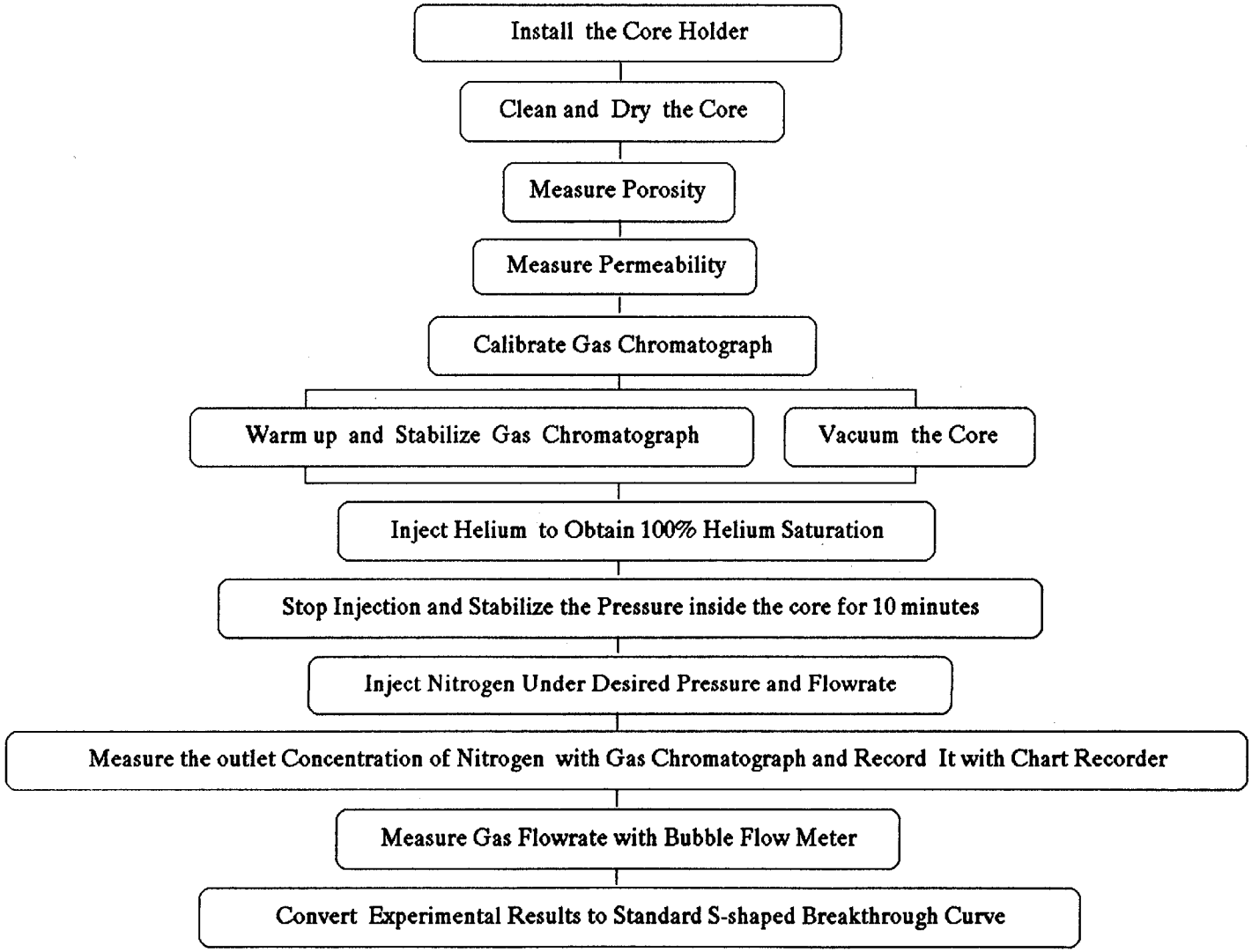

Figure 7.2.2 Flow Chart of Experimental Procedures for Gas-Gas Dispersion

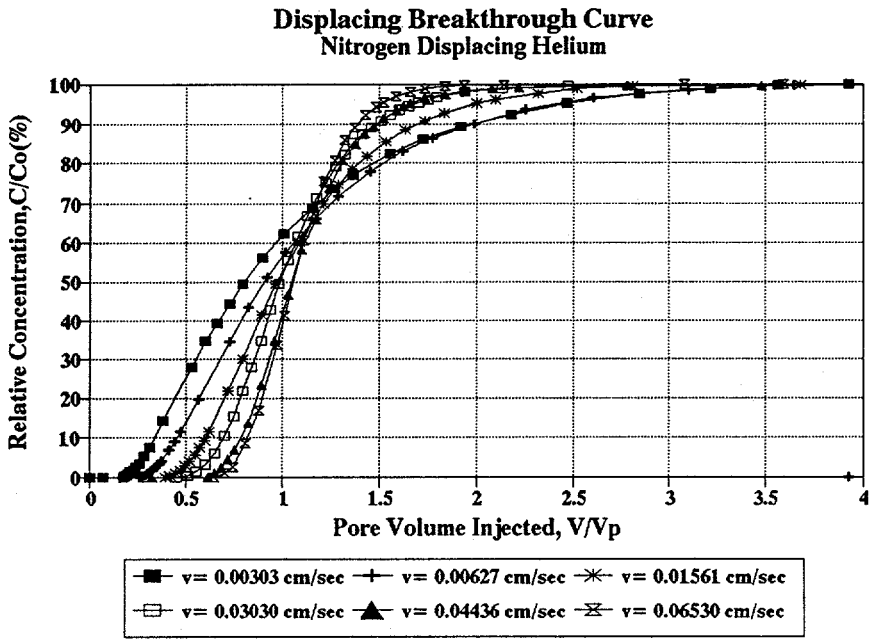

Figure 7.3.1 Experimental Breakthrough Curves Under Different Pore Velocities for Core YD6 (Pi=15 psig)

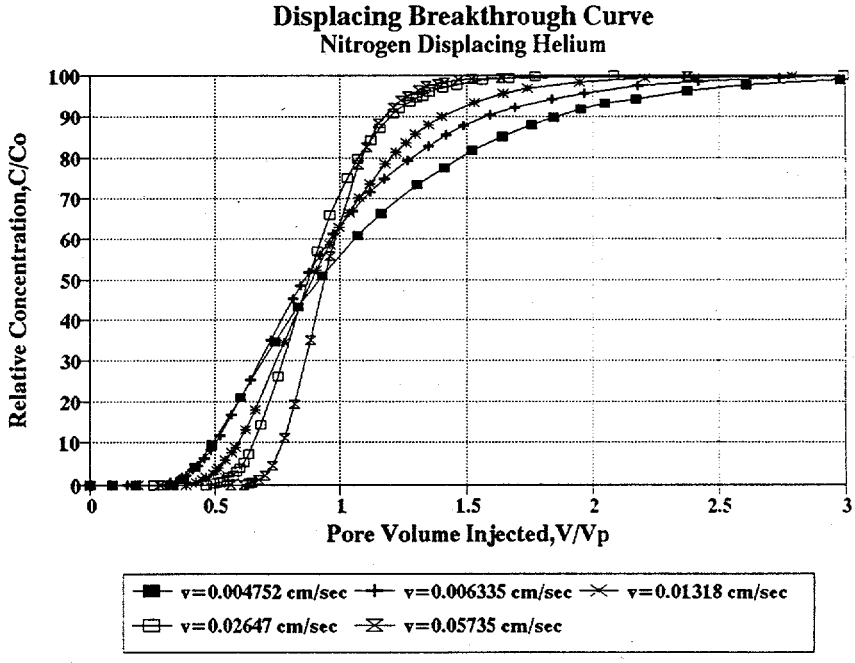

Figure 7.3.2 Experimental Breakthrough Curves Under Different Pore Velocities for Core YA8 (Pi=30 psig)

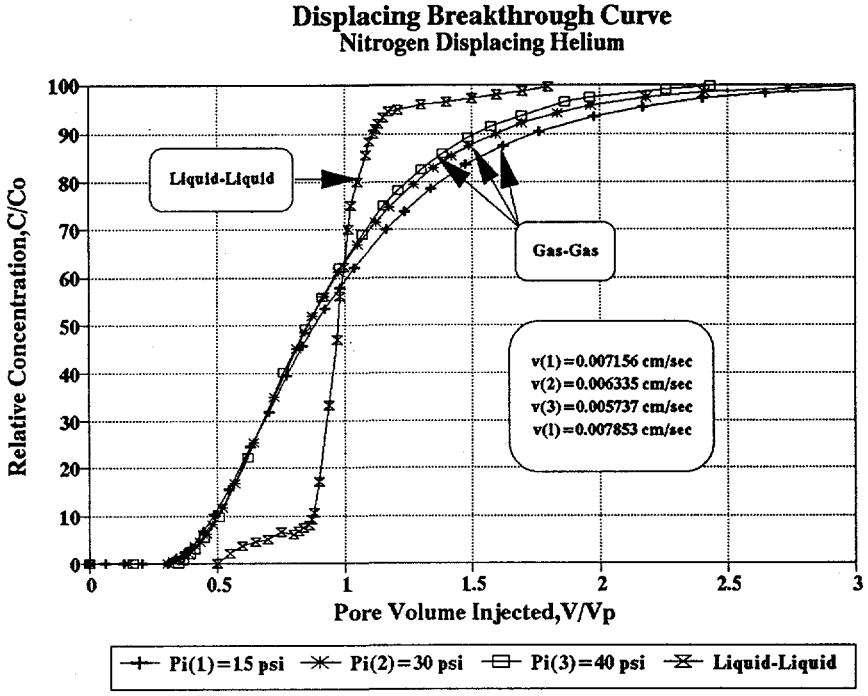

Figure 7.3.3 Effect of Pressure on Gas-Gas Dispersion for Core YA8

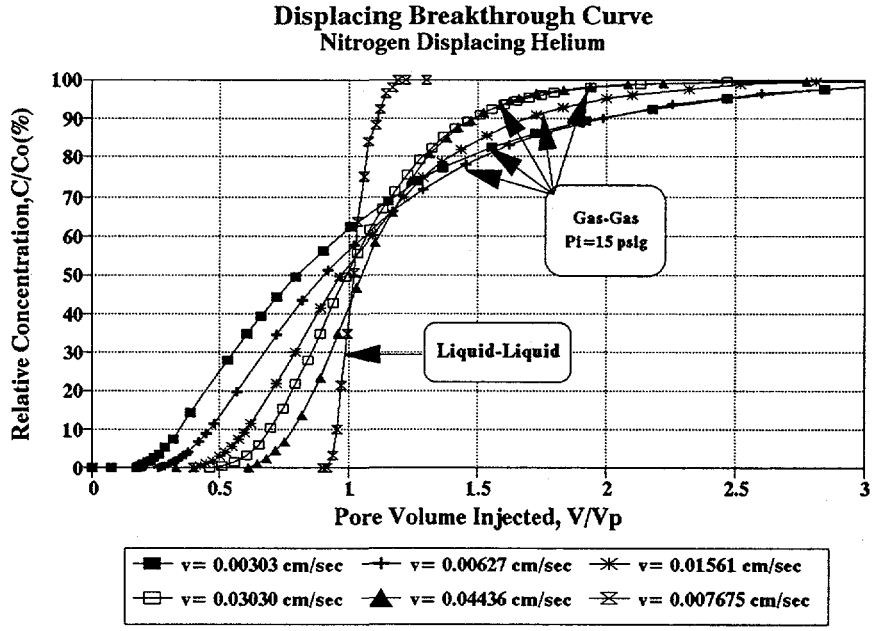

Figure 7.3.4 Comparison of Breakthrough Curves of Gas-Gas Dispersion with Liquid-Liquid Dispersion for Core YD6

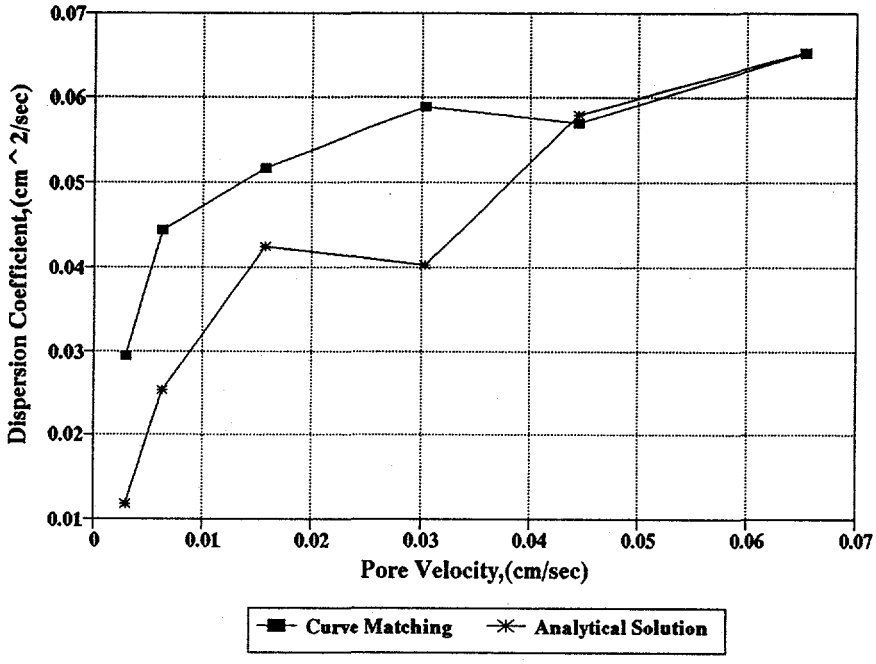

Figure 7.3.5 Dispersion Coefficient Versus Pore Velocity For Core YD6 (Pi=15 psig)

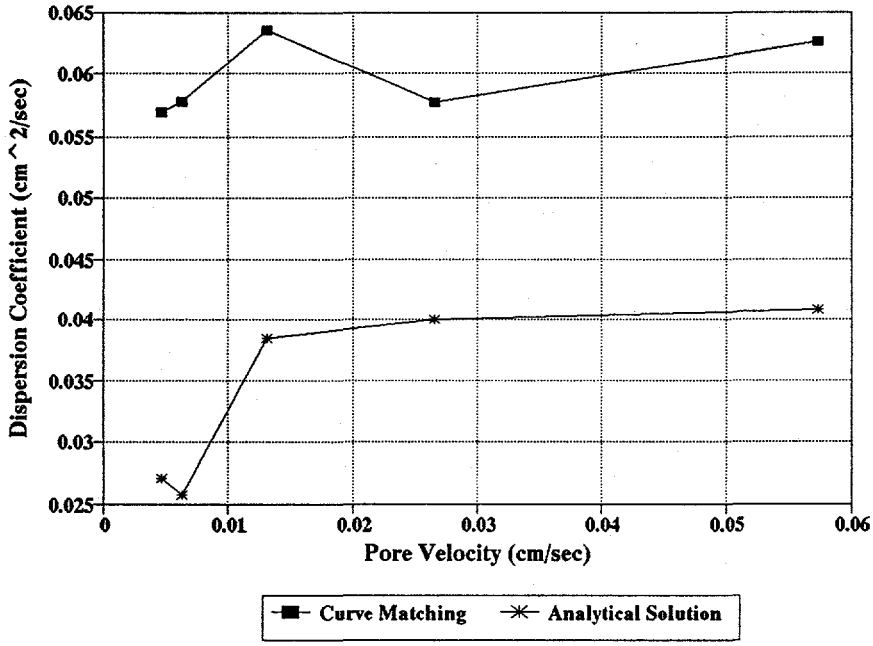

Figure 7.3.6 Dispersion Coefficient Versus Pore Velocity For Core YA8 (Pi=30 psig)

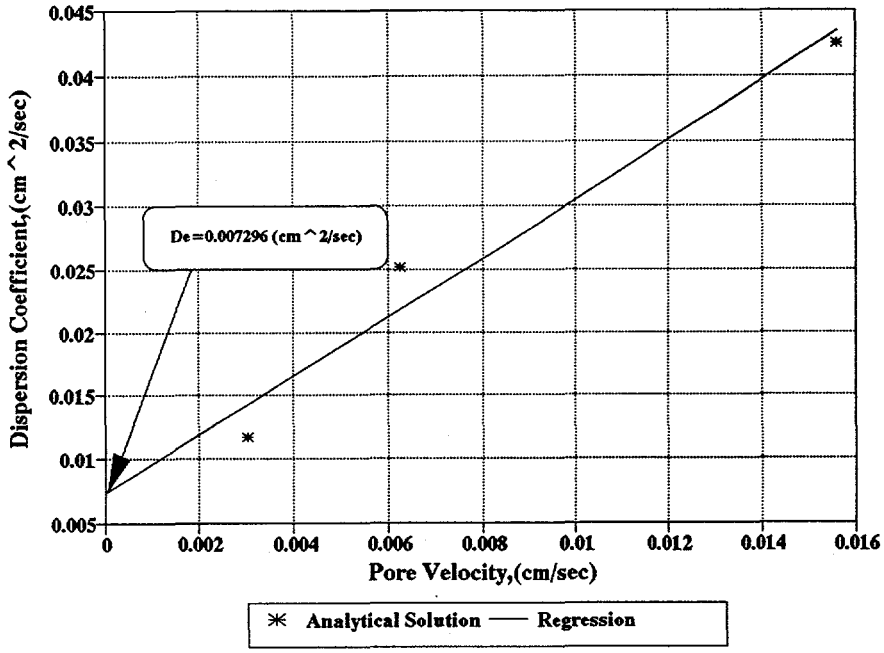

Figure 7.3.7 Obtaining the Effective Diffusion Coefficient by the Dispersion Coefficients Under Low Velocities for Core YD6 (Pi=15 psig)

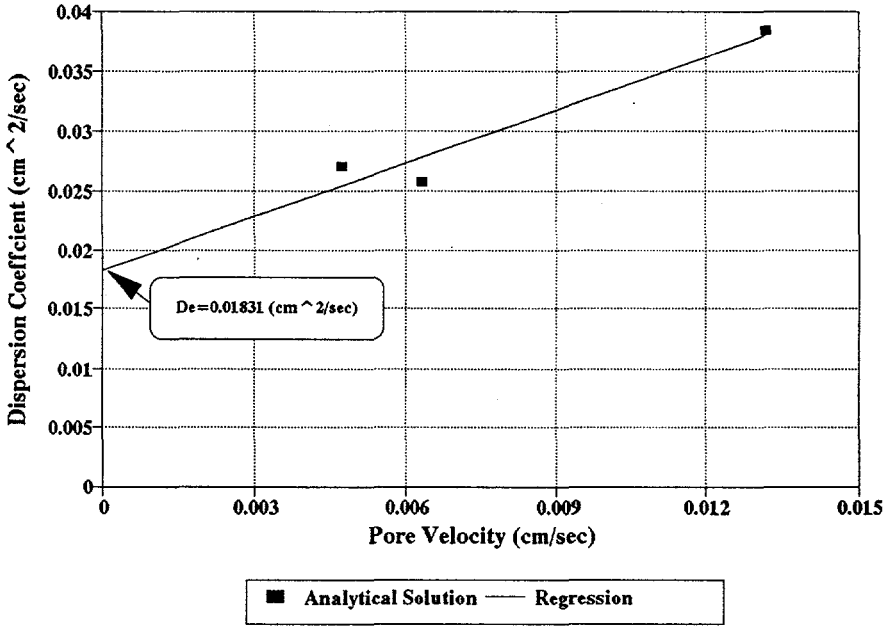

Figure 7.3.8 Obtaining the Effective Diffusion Coefficient by the Dispersion Coefficients Under Low Velocity for Core YA8 (Pi=30 psig)

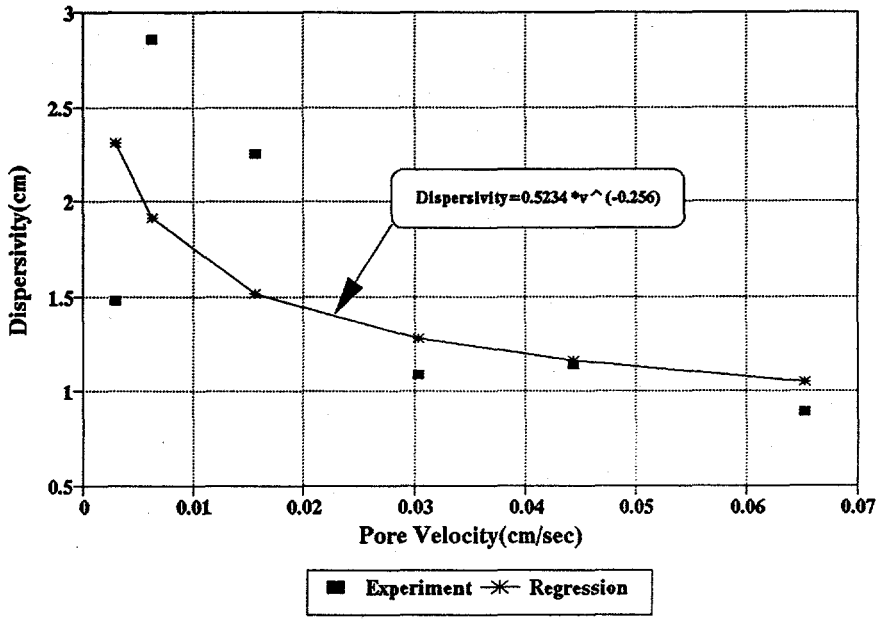

Figure 7.3.9 Dispersivity as a Function of Pore Velocity for Core YD6 (Pi=15 psi)

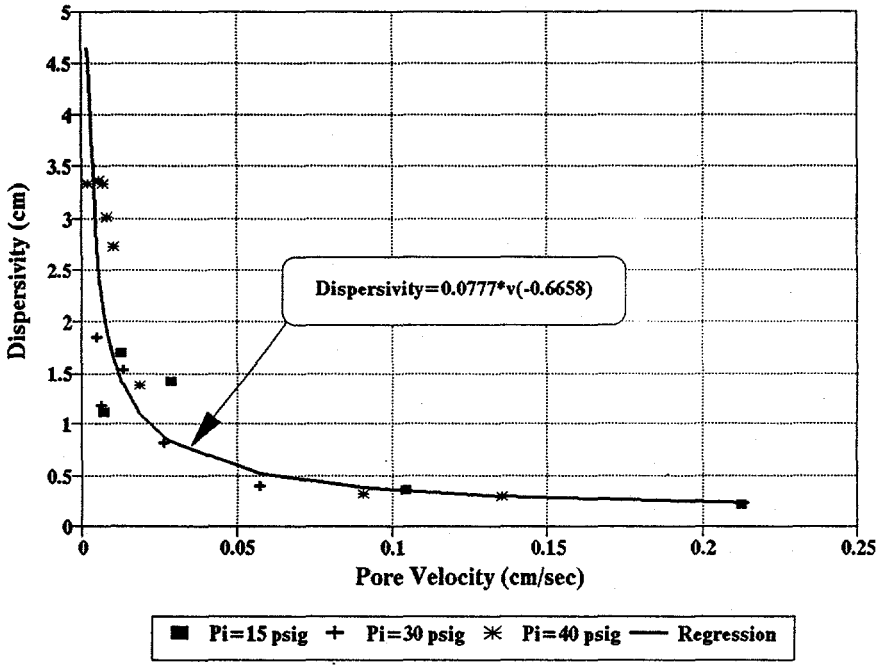

Figure 7.3.10 Dispersivity as a Function of Pore Velocity for Core YA8

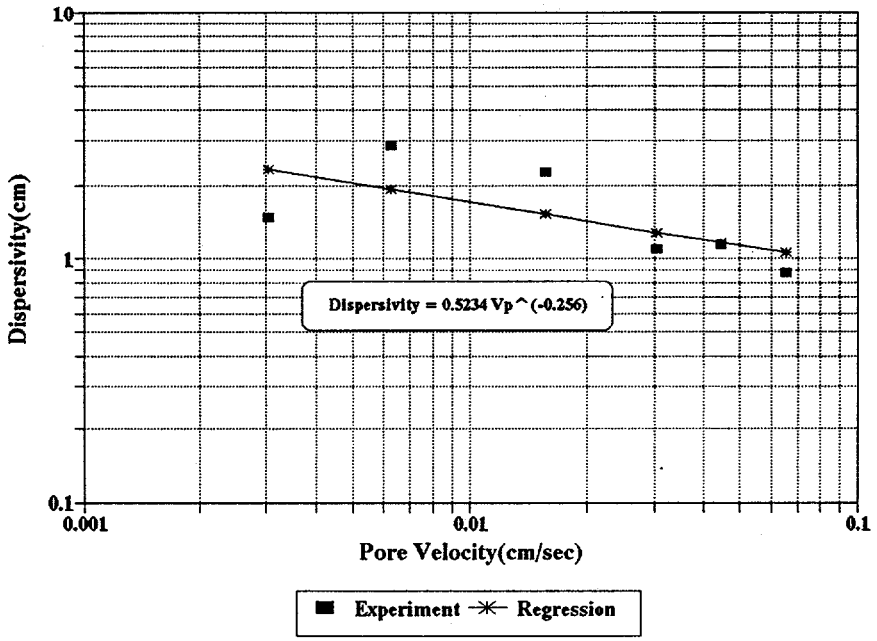

Figure 7.3.11 Dispersivity as a Function of Pore Velocity for Core YD6 on Log-Log Plot (Pi=15 psig)

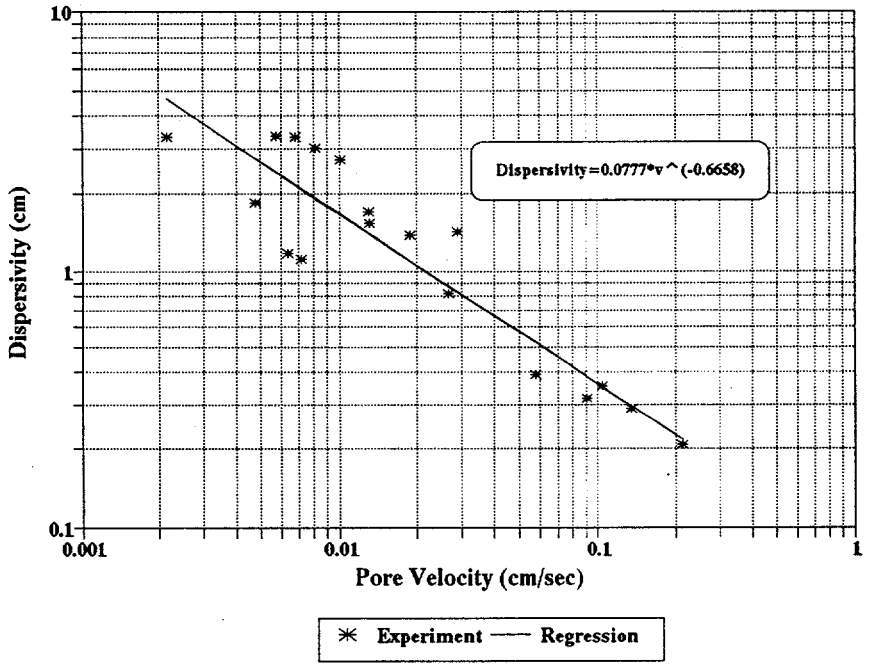

Figure 7.3.12 Dispersivity as a Function of Pore Velocity for Core YA8 on Log-Log Plot (Pi=15, 30 , 40 psig)

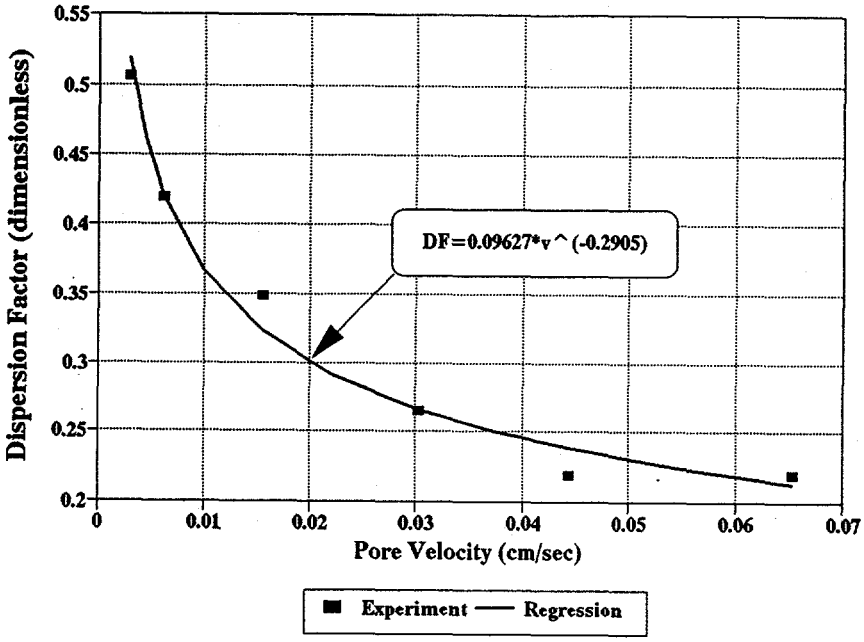

Figure 7.3.13 Dispersion Factor as a Function of Pore Velocity For Core YD6 (Pi=15 psig)

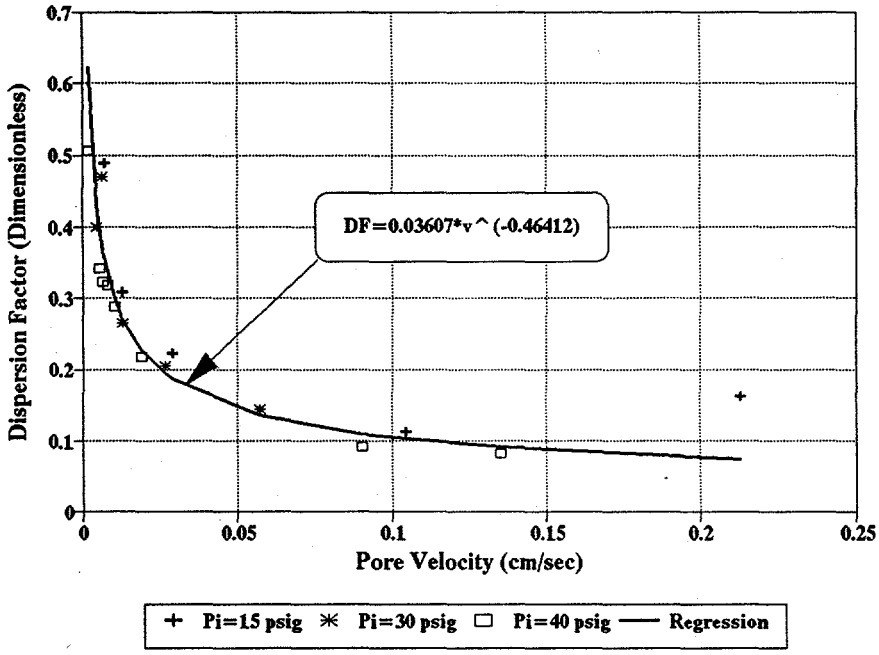

Figure 7.3.14 Dispersion Factor as a Function of Pore Velocity For Core YA8

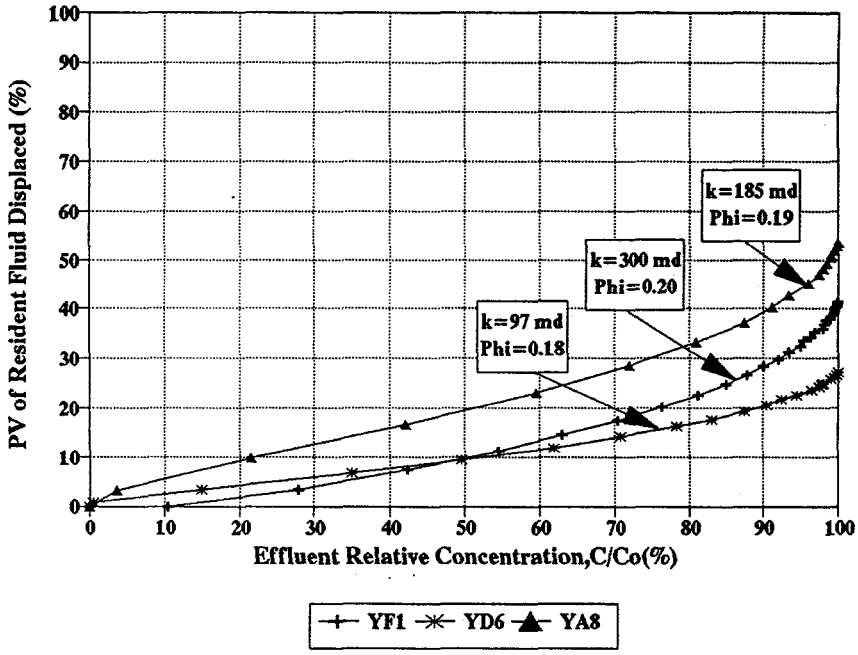

Figure 7.4.1 Pore Volume of Resident Fluid Displaced versus Effluent Relative Concentration

CHAPTER 8

Results and Conclusions

Experimental techniques for determining dispersion, the dispersion coefficient, and dispersivity have been developed in this research. The results contribute toward the solution of the phenomenon of the dispersion process in a miscible displacement. The following results and conclusions are indicated by the experimental research.

1. Regression models used as described in Chapter 2 resulted in considerable improvement of the correlation between dispersion characteristics and porosity and permeability. Dispersivity apparently cannot be calculated exclusively from reservoir rock properties.

2. The experimental method described in Chapter 3 using water labeled with ^{18}O can be used to determine the miscible dispersion effect in an oil reservoir flow system.

3. The CT scan and X-ray linear scan applied as described in Chapter 4 were successful in measuring the dispersion effect within a porous medium. The scans measured the effect of small-scale heterogeneity in the sandstone samples. The vertical length of the flow system appears to have an effect on dispersion, the dispersion coefficient and dispersivity. A new parameter, dispersion factor DF_{ML}, was introduced. A field determined dispersion factor was found to be of much larger value than a laboratory determined dispersion factor.

4. Tortuosity is an important pore property and indicates the relationship of fluid flow, dispersion, and the electrical properties of a reservoir rock. Chapter 5 suggests that both diffusion and capacitance type models can be combined with a tortuous capillary model to describe dispersion flow in a porous medium. An equation was presented to establish, based on well log data, dispersion effects in a reservoir rock.

5. An experimental apparatus and procedure to measure transverse dispersion effects have been developed and reported in Chapter 6. The relationship of longitudinal and transverse dispersion coefficients to the Reynolds Number was studied. Gravity effects on transverse dispersion were also studied. Dispersivity appears to be a function of media characteristics and fluid flow parameters.

6. An experimental method has been developed to investigate gas-gas dispersion in a porous rock (Chapter 7). Effect of pressure and flow velocity on the measured dispersion suggest a critical velocity exists. Dispersivity appears to be a function of rock properties, flow velocity, and displacing pressure in gas-gas dispersion.

Much more research remains to be performed before we understand the phenomenon of dispersion in a porous medium. The results of this research may be applied not only to enhanced oil recovery but also to such varied problems as migration of fertilizers toward aquifers and leaks of chemical or nuclear wastes stored in low permeability rocks.

References

[1] Ahmed, U., Crary, S. F., and Coates, G. R., "Permeability Estimation: The Various Sources and Their Interrelationship", JPT, Vol.43, No.5, May 1991, pp.578-587.

[2] Ahn, J. and Suzuki, A., "Radionuclide Transport Within A Low-Level Radioactive Waste Repository with A Cylindrical Nuclide-Path Model", Waste Management, Vol. 10, 1990, pp. 29-40.

[3] Al-Marhoun, A. M., "PVT Correlations for Middle East Crude Oils", JPT, May 1988, pp. 650-666.

[4] Ali, Liaqat, "Quantitative Evaluation of High Rate Flow in Porous Media", Master's Thesis, University of Oklahoma, Norman, 1989.

[5] Amyx, J. W., Bass, Jr. D. M., and Whiting, R. L., Petroleum Reservoir Engineering (Physical Properties), McGraw-Hill Book Company, New York, 1960, pp. 133-210.

[6] Anderson, M. P., "Using Models to Simulate the Movement of Contaminants Through Groundwater Flow Systems", Critical Reviews in Environmental Controls, Vol. 9, No. 2, 1979, pp. 97-156.

[7] Anderson, M. P., "Movement of Contaminant in Groundwater:Ground Water Transport Advection and Dispersion", Groundwater Contamination, National Academy Press, Washington, D.C., 1984, pp. 37-45.

[8] Archie, G. E., "The Electrical Resistivity Log as an Aid in Determining Some Reservoir Characteristics", Trans. AIME, Vol.146, 1942, pp. 54.

[9] Aris, R., "On the Dispersion of a Solute in a Fluid Flowing Through a Tube", Proceedings of the Royal Science Society of London, Series A., Vol. 235, 1956, pp. 67-77.

[10] Aris, R. and Amundson, N. R., "Some Remarks on Longitudinal Miscible Flooding", AIChE Journal, Vol. 3, June, 1957, pp. 280-282.

[11] Aronofsky, J. S., and Heller, J. P., "A Diffusion Model to Explain Mixing of Flowing Miscible Fluids in Porous Media", Petroleum Transactions, AIME. Vol. 210, 1957, pp. 345-349.

[12] Arya, A., Hewett, T. A., Larson, R. and Lake, L. W., "Dispersion and Reservoir Heterogeneity", SPE 14364, Presented at 60th Annual Fall SPE Meeting, Las Vegas, Nevada, September, 1985.

[13] Arya, A., "Dispersion and Reservoir Heterogeneity", PhD Dissertation, University of Texas at Austin, August, 1986, pp. 35-124.

[14] Arya, A., Hewett, T. A., Larson, R. G., and Lake, L. W.,"Dispersion and Reservoir Heterogeneity", SPE Reservoir Engineering, February 1988, pp. 139-147.

[15] Bailey, R. H., and Gogarty, W. B., "Diffusion Coefficients from Capillary Flow", SPE Journal, September 1963, pp. 256-266.

[16] Baker, L. E., "Effects of Dispersion and Dead-End Pore Volume in Miscible Flooding", SPE Journal, June 1977, pp. 219-227.

[17] Batu, V., "A Generalized Two-Dimensional Analytical Solution for Hydrodynamic Dispersion in Bounded Media with the First-Type Boundary Condition at the Source", Water Resources Research, Vol. 25, No. 6, June 1989, pp. 1125-1132.

[18] Bear, J., "The Transition Zone between Fresh and Salt Waters in Coastal Aquifers", Ph.D. Dissertation, Univ. of Calif., Berkley, 1960.

[19] Bear, J., "Some Experiments in Dispersion", Journal of Geophysical Research, Vol. 66, No. 8, August 1961, pp. 2455-2467.

[20] Bear, J., "On the Tensor Form of Dispersion in Porous Media", Journal of Geophysical Research, Vol. 66, No. 4, April, 1961, pp. 1185-1197.

[21] Bear, J., Dynamics of Fluids in Porous Media, American Elsevier Publishing Company Inc., New York, 1972.

[22] Bear, J., and Verruijt, A. "Modeling Groundwater Pollution", Modeling Groundwater Flow and Pollution, D. Reidel, Dordrecht, Holland, 1987.

[23] Bentsen, R. G. and Nielsen, R. F., "A Study of Plane, Radial Miscible Displacement in a Consolidated Porous Medium", SPE Journal, March 1965, pp. 1-5.

[24] Bertin, E. P., Principles and Practices of X-Ray Spectrometric Analysis, 2nd. ed., Plenum Press, New York, 1984, pp. 35-63.

[25] Biot, M. A., "Propagation of Elastic Waves in a Cylindrical Bore Containing a Fluid", Jour. of Applied Physics, Vol.23, No.9, September, 1952, pp. 997.

[26] Blackwell, R. J., "Experiment on Mixing by Fluid Flow in Porous Media", Presented at American Institute of Chemical Engineering and Society of Petroleum Engineering 52nd Annual Meeting, San Francisco, 1959.

[27] Blackwell, R. J., "Laboratory Studies of Microscopic Dispersion Phenomena", SPE Journal, Vol. 2, March, 1962, pp. 1-8.

[28] Blackwell, R. J., Rayne, J. R., and Terry, W. M., "Factors Influencing the Efficiency of Miscible Displacement", Petroleum Transaction, AIME, Vol. 216, 1959, pp. 1-8.

[29] Blatz, S. K. H., "Transient Flow Through Porous Media", Master's Thesis, University of Oklahoma, Norman, 1988.

[30] Boyer, R. L., Morgan, F., and Muskat, M., "A New Method for Measurement of Oil Saturation in Cores", Petroleum Transaction, AIME, Vol. 170, 1947, pp. 15-33.

[31] Bretz, R. E., and Orr, F. M., "Interpretation of Miscible Displacement in Laboratory Cores", SPE/DOE paper 14898, 1986, pp. 251-258.

[32] Bretz, R. E., Specter, R. M., and Orr, F. M., "Effect of Pore Structure on Miscible Displacements in Laboratory Cores", SPE 15017, Presented at the Permian Basin Oil & Gas Recovery Conference of the Society of Petroleum Engineers held in Midland, Texas, March 13-14, 1986.

[33] Bretz, R. E., Specter, R. M., and Orr, F. M., "Mixing During Single-Phase Flow in Reservoir Rocks: Model, Effects of Pore Structure and Interpretation of Experiments", Reservoir Characterization, Edited by Lake, L.W. and Carroll, H.B., Academic Press, Inc., New York, 1986, pp. 585-642.

[34] Bretz, R. E., Welch, S. L. and Morrow, N. R., "Mixing During Two-Phase, Steady State Laboratory Displacements in Sandstone Cores", SPE 15389, Presented at the 61st Ann. Tech. Conf. and Exhibition of Soc. Petr. Eng., New Orleans, LA, Oct.5-8, 1986.

[35] Brigham, W. E.,"Mixing Equation in Short Laboratory Cores", SPE Journal, Feb. 1974, pp. 91-99.

[36] Brigham, W. E., Reed, P. W., and Dew, J. N., "Experiments on Mixing During Miscible Displacement in Porous Media", SPE Journal, Vol. 1, March 1961, 1-8.

[37] Brown, R. J. S., "Connection Between Formation Factor for Electrical Resistivity and Fluid-Solid Coupling Factor in Biot's Equations for Acoustic Waves in Fluid-Filled Porous Media", Geophysics, Vol.45, 1980, pp.1269-1275.

[38] Bruch, J. C., "Two-Dimensional Dispersion Experiments in a Porous Medium", Water Resources Research, Vol. 6, No. 3, June 1970, pp. 791-800.

[39] Burns, D. R. and Cheng, C. H., "Determination of In-Situ Permeability from Tube Wave Velocity and Attenuation", Paper KK in Transac. of the 27th SPWLA Ann. Logging Symp., Houston, TX, June 9-13, 1986.

[40] Calhoun, J. C., Jr., "Basic Parameters for Describing Porous Systems", Producers Monthly, Vol.18, No.11, Sept. 1954, pp.35-39.

[41] Garabedian, S. P., LeBlanc, D. R., Hess, K. M. and Quadri, R. D.:"Natural-Gradient Tracer Test in Sand and Gravel: Results of Spatial Moments Analysis", U.S. Geological Survey

Open File Report 87-109, USGS Program on Toxic Waste-Ground Water Contamination: Proceedings of the 3rd Technical Meeting, Pensacola, Florida, March 23-27, 1987, pp. B13-B16.

[42] Carberry, J. J., "Axial Dispersion and Void-cell Mixing Efficiency in Fluid Flow in Fixed Beds", AIChE Jour., Vol.4, No.1, 1958, pp.13M.

[43] Carberry, J. J., and Bretton, R. H., "Axial Dispersion of Mass in Flow Through Fixed Beds", AIChE Journal, Vol. 4, No. 3, September, 1958, pp. 367-375.

[44] Carberry, J. J., Chemical and Catalytic Reaction Engineering, Chemical Engineering Series, McGraw-Hill Book Company, New York, 1976, pp. 642.

[45] Carman, P. C., "Fluid Flow Through Granular Beds", Trans. Insti. of Chem. Eng., London, Vol.15, 1937, pp.150.

[46] Carman, P. C., Flow of Gases Through Porous Media, Academic Press Inc., New York, 1956.

[47] Cashdollar, B. H., "The Effect of Viscosity Ratio and Path Length on Miscible Displacement in Porous Media", M.S. Thesis, The Pennsylvania State University, January 1959, pp. 1-68.

[48] Castanga, J. P., Zucker, S. M., Shoberg, T. G., "Permeability Indication with Conventional Sonic Waveforms", Paper MM in Transac. of the 28th SPWLA Ann. Logging Symp., London, June 29-July 2, 1987.

[49] Chandrasekhara, B. C., Rudraiah, N., and Nagaraj, S. T., "Velocity and Dispersion in Porous Media", Engineering Science, Vol. 18, 1980, pp. 921-929.

[50] Charlaix, E., Hulin, J. P., Leroy, C., and Zarcone, C., "Experimental Study of Tracer Dispersion in Flow Through Two-Dimensional Networks of Etched Capillaries", Physical Review, 1988, pp.1727-1732.

[51] Cheng, P. "Thermal Dispersion Effects in Non-Darcian Convective Flows in a Saturated Porous Medium", Letters in Heat and Mass Transfer, Vol. 8, 1981, pp. 267-270.

[52] Cheng, P. and Vortmeyer, D. "Transverse Thermal Dispersion and Wall Channelling in a Packed Bed with Forced Convective Flow", Chemical Engineering Science, Vol. 43, No. 9, 1988, pp. 2523-2532.

[53] Chen, S. X., "Investigation of Dispersivity as a Reservoir Rock Characteristic and Its Determination From Well Logs", PhD Dissertation, University of Oklahoma, Norman, 1991.

[54] Chen, S. M., Allard, D. R., and Anli, J., "Factors Affecting Solvent Slug Size Requirements in Hydrocarbon Miscible Flooding", SPE/DOE 12636, Presented at the SPE/DOE Fourth Symp. on Enhanced Oil Recovery, Tulsa, OK, April 15-18, 1984.

[55] Chin, D. A. and Wang, T., "An Investigation of the Validity of First-Order Stochastic Dispersion Theories in Isotropic Porous Media", Water Resources Research, Vol. 28, No. 6, June 1992, pp. 1531-1542.

[56] Ci-Qun, L. and Jie, Y., "Radial Transport in Porous Media with Dispersion and Adsorption", Institut Francais du Petrole, 2nd European Conference on the Mathematics of Oil Recovery, Paris, France, 1990, pp. 323-325.

[57] Clement, K. and Jorgensen, S. B.,"Experimental Investigation of Axial and Radial Thermal Dispersion in a Packed Bed", Chemical Engineering Science, Vol. 38, No. 6, 1983, pp. 835-842.

[58] Coats, K. H. and Smith, B. D., "Dead-End Pore Volume and Dispersion in Porous Media", SPE Journal, Vol. 4, March 1964, pp. 73-84.

[59] Coelho, M. A. N. and Guedes de Carvalho, J. R. F., "Transverse Dispersion in Granular Beds. Part I. Mass Transfer from a Wall and the Dispersion Coefficient in Packed Beds", Chemical Engineering Research and Design, Vol. 66, March 1988, pp. 165-177.

[60] Coelho, M. A. N. and Guedes de Carvalho, J. R. F.,"Transverse Dispersion in Granular Beds. Part II. Mass Transfer from Large Spheres Immersed in Fixed or Fluidised Beds of Small Inert Particles", Chemical Engineering Research and Design, Vol. 66, March 1988, pp. 178-189.

[61] Collins, R. E., Flow of Fluid Through Porous Media, The Petroleum Publishing Company, Tulsa, Oklahoma, 1961, pp. 1-46.

[62] Correa, A. C., Pande, K. K., Ramey Jr., H. J. and Brigham, W. E., "Computation and Interpretation of Miscible Displacement Performance in Heterogeneous Porous Media", SPE Reservoir Engineering, February 1990, pp. 69-78.

[63] Cornell, D. and Katz, D. L., "Flow of Gases Through Consolidated Porous Media", Ind. Eng. Chem., Vol.45, No.10, 1953, pp.2145-2152.

[64] Crank, J., The Mathematics of Diffusion, Oxford University Press, Oxford, England, 1956, pp. 347.

[65] Cromwell, V., Kortum, D. J., and Bradley, C., "The Use of a Medical Computer Tomography (CT) System to Observe Multiphase Flow in Porous Media", SPE 13098, Presented at the 59th Annual Technical Conference and Exhibition, Houston. Texas, September 16-19, 1984.

[66] Csaszar, A. K., and Tinklepaugh, B. M., "New Apparatus and Technique for Characterization of Reservoir Rocks", Mineral Industries Experiment Station Circular, No. 66, The Pennsylvania State University, October 23-25, 1963, pp. 131-139.

[67] Cunningham, R. E. and Williams, R. J. J., Diffusion in Gases and Porous Media, Plenum Press, New York, 1980.

[68] Cussler, E. C., Diffusion: Mass Transfer in Fluid Systems, London, Cambridge Univ. Press, 1984.

[69] Dagan, G., Flow and Transport in Porous Formations, New York, Springer-Verlag, 1989.

[70] David, D. J., Gas Chromatograph Detectors, John Wiley & Sons, New York, 1974.

[71] Davies, G. W., Muggeridge, A. H. and Jones, A. D. W., "Miscible Displacements in a Heterogeneous Rock: Detailed Measurements and Accurate Predictive Simulation", SPE 22615, Presented at the 66th Annual Technical Conference and Exhibition of the Society of Petroleum Engineers, Dallas, Texas, October 6-9, 1991, pp. 223-237.

[72] De Jong, G. D. J., "Longitudinal and Transverse Diffusion in Granular Deposits", Transactions of the American Geophysical Union, Vol. 39, No. 1, February 1958, pp. 67-74.

[73] De Jong, G. D. J. and Van Duijn, C. J., "Transverse Dispersion from an Originally Sharp Fresh-Salt Interface Caused by Shear Flow", Journal of Hydrology, Vol. 84, 1986, pp. 55-79.

[74] Deans, H. A.,"A Mathematical Model for Dispersion in the Direction of Flow in Porous Media", SPE Journal, March 1963, pp. 49-52.

[75] Dillon, P. J., "An Analytical Model of Contaminant Transport from Diffuse Sources in Saturated Porous Media", Water Resources Research, Vol. 25, No. 6, June 1989, pp. 1208-1218.

[76] Donalson, E. C., Kendall, R. F., and Manning, F. S., "Dispersion and Tortuosity in Sandstones", SPE 6190, (1976).

[77] Dowling, A. J. and Boyd, J. F., "Acoustic Permeability Log Utilizing Differential Travel Time Measurements", U.S. Patent 3,900,826, August 19, 1975.

[78] Dullien, F. A. L., Porous Media: Fluid Transport and Pore Structure, 2nd ed. Academic Press, Inc., San Diego, California, 1992.

[79] Dumore, J. M., "Stability Considerations in Downward Miscible Displacement", SPE Journal, December, 1964, pp. 358-362.

[80] Dupuit, A. J. E. J., Etudes Theoriques Et Pratiques Sur Le Mouvement Des Eaux, 1863.

[81] Dutta, S., "An Experimental Investigation of Dispersivity and its Role as an Oil Reservoir Rock Property", Master's Thesis, University of Oklahoma, 1984.

[82] Dykstra, H. and Parsons, R. L., "The Prediction of Oil Recovery by Water Flood", Secondary Recovery of Oil in the United States, 2nd ed., API, 1950, pp.160-174.

[83] Enick, R. M., Klara, S. M. and Jones, J.,"The Dispersion of a Nonuniform Slug Flowing in a Porous Medium", SPE Journal , Vol. 8, 1993, pp. 293-301.

[84] Epstein, N., "On Tortuosity and the Tortuosity Factor in Flow and Diffusion Through Porous Media", Chem. Eng. Sci., Vol.44, No.3, 1989, pp.777-779.

[85] Flagg, A. H., Myers, J. P., Campbell, J. L. P., Terry, J. M. and Mardock, E. S., "Radioactive Tracers in Oil production problems", SPE Reprint Series No. 2a (1973) p. 97.

[86] Franzini, J. B., "Porosity Factor for Case of Laminar Flow Through Granular Media", Trans. Amer. Geophys. Union, Vol. 32, 1951, pp. 443.

[87] Freeze, R. A. and Cherry, J. A., "Groundwater Contamination", Groundwater, Prentice-Hall, Englewood Cliffs, NJ., 1979.

[88] Fried, J. J., "Some Recent Applications of the Theory of Dispersion in Porous Media", Proceedings of the Second Symposium on Transport Phenomena in Porous Media, Vol. 2, August 7-11, 1972, University of Guelph, Ontario, Canada.

[89] Fried, J. J., Groundwater Pollution, Elsevier, New York, 1975, pp. 330.

[90] Gelhar, L. J., Mantoglou, A., Welty, C., and Rehfeldt, K. R., "A Review of Field-scale Physical Solute Transport Processes in Saturated and Unsaturated Porous Media", Electric Power Research Institute, Report EA-4190, Project RP 2485-5, Final Report, August, 1985.

[91] Gelhar, L. W., and Axness, C. L., "Three-dimensional Stochastic Analysis of Macro-Dispersion in Aquifers", Water Resource Research, 19, 1979.

[92] Gelhar, L. W., Gutjahr, A. L., and Naff, R. L., "Stochastic Analysis of Macro-Dispersion in a Stratified Aquifer", Water Resource Research, Vol. 15, No. 6, Dec. 1979.

[93] Goldstein, S., "Some Two-Dimensional Diffusion Problems with Circular Symmetry", Proceedings of the London Mathematical Society, Series 2, vol. 34, 1932, pp. 51-88.

[94] Goodknight, R. C., Klikoff, W. A. and Fatt, I., "Non-Steady-State Fluid Flow and Diffusion in Porous Media Containing Dead End Pore Volume", Jour. Phys. Chem., Vol.64, 1960, pp.1162.

[95] Grane, F. E. and Gardner, G. F. H.,"Measurements of Transverse Dispersion in Granular Media", Journal of Chemical and Engineering Data, Vol. 6, No. 2, April 1961, pp. 283-287.

[96] Greenkorn, R. A., Flow Phenomena in Porous Media, Marcel Deker, Inc., New York, 1983, pp. 1-251.

[97] Greenkorn, R. A., and Kessler, D. P., "Dispersion in Heterogeneous Nonuniform Anisotropic Porous Media", Flow Through Porous Media, American Chemical Society, Washington, DC., Chapter 8, 1970, pp. 160-178.

[98] Guiochon, G. and Guillemin, C. L., Quantitative Gas Chromatograph, Elsevier Science Publishing Company Inc., New York, 1988.

[99] Gunn, D. J.,"Axial and Radial Dispersion in Fixed Beds", Chemical Engineering Science, Vol. 42, No. 2, 1987, pp.363-373.

[100] Gupta V. K., Bhattacharya, R. N. and Sposito, G., "A Molecular Approach to the Foundations of the Theory of Solute Transport in Porous Media. I. Conservative Solutes in Homogeneous Isotropic Saturated Media", Journal of Hydrology, Vol. 50, 1981, pp. 355-370.

[101] Hall, H. N. and Geffen, T. M., "A Laboratory Study of Solvent Flooding", Petroleum Transactions, AIME, Vol. 210, 1957, 58-57.

[102] Hansbo, P., "The Characteristic Streamline Diffusion Method for Convection-Diffusion Problems", Computer Methods in Applied Mechanics and Engineering, Vol. 96, 1992, pp. 239-253.

[103] Handy, L. L., "An Evaluation of Diffusion Effects in Miscible Displacement", Petroleum Transactions AIME, Vol. 216, 1959, pp. 382-384.

[104] Haring, R. E., and Greenkorn, R. A., "A Statistical Model of a Porous Medium With Non-Uniform Pores", American Institute of Chemical Engineering Journal, Vol. 16, 1970, pp. 477-483.

[105] Harleman, D. R. E., Mehlhorn, P. E., and Rumer, R. R., "Dispersion-Permeability Correlation in Porous Media", Jour. Hydraulic Division, Proc. Amer. Soc. Civil Eng., March 1963, pp.67-85.

[106] Harleman, D. R. F. and Rumer, R. R., "Longitudinal and Lateral Dispersion in an Isotropic Porous Medium", Journal of Fluid Mechanics, Vol. 16, 1963, pp. 385-394.

[107] Harris, M. and Bissey, L. T., "A Study of Gas-Gas Displacements in Linear Unconsolidated Porous Media", Mineral Industries Experiment Station Circular, No. 61,'The Pennsylvania State University, 1961, pp. 58-87.

[108] Hassinger, R. G. and von Rosenberg, D. W. "A Mathematical and Experimental Examination of Transverse Dispersion Coefficients", SPE Journal, June 1968, pp. 195-204.

[109] Herron, M., "Estimating the Intrinsic Permeability of Clastic Sediments from Geochemical Data", Paper HH in Transac. of the 28th SPWLA Ann. Logging Symp., London, June 29-July 2, 1989.

[110] Hetherington, Charles Ray, "The Unsteady Flow of Natural Gas Through Porous Media", Master's Thesis, University of Oklahoma, Norman, 1941.

[111] Hicks, P. J., Narayanan, R., and Deans, H. A., "An Experimental Study of Miscible Displacements in Heterogeneous Carbonate Cores Using X-Ray CT", SPE 20492, Presented at the 65th Annual Technical Conference and Exhibition of the Society of Petroleum Engineers, New Orleans, Louisiana, September 23-26, 1990.

[112] Hong, J. T. and Tien, C. L.,"Analysis of Thermal Dispersion Effect on Vertical-Plate Natural Convection in Porous Media", International Journal of Heat and Mass Transfer, Vol. 30, No. 1, 1987, pp. 143-150.

[113] Hong, J. T., Yamada, Y. and Tien, C. L.,"Effects of Non-Darcian and Nonuniform Porosity on Vertical Plate Natural Convection in Porous Media", Transactions of the American Society of Mechanical Engineers, Vol. 109, May 1987, pp. 356-362.

[114] Hounsfield, G. N., "A Method and Apparatus for Examination of a Body by Radiation Such as X- or Gamma-Radiation", British Patent No. 1,283,915, London, 1972.

[115] Hove, A., Ringen, J. K., and Road, P. A., "Visualization of Laboratory Corefloods with the Aid of Computerized Tomography of X-Rays", SPE 13654, Presented at the Society of Petroleum Engineers 1985 California Regional Meeting, Bakersfield, California, March 27-29, 1985.

[116] Hudson, H. E. and Roberts, R. E., Proc. 2nd Midw. Conf. Fluid Mech. Eng. Series, Vol.31, No.3, 1952, pp.105.

[117] Hulin, J. P., Charlaix, E., Plona, T. J., and Guyon, L. O., "Tracer Dispersion in Sintered Glass beads with a Bidisperse Size Distribution", AIChE Jour., Vol.34, No.4, April 1988, pp.610-617.

[118] Hunt, H. B., "Method for Detecting Subsurface Mineral Bodies", SAFR. 77/2, 442, C 2/15/78, F 4/22/77 Pr US 5/3/76 Texas Pacific Oil Co. 1978 SRPA #245897.

[119] Hunt, P. K., Engler, P., and Bajsarowicz, C., "Computed Tomography as a Core Analysis Tool: Applications, Instrument Evaluation, and Image Improvement Techniques", JPT, September 1988, pp. 1203-1210.

[120] Hurst, William, Advances in Petroleum Engineering, Pennwell Publishing Co., Tulsa, Oklahoma, 1981.

[121] Jacob, C. E., "Report of the Subcommittee on Permeability", Trans. Amer. Geophys. Union, Vol. 27, 1946, pp.245.

[122] Jasti, J. K., Jesion, G., and Feldkamp, L., "Microscopic Imaging of Porous Media Using X-Ray Computer Tomography", SPE 20495, Presented at the 65th Annual Technical Conference and Exhibition of the Society of Petroleum Engineers, New Orleans, Louisiana, September 23-26, 1990.

[123] Jasti, J. K., Vaidya, R. N., and Fogler, H. S., "Capacitance Effects in Porous Media", SPE Reservoir Eng., November 1988, pp.1207-1214.

[124] Johnson, D. L., Koplik, J., and Dashen, R., "Theory of Dynamic Permeability and Tortuosity in Fluid-Saturated Porous Media", Jour. Fluid Mech., Vol.176, 1987, pp.379-402.

[125] Johnson, D. L., Plona, T. J., and Scala, C., "Tortuosity and Acoustic Waves", Physical Review Letters, Vol.49, No.25, December 20, 1982, pp.1840-1844.

[126] Johnson, D. L. and Sen, P. N., "Multiple Scattering of Acoustic Waves with Application to the Index of Refraction of Fourth Sound", Physical Review B, Vol.24, No.5, Sept. 1981, pp.2486-2496.

[127] Kelkar, B. G. and Gupta, S. P., "A Numerical Study of Viscous Instabilities: Effect of Controlling Parameters and Scaling Considerations", SPE 18094, Presented at the 63rd Annual Technical Conference and Exhibition of the Society of Petroleum Engineers, Houston, Texas, October 2-5, 1988, pp. 409-420.

[128] Kenyon, W. E., Day, P. I., Straley, C., and Willemsen, J. F., "Compact and Consistent Representation of Rock NMR Data for Permeability Estimation", SPE 15643, Presented at the SPE Ann. Conf. and Exhibition, October 5-8, 1986.

[129] Khan, Abdul Raoof, "Laboratory Investigation of Linear Unsteady-State Gas Flow Through Porous Media Including the Effect of Non-Darcy Flow", Master's Thesis, University of Oklahoma, 1967.

[130] Kincaid, D., Cheney, E.W., Numerical Mathematics and Computing, Calif: Brooks/Cole Publishing Co., 1980.

[131] Kitagawa, K., "Sur le Dispersement et l'ecart Moyen de l'econlement des eaux Sonterraines, I. Experiences avee un modele le Laboratoire", Kyoto Imperial Univ., Coll. Sci. Mem. Series A, Vol.17, 1934, pp.37-42.

[132] Kitagawa, K., "Sur le Dispersement et l'Ecart Moyen de l'Ecoulement des Eaux Souterraines", Memoirs of the College of Science, Series A, Kyoto University, 1934, pp. 431-441.

[133] Klotz, D., and Moser, H., "Hydrodynamic Dispersion as Aquifer Characteristic: Model Experiments With Radioactive Tracers", Proceedings of Isotope Techniques in Groundwater Hydrology, Vol. 2, 1974, pp. 341-355.

[134] Klotz, D., Seiler, K. P., Moser, H. and Neumaier, F., "Dispersivity and Velocity Relationship from Laboratory and Field Experiments", Jour. Hydrology, Vol.45, 1980, pp.169-184.

[135] Kobus, H. E. and Spitz, K., "Transverse Mixing of Stratified Flows in Porous Media", Presented at the 21st Congress of the International Association for Hydraulic Research, Melbourne, Australia, August 19-23, 1985, pp. 169-174.

[136] Koch, D. L. and Brady, J. F.,"Diffusion in Fixed Beds", Journal of Fluid Mechanics, Vol. 154, 1985, pp. 399-427.

[137] Koch, H. A., and Slobod, R. L., "Miscible Slug Process", Petroleum Transaction, AIME, Vol. 210, 1957, pp. 39-47.

[138] Konikow, L. F. and Bredehoeft, J. D., "Modeling Flow and Chemical Quality Changes in an Irrigated Stream-Aquifer System", Water Resources Research, Vol. 10, No. 3, 1974, pp. 546-562.

[139] Koval, E. J., "A Method for Predicting the Performance of Unstable Miscible Displacement in Heterogeneous Media", SPE Journal, June 1963, pp. 145-154.

[140] Kozeny, J., "Über Kapillare Leitung des Wassers in Boden", Ber. Wien Akad., 136A, 1927, pp.271.

[141] Kreft, A. and Zuber, A., "On the Physical Meaning of the Dispersion Equation and Its Solutions for Different Initial and Boundary Conditions", Chem. Eng. Sci., Vol.33,1978, pp.1471-1480.

[142] Kukal, G. C., "Log Analysis in Low-Permeability Gas Sand Sequences --- Correcting for Variable Unflushed Gas Saturation", Transac. of the 24th SPWLA Ann. Logging Symp., Paper F, June 1983.

[143] Kukal, G. C., "A Systematic Approach for the Effective Log Analysis of Tight Gas Sands", SPE/DOE/GRI 12851, Presented at the 1984 SPE/DOE/GRI Unconventional Gas Recovery Symp., Pittsburg, PA, May 13-15, 1984.

[144] Laird, A. D. K. and Putnam, J. A., "Fluid Saturation in Porous Media By X-Ray Technique", Petroleum Transactions, AIME, Vol. 192, 1951, pp. 275-284.

[145] Laird, A. D. K., and Putnam, J.A., "Three Component Saturation in Porous Media by X-Ray Techniques", Petroleum Transactions, AIME, Vol. 216, 1959, pp. 216-220.

[146] Lake, L. W., Enhanced Oil Recovery, Prentice Hall, Englewood Cliffs, New Jersey, 1989.

[147] Lake, L. W. and Hirasaki, G. J., "Taylor's Dispersion in Stratified Porous Media", SPE Journal, August, 1981, pp. 459-468.

[148] Lallemand-Barres, A. and Peaudecerf, P., "Rechereche des Relations Entre la Valeur de la Dispersivite Macroscopique d'un Milieu Aquifere, ses Autres Caracteristiques et les Conditions de Mesure", Bulletin du BRGM, 2e Serie, Section III, No. 4, 1978.

[149] Lambert, M.E., "A Statistical Study of Reservoir Heterogeneity", M.S. Thesis, University of Texas at Austin, 1981, pp. 1-25.

[150] Lawson, D. W., and Elrick, E. E., "A New Method For Determining and Interpreting Dispersion Coefficients in Porous Media", Proceedings, Fundamentals of Transport Phenomena in Porous Media: International Association for Hydraulic Research, International Society of Soil Science, Second Symposium, University of Guelph, Canada, August 7-11, 1972, pp. 753-777.

[151] Lebreton, F., Sarya, J. P., and Moriher, P., "Acoustic Method and Device for Determining Permeability Logs in Boreholes", U.S. Patent 3,622,969, Nov. 23, 1971.

[152] Lee, S. T., and Okyiga, M., "Analysis of Dispersion in a Layered Porous Medium with Micro-Heterogeneity of Arbitrary Shapes and Size Distribution", SPE 15387, 61th Annual Conference in New Orleans, LA, Oct. 5-8, 1986.

[153] Lee, S. L. P. and De Lasa, H. I., "Radial Dispersion Model for Bubble Phenomena in Three-Phase Fluidized Beds", Chemical Engineering Science, Vol. 43, No. 9, 1988, pp. 2445-2449.

[154] Legatski, Max W., and Katz, Donald L., "Dispersion Coefficients for Gases Flowing in Consolidated Porous Media", SPE Journal, March 1967, pp. 43-53.

[155] Lenormand, R., Kalaydjan, F., Bieber, M. T., and Lombard, J. M., "Use of a Multifractal Approach for Multiphase Flow in Heterogeneous Porous Media; Comparison with CT-Scanning Experiment", SPE 20475, Presented at the 65th Annual Technical Conference and Exhibition of the Society of Petroleum Engineers, New Orleans, Louisiana, September 23-26, 1990.

[156] Ligthelm, D. J., "Reservoir Engineering Approach to Viscosity Grading in Polymer Drives", SPE Journal, Vol. 2, 1989, pp. 159-166.

[157] Li, Y., "An Experimental Study of Dispersion Characteristics in Consolidated Porous Media and The Determination of The Flow Characterization in Miscible Displacement Flooding", PhD Dissertation, University of Oklahoma, Norman, 1992.

[158] Maini, B. B., Lonescu, E., and Batycky, J. P., "Miscible Displacement of Residual Oil-Effect of Wettability on Dispersion in Porous Media", Jour., Cand. Pet. Tech., May-June 1986, pp. 36-41.

[159] Malik, N. A., "Determination of Dispersivity and Its Correlation with Reservoir Rock Properties", M.S. Thesis, Univ. of Okla., Norman, OK., 1989.

[160] Mardock, E. S., and Watkins, J. W., "Use of Radioactive Iodine as a Tracer in Water-Flooding Operations", Trans. AIME, Vol. 201, 1954, pp. 209.

[161] Matheron, G., and DeMarsily, G., "Is Transport in Porous Media Always Diffusive?", Water Resour. Res. 16, 1980, 901-917.

[162] Meegoda, N. J., "An Expression for the Permeability of Anisotropic Granular Media", Intern. Jour. for Numeri. and Analyt. Methods in Geomechanics, Vol.13, 1989, pp.575-598.

[163] Mendenhall, W., Statistics for the Engineering and Computer Sciences, Dellen Publishing Company, San Francisco, 1985, pp. 176-214.

[164] Menzie, D. E., Dutta, S., and Shadizadeh, R., "A New Method of Coating Oilfield Core for Laboratory Studies", JPT, May 1988, pp.643-644.

[165] Menzie, D. E. and Dutta, S., "Dispersivity as an Oil Reservoir Rock Characteristic", Final Report to the Department of Energy, DOE/BC/10851-15, University of Oklahoma, December, 1989, pp. 1-83.

[166] Menzie, D. E., "Study of Dispersion Characteristics in Consolidated Porous Media and Determination of the Flow Characterization", Annual Report to the Department of Energy, DOE/BC/14652.000, University of Oklahoma, October 1992.

[167] Menzie, D. E., "Dispersion Measurement as a Method of Quantifying Geologic Characterization and Defining Reservoir Heterogeneity", Final Report to the Department of Energy, DOE-22-90BC14652.000, University of Oklahoma, 1994, (work in progress).

[168] Mercado, A., "The Spreading Pattern of Injected Water in a Permeability Stratified Aquifer," Proceeding of International Associate Society Hydraulic Symposium, Haifa, Publ. No. 72, 1967, pp. 23-36.

[169] Mertz, V., "Mixing of Gases in Porous Media", Master's Thesis, University of Oklahoma, Norman, 1941.

[170] Millheim, K., "An Experimental Study of Linear Unsteady State Gas Flow Through Low Permeability Porous Media", Master's Thesis, University of Oklahoma, Norman, 1964.

[171] Mohanty, K. K. and Salter, S. J., "Multiphase Flow in Porous Media: III. Oil Mobilization, Transverse Dispersion, and Wettability", SPE 12127 presented at the 58th Annual Technical Conference of the Society of Petroleum Engineers of AIME, San Francisco, CA, October 5-8, 1983.

[172] Moltyaner, G. L. and Killey, R. W. D., "Twin Lake Tracer Tests: Transverse Dispersion", Water Resources Research, Vol. 24, No. 10, October 1988, pp. 1628-1637.

[173] Morgan, F., McDowell, J. M. and Doty, F. C., "Improvements in X-Ray Saturation Technique of Studying Fluid Flow", Petroleum Transactions, AIME, Vol. 189, 1950, pp. 183-194.

[174] Narayanan, K., "Flow Models Based on the Structure of Heterogeneous Carbonate Formations" , PhD Dissertation, University of Houston, Texas, May 1988, pp. 106-167.

[175] Narayanan, K., and Deans, H. A., "A Flow Model Based on the Structure of Heterogeneous Porous Media", SPE 18328, Presentation at the 63rd Annual Technical Conference and Exhibition of the Society of Petroleum Engineers, Houston, Texas, October 2-5, 1988, pp. 675-690.

[176] Novak, J., Quantitative Analysis by Gas Chromatograph, 2nd. ed. revised, Marcel Dekker, Inc., New York, 1988.

[177] Nwosu, S. N., "Stable Isotope Analysis by Nuclear Reaction with Applications to Medicine and Geology", PhD Dissertation, University of Oklahoma, Norman, 1988.

[178] Oak, W.J. and Ehrlich, R., "A New X-Ray Absorption Method For Measurement of Three-Phase Relative Permeability", SPE Reservoir Engineering, February 1988, pp. 199-206.

[179] Oaks, D. B. and Edworthy, K. J., "Field Measurements of Dispersion Coefficients in the United Kingdom", Presented at the Groundwater Quality -- Measurement, Prediction and Protection Conf. at the Univ. of Reading, Berkshire, England, Sept.6-8, 1976.

[180] Ogata, A. and Banks, R. B., "A Solution of The Differential Equation of Longitudinal Dispersion in Porous Media", Geological Survey Professional Paper No. 411-A, United States Department of the Interior, Washington, D.C., 1961, pp. 7.

[181] Ogata, A., "Theory of Dispersion in a Granular Medium", U.S. Geological Survey Professional Paper 411-I, 1970.

[182] Ogata, A., "Transverse Diffusion in Saturated Isotropic Granular Media", Fluid Movement in Earth Materials, Geological Survey Professional Paper 411-B, United States Printing Office, Washington, 1961, pp. B1-B8.

[183] Ogata, A., "Two-Dimensional Steady-State Dispersion in a Saturated Porous Medium", Journal of Research, U.S. Geological Survey, Vol. 4, No. 3, May-June 1976, pp. 227-284.

[184] Orlob, G.T., and Radhakrishna, G.N., "The Effect of Entrapped Gases on the Hydraulic Characteristics of Porous Media", Trans AGU., 1958, Vol. 39, 648.

[185] Parker, J. C. and Genuchten, M. Th. van, Determination of Transport Parameters from Laboratory and Field Tracer Experiments, Virginia Agricultural Experiment Station, Virginia Polytechnic Institute and State University, 1984.

[186] Paterson, M. S., "The Equivalent Channel Model for Permeability and Resistivity in Fluid-Saturated Rocks --- A Reappraisal", Mech. Mater., Vol.2, No.4, 1983, pp.345-352.

[187] Peaudecerf, P., and Santy, J. P., "Application of a Mathematical Model to the Characterization of Dispersion Effects of Groundwater Quality", Progress Water Technology, Vol. 10, No. 5/6, 1978, pp. 443-454.

[188] Percious, D. J., "Aquifer Dispersivity by Recharge-Discharge of a Fluorescent Dye Tracer Through a Single Well", M.S. Thesis, University of Arizona, Tucson, 1969.

[189] Perkins, T. K. and Johnston, O. C., "A Review of Diffusion and Dispersion in Porous Media", SPE Journal, March 1963, pp. 70-84.

[190] Perkins, T. K., Johnston, O. C. and Hoffman, R. N., "Mechanics of Viscous Fingering in Miscible Systems", SPE Journal, December 1965, pp. 301-317.

[191] Peter, et al., "A Stability Theory for Miscible Displacement", SPE of ASME, SPE 13167, 1984, pp. 1-12.

[192] Pfannkuch, H., "Coupling Phenomenon During Miscible Displacement", Experiment Station Circular, Vol. 71, 1966, The Pennsylvania State University, pp. 69-81.

[193] Pfannkuch, H. O., "On the Correlation of Electrical Conductivity Properties of Porous Systems with Viscous Flow Transport Coefficients", Fundamentals of Transport Phenomena in Porous Media, New York, Elsevier Publishing Comp., 1972, pp.42-54.

[194] Pickens, J. F. and Grisak, G. E., "Scale-Dependent Dispersion in a Stratified Granular Aquifer", Water Resources Research, Vol. 17, No. 4, August 1981, pp. 1191-1211.

[195] Pickens, J. F., Cherry, J. A., Gillham, R.W., and Merritt, W.F., "Field Studies of Dispersion in a Shallow Sandy Aquifer", Proceeding of Department of Energy Invitational Well Testing Symposium, Berkeley, California, October 19-21, 1977, pp. 55-62.

[196] Pickens, J. F. and Grisak, G. E., "Modeling of Scale-Dependent Dispersion in Hydrogeologic Systems", Water Resources Research, Vol.17, No.6, December 1981, pp.1701-1711.

[197] Pinder, G. F., "A Galerkin-Finite Element Simulation of Groundwater Contamination on Long Island, New York", Water Resources Research, Vol. 9, No. 6, 1973, pp. 1657-1669.

[198] Potter, G.F. and Groves, D.R., "Displacements, Saturations, and Porosity Profiles From Steady-State Permeability Measurements", SPE 19679, Presented at the 64th Annual Technical Conference and Exhibition of the Society of Petroleum Engineers, San Antonia, Texas, October 8-11, 1989.

[199] Poulin, T. J., "The Determination of the Coefficient of Dispersion in Sandstones", Master's Thesis, University of Oklahoma, Norman, 1985.

[200] Pozzi, A. L. and Blackwell, R. J., "Design of Laboratory Models for Study of Miscible Displacement", SPE Journal, March 1963, pp. 28-40.

[201] Prausnitz, J. M., "Longitudinal Dispersion in a Packed Bed", AIChE Jour., Vol.4, No.1, 1958, pp.14M.

[202] Raimondi, P., Gardner, G. H. F. and Petrick, C. B., "Effect of Pore Structure and Molecular Diffusion on the Mixing of Miscible Liquids Flowing in a Porous Media", Reprint 43 Presented at AICHE-SPE Joint Symposium, San Francisco, California, December 6-9, 1959.

[203] Rameriez, W. F., Shular, P. J., and Friedman, F., "Convection, Dispersion and Adsorption of Surfactant in Porous Media", SPE Journal, Dec. 1980, pp. 430-438.

[204] Ravnaas, R. D., "Determination of Field Scale Dispersivities by Mathematical Modeling", M.S. Thesis, University of Texas at Austin, Texas, August, 1981.

[205] Robbins, G. A., "Methods for Determining Transverse Dispersion Coefficients of Porous Media in Laboratory Column Experiments", Water Resources Research, Vol. 25, No. 6, June 1989, pp. 1249-1258.

[206] Robson, S. G., "Application of Digital Profile Modeling Techniques to Ground-Water Solute Transport at Barstow, California", U. S. Geological Survey Water Supply Pap., 2050, 1978, pp. 28.

[207] Rohovets, N. and Fertl, W. H., "Digital Shaly Sand Analysis Based on Waximan-Smits Model and Log-Derived Clay Typing", The Log Analyst, May-June, 1982, pp.7-23.

[208] Rosenbaum, J. H., "Synthetic Microseismograms: Logging in Porous Formations", Geophysics, Vol.39, No.1, Feb., 1974, pp.14-32.

[209] Rumer, R. R. Jr., "Longitudinal Dispersion in Steady and Unsteady Flow", Journal of the Hydraulics Division of Proceedings of the American Society of Civil Engineers, HY4, July 1962, pp. 147-172.

[210] Russo, D., "Stochastic Modeling of Macrodispersion for Solute Transport in a Heterogeneous Unsaturated Porous Formation", Water Resources Research, Vol. 29, No. 2, February 1993, pp. 383-397.

[211] Rust, C. F., "Electrical Resistivity Measurements on Reservoir Rock Samples by the Two-Electrode and Four-Electrode Methods", Petr. Transactions of AIME, Vol.195, 1952.

[212] Saffman, P.G., "Dispersion in Flow through a Network of Capillaries", Chemical Engineering Science, Vol. 11, 1959, pp. 125-129.

[213] Saffman, P.G., "A Theory of Dispersion in a Porous Medium", Journal of Fluid Mechanics, Vol. 6, January 1959, pp. 21-129.

[214] Saffman, P. G., "Dispersion Due to Molecular Diffusion Through a Network of Capillaries", Jour. of Fluid Mech., Vol.7, 1960, pp.194.

[215] Sahimi, et al., "Dispersion in Flow Through Porous Media-1. One Phase Flow", Chemical Engineering Science, Vol. 41, No. 8, 1986, pp. 2103-2122.

[216] Sahimi, M., Davis, H. T. and Scriven, L. E., "Dispersion in Disordered Porous Media", Chemical Engineering Commun. Vol. 23, 1983, pp. 329-341.

[217] Sandrea, R., Dynamics of Petroleum Reservoirs Under Gas Injection, Gulf Publishing Company, Houston, Texas, 1974.

[218] Sawyer, W. K., Pierce, C. I., and Lowe, R. B., "Electrical and Hydraulic Flow Properties of Appalachian Petroleum reservoirs", Bureau of Mines Report of Investigations No.7519, June 1971.

[219] Scheidegger, A. E., "Statistical Hydrodynamics in Porous Media", Journal of Applied Physics, Vol. 25, No.8, August, 1954, pp. 994-1001.

[220] Scheidegger, A. E., "General Theory of Dispersion in Porous Media", Journal of Geophysical Research, Vol.66, No. 10, October 1961, pp. 3273-3270.

[221] Scheidegger, A. E., The Physics of Flow Through Porous Media, University of Toronto Press, Vienna, Austria, February, 1972.

[222] Scheidegger, A. E. and Larson, V. C., "Asymmetry of the Concentration Front During Miscible Displacement in Porous Media", Can. Jour. Phys., Vol.36, 1958, pp.1476.

[223] Schwartz, F. W., "Macroscopic Dispersion in Porous Media: The Controlling Factors", Water Resources Research, Vol. 13, No. 4, August 1977, pp. 743-752.

[224] Schwartz, F. W., "On Radioactive Waste Management, Model Analysis of a Proposed Site", Journal of Hydrology, Vol. 32, 1977, pp. 257.

[225] Seevers, D. O., "A Nuclear Magnetic Method for Determining the permeability of Sandstones", Paper L in Transc. of the 7th SPWLA Ann. Logging Symp., Tulsa, OK, May 8-11, 1966.

[226] Shadizadeh, S. R., "An Experimental Investigation of the Dependence of Dispersion on Flow Parameters and Porous Media Properties During Solute Transport Through Consolidated Porous Media Independent of Fickian Assumptions", PhD Dissertation, University of Oklahoma, Norman, 1991.

[227] Schmidt, C.D., "Mixing of Gas in Porous Media", Master's Thesis, University of Oklahoma, Norman, 1940.

[228] Shamir, U., and Herleman, D. R., "Dispersion in Layered Porous Media", Journal of Hydraulics Division. Proceedings of the American Society of Civil Engineers, HY5, Sept. 1967, pp. 237-260.

[229] Shen, H. T., "Transient Dispersion in Uniform Porous Media Flow", Journal of the Hydraulics Division, June 1976, pp.707-716.

[230] Simpson, E. S., "Transverse Dispersion in Liquid Flow Through Porous Media", Fluid Movement in Earth Materials, Geological Survey Professional Paper 411-C, United States Printing Office, Washington, 1962, pp. C1-C30.

[231] Slawinski, A., "Conductibite Dun Electrolyte Contenant Des Spheres Dielectriques", Jour. Chem. Phys., Vol.23, 1926, pp.710.

[232] Slichter, C. S., "Field Measurements of the Rate of Movement of Underground Water", U.S.Geological Survey Water-Supply Paper, Vol. 140, 1905, pp. 9-85.

[233] Slobod, R. L., and Caudle, B. H., "X-ray Shadowgraph Studies of Areal Sweepout Efficiencies", Petroleum Transactions, AIME, Vol. 195, 1952, pp. 265-270.

[234] Sohlo, J. and Kouri, R. J., "An Analysis of Enhanced Transverse Dispersion on Distillation Plates", Chemical Engineering Science, Vol. 37, No. 2, 1982, pp. 193-197.

[235] Sorbie, K. S. and Clifford, P. J., "The Inclusion of Molecular Diffusion Effects in the Network Modeling of Hydrodynamic Dispersion in Porous Media", Chemical Engineering Science, Vol. 46, No. 10, 1991, pp. 2525-2542.

[236] Srivastava, R. K., Chatzis, I. and Dullien, F. A. L., "A Computerized Technique for Measuring In-Situ Concentrations During Miscible Displacements in Porous Media", Transport in Porous Media, Vol. 7, No. 2, 1992, pp. 127-145.

[237] Staal, J. J. and Robinson, J. D., "Permeability Profile from Acoustic Logging", SPE 6821, Presented at the 52nd Ann. Fall Meeting of SPE in Denver, Colorado, Oct.9-12, 1977.

[238] Stalkup, F. I., Miscible Displacement, SPE Monograph Series, Society of Petroleum Engineers, New York, 1984, pp. 204.

[239] Starr, R. C., Gillham, R. W. and Sudicky, E. A., "Experimental Investigation of Solute Transport in Stratified Porous Media. 2. The Reactive Case", Water Resources Research, Vol. 21, No. 7, July 1985, pp.1043-1050.

[240] Street, N., "Tortuosity Concepts (Short Communications)", Austr. Jour. of Chem., Vol.11, No.4, 1958, pp.607-609.

[241] Sudicky, E. A., Gillham, R. W. and Frind, E. O., "Experimental Investigation of Solute Transport in Stratified Porous Media. 1. The Nonreactive Case", Water Resources Research, Vol. 21, No. 7, July 1985, pp. 1035-1041.

[242] Tahmassebi, S., "An Experimental Evaluation of Transverse Dispersivity and Plume Propagation in Porous Media", PhD Dissertation, University of Oklahoma, Norman, 1993.

[243] Tang, Y. and Aral, M. M., "Contaminant Transport in Layered Porous Media. 1. General Solution", Water Resources Research, Vol. 28, No. 5, May 1992, pp. 1389-1397.

[244] Tang, Y. and Aral, M. M., "Contaminant Transport in Layered Porous Media. 1. Applications", Water Resources Research, Vol. 28, No. 5, May 1992, pp. 1399-1406.

[245] Taylor, S.G., "Dispersion of Soluble Matter in Solvent Flowing Slowly Through a Tube", Proceedings of the Royal Science Society, Vol. 219, No. 1137, 1953, pp. 186-203.

[246] Theis, C.V., "Notes on Dispersion in Fluid Flow by Geologic Features, Proceedings of Conference on Ground Disposal of Radioactive Wastes", Chalk River, Ontario, Canada, Report

TAD-7628, Edited by J.M. Morgan, D.K. Kamison, and J.D. Stevenson, U.S. Atomic Energy Commission, Washington, D.C., 1962, pp. 166-178.

[247] Timur, A., "An Investigation of Permeability, Porosity and Residual Water Saturation Relationships for Sandstone Reservoirs", The Log Analyst, Vol.9, No.4, July-August, 1968.

[248] Tixier, M. P., "Evaluation of Permeability from Electric-Log Resistivity Gradients", The Oil and Gas Jour., Vol.48, No.6, June 16, 1949, pp.113-122.

[249] Van Der Poel, C., "Effect of Lateral Diffusivity on Miscible Displacement in Horizontal Reservoirs", Presented at the 36th Annual Fall Meeting of the Society of Petroleum Engineers, Dallas, Texas, October 2-5, 1961.

[250] Walsh, J. B. and Brace, W. F., "The Effect of Pressure on Porosity and the Transport Properties of Rock", Jour. of Geophys. Res., Vol.89, No.11, October 10, 1984, pp.9425-9431.

[251] Wang, F. H. L., "Effect of Wettability Alteration on Water/Oil Relative Permeability, Dispersion, and Flowable Saturation in Porous Media", SPE Reservoir Engineering, May 1988, pp.617-628.

[252] Wang, S. Y., Ayral, S., and Gryte, C. C., "Computer-Assisted Tomography for the Observation of Oil Displacement in Porous Media", SPE Journal, February, 1984, pp. 53-55.

[253] Wang, W.,"An Experimental Study of Gas-Gas Dispersion in Consolidated Porous Media to Characterize Reservoir Rocks", Master's Thesis, University of Oklahoma, Norman, 1994.

[254] Warren, J. E., and Skiba, F. F., "Macroscopic Dispersion", SPE Journal, September, 1964, pp. 215-230.

[255] Warner, M. J., "Characterizing Reservoir Core Samples and Measuring The Dispersion Coefficient Through Miscible Displacement Experiments", Master's Thesis, University of Oklahoma, Norman, 1987.

[256] Weisbrod, K. R. and Ring, W. W., "Simulation of Miscible Laboratory Displacements by the Total Dispersion Method", Presented at the 66th Annual Technical Conference and Exhibition of the Society of Petroleum Engineers, Dallas, Texas, October 6-9, 1991, pp. 239-254.

[257] Wellington, S. L., and Vinegar, H. J., "X-Ray Computerized Tomography", JPT, August, 1987, pp. 885-898.

[258] Wheat, M. R. and Dawe, R. A., "Transverse Dispersion in Slug-Mode Chemical EOR Processes in Stratified Porous Media", SPE Reservoir Engineering, May 1988, pp. 466-478.

[259] Wheatcraft, S.W., and Tyler, S.W., "An Explanation of Scale-Dependent Dispersivity in Heterogeneous Aquifers Using Concepts of Fractal Geometry", Water Resources Research, Vol. 24, No. 4, 1988, pp. 566-578.

[260] Willhite, G. P., Waterflooding, SPE Textbook Series, Vol. 3, Society of Petroleum Engineers, Richardson, Texas, 1986, pp. 326.

[261] Wilson, L.G., "Investigations on the Subsurface Disposal of Waste Effluent at Inland Sites", Research Development Program Report 650, U.S. Department of Interior, Washington, D. C., 1971, pp. 106.

[262] Wilson, J. L. and Miller, P. J., "Two Dimensional Plume in Uniform Ground-Water Flow", Journal of the Hydraulics Division, 1978, pp. 504-514.

[263] Winsauer, W. O., Shearin, H. M., Jr., Masson, P. H., and Williams, M., "Resistivity of Brine-Saturated Sands in Relation to Pore Geometry", AAPG Bull., Vol.36, No.2, Feb. 1952, pp.253-277.

[264] Withjack, E. M., "Computed Tomography for Rock-Property Determination and Fluid Flow Visualization", SPE Formation Evaluation, December 1988, pp. 696-704.

[265] Withjack, E. M., Graham, S. K., and Yang, C. T., "Determination of Heterogeneities and Miscible Displacement Characteristics in Corefloods by CT Scanning", SPE 20490, Presented in the 65th Annual Technical Conference and Exhibition of the Society of Petroleum Engineers, New Orleans, Louisiana, September 23-26, 1990.

[266] Wood, W. W., "A Geochemical Method of Determining Dispersivity in Regional Ground Water Systems", Journal of Hydrology, Vol. 54, 1981, pp. 209-224.

[267] Wright, R. J., Dawe, R. A. and Allmen, M. J., "Miscible, Equal Mobility Displacement within Layered Porous Media. The Influence of Transverse Dispersion", Revue de l'Institut Francais du Petrole, Vol. 38, No. 6, November-December 1983, pp. 735-750.

[268] Wyllie, M. R. J. and Gregory, A. R., "Fluid Flow Through Unconsolidated Porous Aggregates", Ind. Eng. Chem., Vol. 47, No.7, 1955, pp.1379-1388.

[269] Wyllie, M. R. J. and Rose, W., "Some Theoretical Considerations Related to the Quantitative Evaluation of the Physical Characteristics of Reservoir Rock from Electrical Log Data", JPT, Vol. 2, No. 4, 1950, pp. 105.

[270] Wyllie, M. R. J. and Spangler, M. D., "Application of Electrical Resistivity Measurements to Problems of Fluid Flow in Porous Media", Am. Assoc. Pet. Geol. Bull., Vol. 36, No. 2, 1952, pp. 359-403.

[271] Yaalon, D. H., "Mineral Composition of the Average Shale", Clay Minerals Bull, Vol. 5, No. 27, 1962, pp. 31-36.

[272] Yellig, W. F., and Baker, L. E., "Factors Affecting Miscible Flooding Dispersion Coefficients", Journal of Canadian Petroleum Technology, October-December, 1981, pp. 69-74.

[273] Youngquist, G. S., "Diffusion and Flow of Gases in Porous Solids", Flow Through Porous Media, American Chemical Society Publications, Washington, D.C., 1970, pp. 57-69.

[274] Yuan, Z. G., Somerton, W. H. and Udell K. S., "Thermal Dispersion in Thick-Walled Tubes as a Model of Porous Media", International Journal of Heat and Mass Transfer, Vol. 34, No. 11, 1991, pp. 2715-2726.

[275] Ziolkowski, D. and Szustek, S., "Effect of Fluid Velocity Radial Profile on the Radial Mass Dispersion in a Fluid Stream in a Packed Bed Tubular Apparatus", Chemical Engineering Science, Vol. 44, No. 5, 1989, pp. 1195-1204.

☆U.S. GOVERNMENT PRINTING OFFICE: 1995 - 660-029/20015